Title
Local Solvent Environment Can Define Solute Chemical Identity, Dynamics, and Reactivity

Author
Widmer, Devon Rose

Publication Date
2020

Peer reviewed|Thesis/dissertation

UNIVERSITY OF CALIFORNIA

Los Angeles

Local Solvent Environment Can Define Solute Chemical Identity, Dynamics, and Reactivity

A dissertation submitted in partial

satisfaction of the requirements for the degree

Doctor of Philosophy in Chemistry

by

Devon Rose Widmer

2020

ABSTRACT OF THE DISSERTATION

Local Solvent Environment Can Define Solute Chemical Identity, Dynamics, and Reactivity

by

Devon Rose Widmer

Doctor of Philosophy in Chemistry

University of California, Los Angeles, 2020

Professor Benjamin Joel Schwartz, Chair

Is it acceptable to assume that when a molecule is placed in solution, it retains the chemical identity and general behavior of its gas-phase counterpart? In this thesis, I explore this question through mixed quantum classical (MQC) molecular dynamics (MD) simulations of sodium dimer (Na_2) and sodium dimer cation (Na_2^+) in liquid tetrahydrofuran (THF). Although most chemical reactions, particularly those relevant to biological systems, take place in the condensed phase, the solvent is generally thought of as a mere medium that holds the reactants and allows them to encounter each other via diffusion. Of course, there are scenarios where the solvent is known to influence the chemistry of the solute, but these cases are usually straightforward and are only thought about for a small subset of chemical reactions. However, no studies have yet described the local solvent environment as part of the chemical identity of the solute. In this thesis, I show that when there are even modest local specific interactions between a solute and solvent, the solvent controls the chemical identity of the solute, entirely changing the types of chemistry that can take place.

In the specific case of an Na_2 or Na_2^+ solute in liquid THF, I show that local solvent molecules actually integrate as part of the the solute's identity, thus, stabilizing the solute in multiple states that differ only in the number of solvent molecules associated with the

solute's identity. These stable states, which can interconvert only by surmounting a large free energy barrier, behave as chemical species distinct not only from their gas-phase counterpart but also from each other. In addition, solvent interactions can also affect the dynamics of chemical reactions, such as photodissociation. Because the lowest energy excited state of gas-phase Na_2^+ is dissociative, this molecule makes an ideal basis for studies of photodissociation in the condensed phase, an important probe for understanding complex reaction dynamics. In this thesis, I show that when Na_2^+ is photoexcited in liquid THF, the initial shape of the bonding electron is completely different than that of excited state Na_2^+ in the gas phase. This means that unlike its gas-phase counterpart, upon photoexcitation, the bond of Na_2^+ solvated in liquid THF does not immediately break. Instead, the electron must dynamically rotate into an orientation more favorable for dissociation.

To investigate the dynamics of this process, I first pose a question fundamental to theoretical studies of the condensed phase: can a nonequilibrium system be understood through observation of the fluctuations of its equilibrium dynamics? This approximation, known as linear response (LR), is commonly assumed for condensed phase systems, but in this thesis I show that LR breaks down for the photodissociation of Na_2^+ in THF precisely because the local solvent environment experienced by the molecule varies between the equilibrium and nonequilibrium dynamics. In particular, I show that the solvent molecules associated with the solute's identity must shift from their preferred ground state positions to facilitate the rotation of the solute bonding electron into the position favorable for dissociation. Furthermore, in THF, the chemical identity of the solute can change during dissociation via the integration of new THF molecule's into the solute's identity. These processes consume most of the solute's dissociation energy, thus hindering its ability to fully dissociate.

Thus, one cannot simply assume that a solute's chemical identity is retained in solution. In fact, when there are even modest solute–solvent interactions present, the local solvent environment actually controls the solute's chemical identity, and thus also its dynamics and reactivity.

The dissertation of Devon Rose Widmer is approved.

Raphael D. Levine

Justin Ryan Caram

William M. Gelbart

Benjamin Joel Schwartz, Committee Chair

University of California, Los Angeles

2020

For Mei,

without whom

this dissertation would surely

have been completed

two years earlier,

but without whom

the process would surely

have held far less joy,

laughter,

and love.

I hope one day

you can read

Mommy's dissertation

with pride.

We did it!

Contents

List of Figures

List of Tables

ACKNOWLEDGEMENTS

For several long years now, I've adventured down the rugged, winding path of graduate school in pursuit of that most glittering of treasures: a PhD in chemistry. Although the road has taken me in unexpected and challenging directions, I have fortunately not had to journey alone. I here thank the individuals whose aid, whether academic or emotional, proved integral to the success of my ventures.

First, I thank my advisor Ben Schwartz for his guidance in my research and support as I navigated the difficult process of switching from experiment to theory while balancing graduate school with first pregnancy and then parenthood. I also thank the members of the Schwartz group, all of whom have been so supportive and kind throughout my years at UCLA. In particular, I single out Erik Farr and Matt Fontana who entered the Schwartz group the same summer as I and proved to be invaluable friends through grueling grad school classes and early research woes. I also thank Chen-Chen Zhou. Her friendship has kept my mental health from plunging off a cliff during the many emotional ups and downs of graduate school. Finally, I thank Andy Vong for becoming my partner in resurrecting ancient group code and exploring finicky condensed phase systems.

I also thank my family. Since childhood, my parents have supported and inspired me to pursue higher education. They even put up with my precocious six-year-old self declaring that I was going to pursue multiple PhD's when I was old enough (a dream that has lost all luster after the grueling process of pursing just the single PhD!). I would not have developed my passion for science without my parents. Some of my fondest science memories are of putting together middle school science fair projects with my dad and decorating my display board with my mom. Doing well at science projects as a child made me feel like I was *good* at science in a way that empowered me to seek out more scientific opportunities.

My amazing husband Alfie has been an endless source of support during my studies. He has spent countless hours listening to me cry or rant about difficult graduate school classes and research woes. I'm sure I have also bored him many times with my ravings about code

and plots and lovely bits of data, but he was always there to listen regardless. Without him, I would never have been able to complete this challenging degree, particularly after the arrival of our energetic, tenacious daughter Mei. Life has been so hectic these last few years, but I am so thankful for my wonderful Mei who helps (and distracts) me every day with dancing contests and hugs. I hope that one day she will be able to read Mommy's thesis and be inspired by all of the hard work her mom did during graduate school!

I also acknowledge that Chapter 2 is a version of D. R. Widmer and B. J. Schwartz. Solvents can control solute molecular identity. *Nature Chem.*, 10:910-916, 2018 (Copyright 2018 Nature Chemistry), reprinted with permission from the journal. For this work, co-author B. J. Schwartz was the PI. Chapter 3 is a version of D. R. Widmer and B. J. Schwartz. The role of the solvent in the condensed-phase dynamics and identity of chemical bonds: The case of the sodium dimer cation in THF. *J. Phys. Chem. B*, Under Review 2020. For this work, co-author B. J. Schwartz was the PI. Chapter 4 is a version of D. R. Widmer, A. Vong, and B. J. Schwartz. Linear response breakdown in liquid photodissociaiton: Caging and chemical identity. *Nature Chem.*, Submitted 2020. For this work, co-author A. Vong completed the simulations of Na_2^+ in liquid Ar and co-author B. J. Schwartz was the PI. Chapter 5 is a version of D. R. Widmer and B. J. Schwartz. How local solvent environment can alter solute electronic structure during photodissociation dynamics. *J. Phys. Chem. B*, In Preparation 2020. For this work, co-author B. J. Schwartz was the PI. I would also like to note that Chapter 1 Section 3 is based on an article I wrote for the Royal Society of Chemistry's *Chemistry World* magazine: D. R. Widmer. Why Choice of Solvent Matters More Than You Think. *Chemistry World* (May 2018).

The work described in this thesis was supported by the National Science Foundation under Grant No. CHE-1565434 and by the U.S. Department of Energy Condensed Phase and Interfacial Molecular Science program under Grant No. DOE-CPIMS-0000228903. I also gratefully acknowledge the Institute for Digital Research and Education (IDRE) at UCLA for use of the hoffman2 computing cluster.

VITA

For her undergraduate studies, Devon Rose Widmer attended Denison University, where she went on to earn duel degrees, a Bachelor of Science in Chemistry and a Bachelor of Art in English Literature. While at Denison, Widmer conducted research on water diffusivity in mixed phase binary systems, culminating in a final thesis on effective water diffusion coefficients in tetradecanol-eicosanol mixtures which was published in Fluid Phase Equilibria. In honor of her achievements in undergraduate research, Widmer was awarded the Anderson Scholarship for Excellence in Science, Denison's highest award for undergraduate scientists. During her time at Denison, Widmer was inducted into a variety of honors societies, including the Phi Beta Kappa Honor Society, the Sigma Xi Scientific Research Honor Society, and the Sigma Tau Delta English Honor Society. In 2012, Widmer graduated summa cum laude and was accepted into the chemistry program at the University of Chemistry, Los Angeles.

Widmer began her time at UCLA by participating in the summer research program, initiating her graduate studies with Dr. Benjamin Schwartz and continuing on with the Schwartz group thereafter. Her early research within the group focused on ultrafast spectroscopy, but Widmer made a dramatic switch mid-way through her degree to theoretical research, specifically mixed quantum classical molecular dynamics simulations of diatomic molecules in the condensed phase.

In 2013 Widmer was awarded the UCLA Department of Chemistry and Biochemistry Excellence in Teaching Award. Then, in 2018, Widmer had the immense honor to receive UCLA's Distinguished Teaching Award for Teaching Assistants, the highest teaching award given by the university.

Widmer's research has also found considerable acclaim. In 2014, she received an honorable mention in the National Science Foundation Graduate Research Fellowship Program, and in 2018 her work was published in the top tier journal Nature Chemistry. Widmer's work has also been highlighted by the Department of Energy and the National Science Foundation.

Chapter 1

Introduction

1.1 Solvent Effects on Condensed Phase Systems

Most chemical reactions, particularly those relevant to biological systems, take place in the condensed phase, yet our understanding of the influence of different solvent environments on solute behavior remains incomplete. Oftentimes, the condensed phase is approximated as simply a perturbation to the gas phase with solvent molecules acting as spectators, a medium to hold reactions in place but not a major participant in the reactivity or chemical identity of the solute. For instance, when simulating the electronic states of a solute, the condensed phase potential energy surfaces are often assumed to remain unchanged relative to their gas phase counterparts with the exception of a shift in energy level spacing.[1] However, through mixed quantum/classical (MQC) molecular dynamics (MD) simulations of simple diatomics in the condensed phase, this thesis reveals that trying to extrapolate how a solute will behave in the condensed phase based on that solute's gas phase behavior at best misses interesting chemical features and at worst gives entirely the wrong picture. In this thesis, I will show that a thorough understand of a solute's behavior in the condensed phase can only be obtained by taking into account the specific local solvent environment around that solute.

There are, of course, several well studied cases where the solvent is known to have significant effects on the solute's electronic structure–for instance by stabilizing the electrons of interest, thus creating the electronic states that are important to the solute's condensed phase behavior. One such example are solvated anions. In the gas phase, most anions have no bound excited states. However, in the condensed phase, the solvent can induce a bound excited state by local confinement.[2–5] This is also the case for solvated electrons, for which the solvent creates both the ground and excited states, states that can vary dramatically based on the specific solvent environment.[6–36] Those stabilized solvent-created electronic states are necessary for processes like charge-transfer-to-solvent transitions, a simple reaction where a solute electron is transferred to a cavity in the surrounding solvent.[2, 5, 26, 37–42] For many condensed phase reactions, including electron transfer reactions, the solvent is often the driving force that moves the electron from donor to acceptor.

Another important condensed phase effect on solute behavior is solvent caging, a concept first described by Franck and Rabinowitch in 1934, where solvent molecules encapsulate the solute.[43] Even for those diatomic molecules that smoothly dissociate in the gas phase, in the condensed phase, this solvent "cage" can trap the geminate atom pair, forcing the atoms to recombine if they are unable to escape the solvent cage through random motions.[1] This leaves the solute with three primary photodissociation/recombination pathways.[44, 45] The fastest pathway occurs when the atoms lose enough energy after the initial collisions with the solvent cage that they react back to form the original solute species. This process, which is referred to as "geminate" recombination since it was the original excited atom pair that reformed the solute, takes place on a timescale of a several hundred femtoseconds. Second, the atoms might escape the solvent cage, diffusing through the solution until they meet each other again, thus recombining on a timescale of a few to several hundred picoseconds in what is referred to as diffusive geminate recombination. The last pathway is "non-geminante" recombination where, after escaping the solvent cage, the atoms diffuse until they encounter other excited fragments with which to combine, a process that occurs on the nanosecond

to microsecond time scale. Clearly, the solvent plays a major role in the rates of many condensed phase processes.[3–5, 44, 45]

In previous work, our group has also shown that a diatomic solute's bonding electrons are compressed through Pauli repulsion interactions with the solute's first-shell solvent molecules.[46] This decreases the average bond length while raising the vibrational frequency of the bond. Meanwhile, collisions with solvent molecules shove the bonding electron density off axis, resulting in relatively large instantaneous dipole moments that induce infrared activity, even in molecules that, in the gas phase, are perfectly symmetrical. However, although the solvent is known to influence chemical reactivity in a wide variety of ways, in all of these scenarios the solute is considered to retain its gas-phase chemical identity. In this thesis, I will also show that in cases where the solute–solvent interactions are at least the strength of a hydrogen bond, the bond dynamics, spectral signatures, electronic structure, and reactivity of the solute is controlled by the local solvent environment. In other words, the solvent creates a new chemical identity for the solute, one which can behave entirely differently than the original gas-phase molecule.

1.2 Simple Diatomics Can Elucidate Complex Dynamics

Although there are a wide variety of chemical systems that could be used to explore the dynamics and reaction mechanics of solutes in the condensed phase, we have chosen for these studies to focus on simple diatomic molecules in solution. Specifically, the studies included in this thesis examine condensed phase systems where the solute is sodium dimer (Na_2) or sodium dimer cation (Na_2^+) and the solvent is argon (Ar) or tetrahydrofuran (THF).

The photodissociation and recombination of simple diatomic molecules in solution have been studied for nearly ninety years now as a probe for understanding complex reaction dynamics in the condensed phase.[1, 43, 47–52] Many of these studies have focused on molecular

iodine, I_2.[53–71] Although there is still much that can be learned about the microscopic processes involved in iodine dissociation and recombination, the timescales of I_2 photoexcitation have been shown to consist of fast dissociation followed by collision with the surrounding cage of solvent molecules within approximately 5 ps that results in direct geminate recombination, temporary escape from the solvent cage followed by delayed geminate recombination, or dissociation and eventual non-geminate recombination.[45]

Because I_2 is stable in a variety of solvent environments, it makes for an ideal experimental probe molecule. However, I_2 has a complicated electronic structure with low-lying bound and dissociative electronic states that cross. An ideal molecule for theoretical studies of condensed phase dynamics and photodissociation must have a simple electronic structure, ideally with an easily accessible state that is purely dissociative. With this in mind, we chose the Na_2 and Na_2^+ molecules due to the relative simplicity of their electronic structure, with only two and one valence electrons respectively. The neutral dimer Na_2 was chosen for preliminary studies exploring solvent effects on the ground state of a simple diatomic solute. However, experimental studies of Na_2 in liquids would require fairly complex methods, such as co-evaporating Na metal with a solvent to prepare solvated Na_2 in low-temperature rare gas matrices[72–78] or a glass-forming liquid.[79] Experimental studies of solvated Na_2^+, on the other hand, are potentially much more accessible. In fact, studies of room temperature Na_2^+ prepared in bulk THF via pulse radiolysis of solutions containing high concentrations of sodium salts are already underway and should prove an excellent opportunity to couple experimental results with the theoretical studies contained in this thesis. Furthermore, the lowest energy excited state of Na_2^+ is dissociative, making photodissociation studies accessible. For these reasons, the Na_2^+ molecule was chosen for the majority of the work discussed in this thesis.

With a solute of study in mind, the next step is to determine the most effective type of simulation to describe a condensed phase system. Though computationally accessible, traditional molecular dynamics simulations based on classical pairwise additive force fields

are not able to take into account how the solute's electronic structure is distorted by the local solvent environment. One method to enhance these classical models is through the inclusion of many-body polarization terms; however, even these improved simulations are not able to capture the changes to the solute's electronic structure which, as this thesis will show, are integral to understanding the condensed phase dynamics and reactivity of a solute. On the other extreme would be to use full quantum mechanics. Such simulations would, of course, be the most ideal method as they would completely capture all of the intricate interactions of the chemical system. However, even for a molecule with a relatively simple electronic structure, like Na_2 and Na_2^+, performing all-quantum condensed phase molecular dynamics simulations is simply not feasible due to the enormous computational cost of accounting for all of the electrons contained in the system, which would include the valence and core electrons of the solute as well as all of the electrons on each of a minimum of several hundred solvent molecules. Regardless, the quantum mechanics of the electrons responsible for the chemical bonding and the interactions of those electrons with the surrounding solvent molecules must be accounted for at the Hamiltonian level. Although there have been some semiempirical studies done to include solvent effects on the bonding electronic structure of I_2 and I_2^- in simulations examining the photodissociation of diatomics in rare gas liquids/matrixes[80, 81] and CO_2 clusters,[82–84] we elected to utilize first-principles quantum mechanics but to reserve use of the Schrödinger's equation (SE) for the electron(s) involved in the chemical bond of interest, here the Na_2 or Na_2^+ bond.

Therefore, the studies included in this thesis were conducted using mixed quantum/classical (MQC) molecular dynamics (MD) simulations in which the majority of the system is treated classically while quantum mechanics is reserved only for the electron(s) involved in the dimer's bond, thus avoiding the formidable task of solving the SE for the thousands upon thousands of electrons present in simulations with even just a few hundred solvent molecules. This means that for simulations of Na_2^+, we need only solve the SE once−for the single valence electron involved in the Na_2^+ bond. This is the primary reason for choosing Na_2^+ as the solute

molecule for the majority of the simulations in this thesis: the Na_2^+ molecule can be accurately modeled with a single-electron description. Simulations of Na_2 were more complicated because we needed to find the electronic states of a pair of valence electrons, a problem that we solved using our group's two-electron Fourier grid (2EFG) method, which is described in detail in previous group work.[46, 85, 86] In short, we represent the wave functions of the two electrons on a six-dimensional real space grid. The SE is then solved variationally at every time step of the simulation. We treat the bonding electrons using configuration-interaction-with-singles-and-doubles (CISD), which, because there are only two explicit electrons, is equivalent to full configuration interaction.[85]

Thus, for all of our MQC MD simulations, we think of the solute as two classical Na^+ cores held together by one or two quantum mechanical valence bonding electrons. The simulations also contain hundreds of classical solvent molecules. While the precise simulation details for each study are provided in the relevant chapters, I will outline the basics of the interactions between the various simulation components here. The interactions between the classical components are calculated using Lennard-Jones (LJ) potentials, except where specified.[87] For the interactions between the classical components and the quantum mechanical electron(s), we used Phillips-Kleinman (PK) based electron$-$Na and electron$-$solvent pseudopotentials.[88] A pseudopotential is an effective potential that is used in place of the explicit interactions between core and valence electrons. Oftentimes, these pseudopotentials are constructed empirically by using adjustable parameters to reproduce an experimental observable, such as ionization energy. PK pseudopotentials, like the ones developed by our group,[27, 33, 89] are instead rigorously derived using the core orbital wavefunctions generated from a Hartree-Fock calculation of the system of interest and guarantee orthogonality between the core and valence electron wavefunctions. Of course, all pseudopotentials are subject to approximations. For instance, because all pseudopotentials are constructed from a single configuration of the molecule's core electrons, if the wavefunction of those core electrons changes under certain situations, the pseudopotential will not

take that change into account. This is known as the frozen core approximation (FCA), which is examined in this thesis in relation to the Na_2^+ molecule at the end of Chapter 2. Nevertheless, the ability to describe the interactions between the classical and quantum components of our system is what allows us to access the chemistry key to understanding solvent effects on chemical bonds.

1.3 Of Jellybeans, Gumballs, and Gummy Bears: Tasty Analogies for Solvent-Solute Interactions

The material in this thesis section is adapted and expanded upon based on a general scientific interest article I wrote for the Royal Society of Chemistry's *Chemistry World* magazine: D. R. Widmer. Why Choice of Solvent Matters More Than You Think. *Chemistry World* (May 2018). As such, the tone is more colloquial. However, despite the lighthearted candy analogies, this section gives a solid overview of the important scientific questions asked and answered in this thesis.

So far, I have established the importance of studying the dynamics and reactivity of condensed phase systems and the utility of mixed quantum/classical molecular dynamics simulations of simple diatomic in solution for exploring such systems. Now, let's chew on some mental sweets to think about the various solute—solvent interactions that will be explored in this thesis.

Depending on the kinds of solute—solvent interactions present in a given condensed phase system, the ways the solute's dynamics and reactivity are effected by the solvent will differ vastly. In cases where the solute and solvent do not strongly interact, we can think of the condensed phase system as a solute jellybean in a jar of solvent gumballs. Shaking the jar causes the gumballs to bash into the jellybean, jiggling it around the jar and smashing it into new shapes. In such scenarios, even though the solute "jellybean" and solvent "gumballs" do not strongly interact chemically, the solvent still has a strong influence on the solute's

behavior. For instance, just like nearest layer of gumballs works to trap the jellybean, solvent molecules form a cage around the solute, compressing the solute's electron density and, for dimer molecules, causing the average bond length to decrease and thus the vibrational frequency to increase. The collisions between the jellybean and nearby gumballs which lead to the squishing and squashing of the jellybean also provide a nice analogy for the way the solute's electron density is distorted through Pauli repulsion interactions with the caging solvent molecules. Such was the case in previous group studies of Na_2 in liquid argon, where the instantaneous dipole moments induced by the jostling of the electron density due to nearby solvent molecules actually led to a large instantaneous dipole moment which made the otherwise completely symmetric solute infrared active.[46]

The "jellybean in a jar of gum balls" model works well for condensed phase systems where the solvent does not strongly interact with the solute, systems where knowledge of the all-encompassing average is sufficient for understand the solute's dynamics. In other words, for such systems, a description of "jellybean in a jar of gum balls" is sufficient, and one could then go on to study the jellybean in a jar of malted milk balls or jawbreakers, which will each jostle and squish the jellybean to different extents. However, this simple analogy breaks down for cases where the solute and solvent interact even relatively weakly, such as with the strength of the hydrogen bonds present in liquid water. In such cases, we can introduce a knew analogy: a jellybean in a jar of gooey gummy bears. Now, instead of simple jostling and squishing the jellybean, the gummy bear "solvent" can actually latch on, grabbing hold of the jellybean and forcing it to move according to their own specific motions. Such interactions have the potential to pull, stretch, and contort the jellybean into a variety of new shapes, each of which need not behave the same as the last.

Such is the case with Na_2 and Na_2^+ in liquid THF. Although apolar argon does not interact with the Na_2 or Na_2^+ solute, negatively charged oxygen sites of the THF molecules are capable of forming dative bonds with the positively charged sodium cores on each end of the solute molecule. Even though these dative bonds are only about as strong as the hydrogen bonding

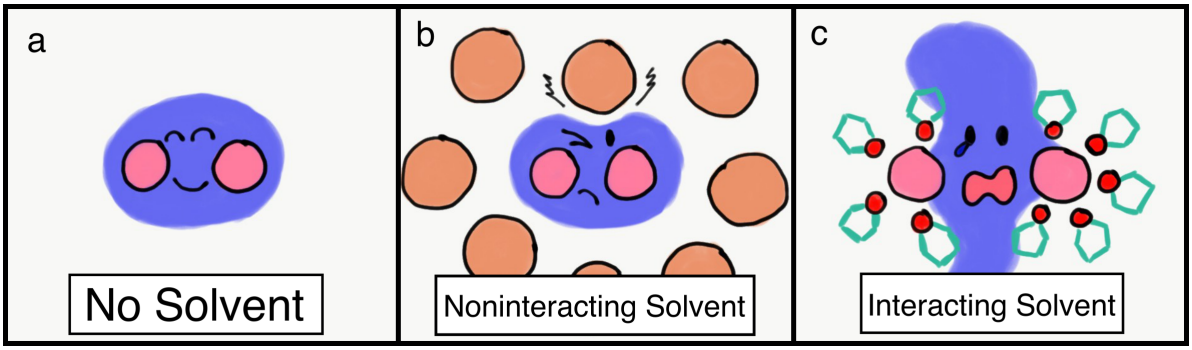

Figure 1.1: Cartoon depictions of the solvent's influence on a simple diatomic solute. Panel (a) shows a happy gas-phase dimer unperturbed by any pesky solvent molecules. However, when that dimer is placed in the condensed phase, it becomes perturbed. Panel (b) shows the "jellybean in a jar of gum balls" scenario: the influence of a solvent that does not interact with the solute, like Na_2 and Na_2^+ in apolar liquid Ar. Instead, solvent molecules form a cage around the dimer, compressing and jostling the solute's electronic density. Finally, panel (c) shows the "jellybean in a jar of gooey gummy bears" scenario: a dimer that has been stretched to a longer bond length while the interacting solvent molecules crowd each end of the solute, squashing the bonding electron into an entirely new structure, like Na_2 and Na_2^+ in polar liquid THF. The atoms of the dimer molecule are drawn as pink spheres while the bonding electron is shown as a pale blue "cloud." Ar atoms are drawn as orange spheres and THF as turquoise sticks with red oxygen atoms.

interactions in liquid water, they dramatically alter the condensed phase behavior of the solute with which they interact. Just like gummy bears pulling on opposite sides of the jellybean "solute" might cause it to elongate, the datively bound solvent stretches the Na_2 and Na_2^+ bonds in liquid THF such that the solute ends up with an average bond length that is significantly longer than in the gas phase—the exact opposite trend of the solute's interaction with argon solvent molecules. Furthermore, just as having different numbers of gooey gummy bears on each end would change the way the solute jellybean is distorted, having different numbers of dative bonds changes the behavior of the Na_2 and Na_2^+ solute. This leads to multiple stable coordination states for these molecules in liquid THF which differ only in the specific local solvent environment.

Although the interactions between the THF and solute would not be conventionally considered chemical bonds, the coordination states must surmount relatively large energy barriers, essentially undergoing a chemical reaction, in order to interconvert. Thus, these states act

as discrete molecules that are not only distinct from the gas phase but also from each other. In such a scenario, we can no longer describe the system as simple a "jellybean in a jar of gummy bears" because the exact number of gummy bears around the "solute" jellybean at a given moment influences how the jellybean will behave. In other words, the local solvent environment is key to understanding the chemical identity of the solute, so we must consider the system as multiple stable states in equilibrium or risk washing out the true solvent effects with a deceptive average.

But does all this talk of jellybean solutes and gumball/gummy bear solvents matter beyond these simulations of simple diatomic in solution? Of course it does! It is already well know that the solvent in which a chemical process occurs can influence a chemical reaction, such as my changing the reaction rate or stabilizing products. But additionally, many of the biological processes necessary for life, such as the folding of a protein into its biologically function form, are controlled by delicate chemical equilibria. Because so many of these processes occur in the condensed phase, understanding the specific ways that the local solvent environment influence the dynamics and reactivity of the solute is of critical importance. This thesis shows that the solvent, far from a mere spectator in chemical processes, can actually become a part of the chemical identity of a solute, changing the solute's behavior in unexpected and exciting ways.

1.4 Summary of Thesis Content

Understanding how the solvent influences the chemical identity and reactivity of a solute is essential in understanding condensed phase dynamics. This thesis will delve into key questions about how a solute interacts with its local solvent environment. In Chapter 2, which was published in *Nature Chemistry* as "Solvents can control solute molecular identity," we utilize MQC MD simulations of Na_2 in THF to explore in detail how the chemical identity of a solute can be influenced, and indeed defined, by its local solvent environment. In

Chapter 3, we focus on the Na_2^+ molecule in the condensed phase with several aims: to show through detailed comparisons to all classical simulations the necessity of treating the the Na_2^+ bonding electron explicitly quantum mechanically if we want to capture the condensed phase dynamics of the solute, to compare to the results of Chapter 2 to understand the extent of the solvent's influence on the condensed phase dynamics of this molecule, and to introduce the concept of stable gas-phase $Na_2(THF)_n^+$ coordinated clusters that have an electronic structure completely different than that of gas phase Na_2^+, which will have important influence on the photodissociation dynamics of Na_2^+ in the condensed phase. Chapter 4 shows that the process by which the Na_2^+ molecule dissociates both in liquid argon and liquid THF differs from the linear response prediction and delves into the reasons for this linear response breakdown. Finally, Chapter 5 gives an in depth analysis of the changes in the Na_2^+ electronic structure as the molecule dissociates in THF.

Chapter 2

Solvents Can Control Solute Molecular Identity

2.1 Abstract

For solution-phase chemical reactions, the solvent is often considered simply a medium to allow the reactants to encounter each other by diffusion. Although examples of direct solvent effects on molecular solutes exist, such as the compression of solute bonding electrons due to Pauli repulsion interactions, the solvent has not yet been considered a part of the chemical species of interest. We show using quantum simulations of Na_2 that when local specific interactions between a solute and solvent are energetically on the same order as a hydrogen bond, the solvent controls not only the bond dynamics but also the chemical identity of simple solutes. In tetrahydrofuran, dative bonding interactions between the solvent and Na atoms lead to several unique coordination states which must cross a free energy barrier of $\sim$8 $k_{\mathrm{B}}T$, essentially undergoing a chemical reaction, to interconvert. Each coordination state has

its own dynamics and spectroscopic signatures, highlighting the importance of considering the local solvent environment in the identity of condensed-phase chemical systems.

2.2 Introduction

Although most chemical reactions take place in solution, the solvent is usually thought of as a spectator, acting merely as a medium to hold the reactants and allow them to encounter each other by diffusion. Of course, for a few special cases, such as solvated electrons[38] and the charge-transfer-to-solvent transitions[2] of simple anions, the solvent creates the electronic states that are of importance, primarily because the electrons of interest are not otherwise bound without the stabilizing presence of the solvent. Moreover, in electron transfer and related reactions, the reorganization of the surrounding solvent molecules is the driving force to move the electron from the donor to the acceptor, and thus determines the reaction rate.[3–5] Dielectric effects from collective solvent motions can lead to solvatochromic shifts in the electronic absorption spectra of solutes,[90] and solvent molecules can provide viscous drag that changes the dynamics and thus branching ratios of unimolecular isomerization reactions.[91] In terms of more direct solvent effects on molecular solutes, in previous work we showed that Pauli repulsion interactions from the electrons on the first-shell solvent molecules can compress a solute's bonding electrons, pushing the solute's electron density off axis and raising the bond's vibrational frequency.[46] But even with these wide-ranging ways in which solvents can affect chemical reactivity, in none of these cases is the solvent thought of as being a part of the chemical species of interest.

In this work, we show using mixed quantum/classical (MQC) molecular dynamics (MD) simulations that local specific interactions between a solute and solvent that are energetically on the same order as a hydrogen bond not only alter solute molecular properties but also play an important role as part of the molecular identity of the solute. By simulating the sodium dimer (Na_2) molecule in both liquid Ar and liquid tetrahydrofuran (THF), we show that Pauli

repulsion interactions between the solvent molecules and the solute bonding electrons deform the Na_2 bonding electron density. This induces large dipole moments and creates infrared activity in what in the gas phase is a symmetric diatomic solute with no infrared absorption. In liquid THF, dative bonding interactions between the THF oxygen atoms and the sodium cation core at the center of each Na atom create a series of distinct, chelated solvation states, causing even further distortion of the bonding electrons and, in some cases, the induction of permanent dipole moments. Furthermore, we find that distinct local THF solvation states each have their own unique Na–Na bond length, bond dynamics and spectroscopic signatures, and that these different chelation states are separated by barriers of many $k_{\mathrm{B}}\,T$ in free energy. Thus, to explain the behavior of Na_2 in liquid THF, the different chelated solvation states, which are distinguished only by the weak solute-solvent dative bonds, must be treated as distinct chemical species.

We chose to study the Na_2 molecule in this work because it can be well described in MQC MD simulations; the molecule can be thought of as two classical Na^+ cores that are held together by two quantum mechanical valence bonding electrons.[46] In our simulations, we treat the two quantum mechanical bonding electrons using configuration-interaction-with-singles-and-doubles (CISD),[85] which is equivalent to full CI since only two explicit electrons are involved. The interactions between the bonding electrons and the Na^+ cores[39] and the THF[27, 41, 86] or Ar[92] solvent molecules are described using previously-developed pseudopotentials.[93] In this way, we can accurately calculate how immersion of Na_2 in solvents like liquid Ar or THF affects the molecular electronic and vibrational structure of this relatively simple solute. Details of the potentials and computational methods we use are given in the Supplementary Information (SI) but in general are similar to those in our previous work.[46, 85, 86] We note that we used these same potentials and level of theory to simulate the structure, spectroscopy and excited-state dynamics of the sodium anion (Na^-) in liquid THF, and obtained excellent agreement with experiment.[39, 41] The Na_2/THF system studied here is theoretically identical to our previously-studied Na^-/THF system

except for the presence of a second identically-theoretically-treated sodium nucleus.

2.3 Results and Discussion

Because there is relatively little exchange and correlation between the bonding electrons and those in the Na^+ core, our MQC description of the Na_2 molecule in the gas phase gives good agreement with high-level quantum chemistry calculations,[46, 94] as summarized in Table 2.1. Figure 2.1a shows that the gas-phase Na_2 valence electron density forms a symmetric ovoid around the Na_2 center of mass, as expected from the ideas of molecular-orbital theory.[95, 96] When we insert the Na_2 molecule into solution, however, interactions between the solvent molecules and bonding electrons produce a valence electron density that is deformed relative to that in the gas phase. Figure 2.1b shows that when Na_2 is placed in liquid Ar, Pauli repulsion interactions from the surrounding cage of Ar atoms, on average, compress the solute's bonding electronic density leading to a stiffer, tighter chemical bond (Table 2.1). As we saw previously,[46] solvent fluctuations, even in apolar liquid argon, induce relatively large instantaneous dipole moments $\overline{\mu}$ (Table 2.1), even though the overall average dipole moment remains zero since the instantaneous dipoles point in random directions.

THF molecules, on the other hand, are known to chelate Na^+ in solution, with THF oxygen sites forming metal-oxygen dative bonds with strength similar to that of a hydrogen bond, about 5 kcal/mol. We have shown previously on the basis of both MQC simulations and ultrafast spectroscopy experiments that when bare Na atoms are created in liquid THF, THF molecules push the Na valence electron off-center to allow the formation of Na–THF oxygen site dative bonds; in other words, the neutral atomic Na species in liquid THF is best though of as a Na^+–solvated electron tight-contact pair rather than a solvated atom.[86, 101] Indeed, when simulated with the same potentials and methods used here,[86, 101] the calculated properties of sodium cation:electron contact pairs were found to be in excellent agreement with experiment.[42, 102] Unlike what happens with bare Na atoms, the Na_2

System	r_e (Å)	ω_e (cm^{-1})	$\overline{\mu}$ (e-Å)
Gas Phase Exp[97–100]	3.08	159.1	0.0
Gas Phase [CCSD(T)]	3.185 ± 0.004	149 ± 26	0.0
Gas Phase [MQC]	3.270 ± 0.004	136 ± 23	0.0
Argon	3.167 ± 0.005	161 ± 48	0.11 ± 0.05
THF (average)	3.617 ± 0.002	112 ± 15	0.6 ± 0.4
$Na(THF)_3$–$Na(THF)_3$	3.472 ± 0.008	119 ± 33	0.4 ± 0.2
$Na(THF)_2$–$Na(THF)_4$	3.66 ± 0.01	108 ± 20	1.2 ± 0.3
$Na(THF)_3$–$Na(THF)_4$	3.692 ± 0.007	113 ± 24	0.7 ± 0.2

Table 2.1: Average bond length (r_e), vibrational frequency (ω_e), and instantaneous dipole moment ($\overline{\mu}$) for Na_2 in the gas phase and in various solution environments. r_e and ω_e values for our work were obtained from Harmonic fits to the well bottom of the potential energy surface (gas phase) or potential of mean force (solution phase); cf. Fig. 2.4, below. The post-Hartree-Fock gas phase fixed-point calculations were performed using coupled-cluster with singles, doubles and perturbative (linearized) triples [CCSD(T)] with the 6-311+G(d,p) basis set using GAUSSIAN 09. The gas-phase values calculated with our plane-wave-based CISD method give good agreement with theory at a similar level using more standard basis sets.[94] The quoted errors are the standard deviations calculated from the non-linear least-squares fit.

molecule simulated here remains intact in liquid THF, but Figure 2.1c shows that, similar to the Na^+-solvated electron tight-contact pair, local interactions with the solvent displace the solute valence electron density to expose part of each Na^+ core for chelation by the THF oxygen sites. The net effect of these dative interactions with the solvent is to cause the solute valence electron density to spill out away from the bond axis, leading to instantaneous dipole moments that are much larger than in liquid Ar. Also in contrast to the bond compression seen in liquid Ar, the THF–Na^+ interactions lead to a large increase in the Na–Na bond length (Table 2.1).

To better understand the local interactions between Na_2 and THF, the black curve in Fig. 2.2 shows the Na^+–THF oxygen site radial distribution function, $g(r)$, averaged over both Na^+ cores. The large peak at 2.35 Å that dominates the $g(r)$ corresponds to THF oxygen sites that coordinate the Na^+ core; this dative bond distance is the same as that for solvation of both bare Na^+ ions and Na^+:solvated electron tight-contact pairs in liquid THF.[86, 103] Although six THF molecules coordinate a bare Na^+ and four coordinate the

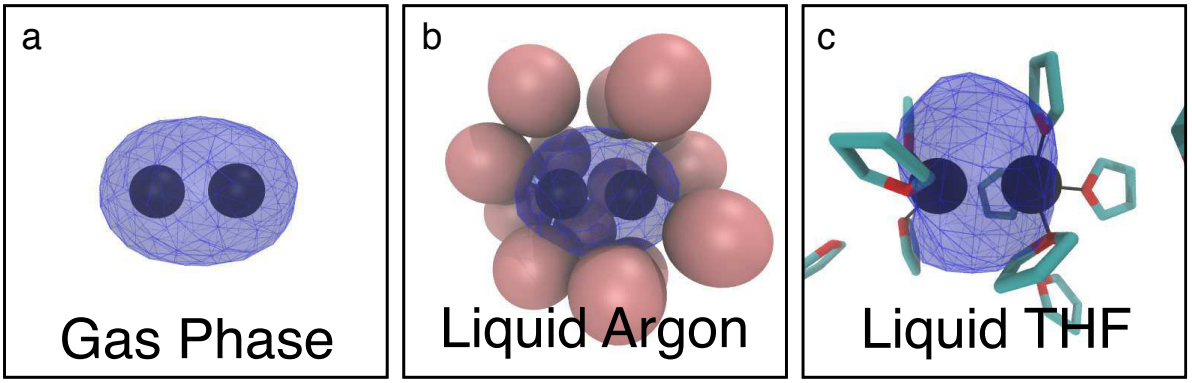

Figure 2.1: Representative simulation snapshots of Na_2 reveal deformation of the bonding electronic density in the condensed phase. The Na^+ cores are plotted as black spheres (scaled to their ionic radius) while the valence electrons' density is represented as a transparent blue surface with a blue wire mesh enclosing 90% of the charge density. The first solvation shell of Ar atoms (with a cutout to enable viewing of the electron density) are plotted as pink spheres (scaled to their van der Waals radius) and THF molecules are plotted as light-blue sticks with red oxygen atoms. The dative bonds between Na^+ and THF oxygen sites within 3.5 Å are drawn with thin black lines. For the sodium dimer in THF, the snapshot shown is for the most commonly-occurring $Na(THF)_3$–$Na(THF)_4$ coordination state; representative snapshots for other coordination states and further discussion is provided in the SI. In the gas phase (**a**), the bonding electron density forms a symmetric ovoid around the dimer center of mass. However, in liquid Ar (**b**), the electron density is compressed, resulting in a slightly shorter average bond length, and in liquid THF (**c**), the Na^+-THF oxygen site dative bonds elongate the Na_2 bond length and distort the electron density.

neutral Na species,[86] integration of the $g(r)$ for Na_2 in THF reveals an average coordination of 3.25 THF oxygens making dative bonds per Na atom.

To understand why the average coordination number is not an integer and why the THF-solvated Na–Na bond length is longer than that in the gas phase or liquid Ar, we examined the free energies involved in THF coordination of Na_2. To do this, we introduce a continuous coordination number n_{Na^+}, defined as the number of THF oxygen sites that reside within a certain distance of the atomic center (actually, the integrated number of THF oxygens weighted by the function $S(r)$, shown as the dashed green curve in Fig. 2.2; this is very similar to the coordinate we used in our previous work on Na^+:solvated electron tight-contact pairs in liquid THF, and details are given below in the methods section). By examining the distribution of n_{Na^+} along our equilibrium Na_2/THF trajectory, we were able to calculate the free energy A, or potential of mean force, as a function of the coordination number coordinate for each Na atom, which is shown in Fig. 2.3a. The figure shows clearly that there are only a few stable Na_2 coordination states, and that the minima in A occur precisely at integer coordination numbers. The coordination states accessible at equilibrium are $Na(THF)_3$–$Na(THF)_3$, $Na(THF)_2$–$Na(THF)_4$, and $Na(THF)_3$–$Na(THF)_4$ (referred to as (3,3), (2,4), and (3,4) in the figures below), which occur at room temperature with relative populations of roughly 50:17:54, respectively, explaining the average THF coordination number of 3.25. The figure also shows that these stable coordination states interconvert along pathways where n_{Na^+} on one Na^+ core remains fixed while the other Na^+ core either gains or loses a single coordinating THF.

Figures 2.3b and 2.3c also show one-dimensional slices along two of the coordination-state conversion pathways, revealing relatively large potential energy barriers ($\sim$8 $k_B T$ high) that must be overcome to convert between coordination states. Indeed, we see that at equilibrium the typical interconversion time at room temperature for the $Na(THF)_3$–$Na(THF)_4$ $\rightarrow$ $Na(THF)_3$–$Na(THF)_3$ reaction is $\sim$37 ps, and $\sim$32 ps for the reverse $Na(THF)_3$–$Na(THF)_3$ $\rightarrow$ $Na(THF)_3$–$Na(THF)_4$ interconversion reaction while we see $\sim$38 ps for the $Na(THF)_3$–

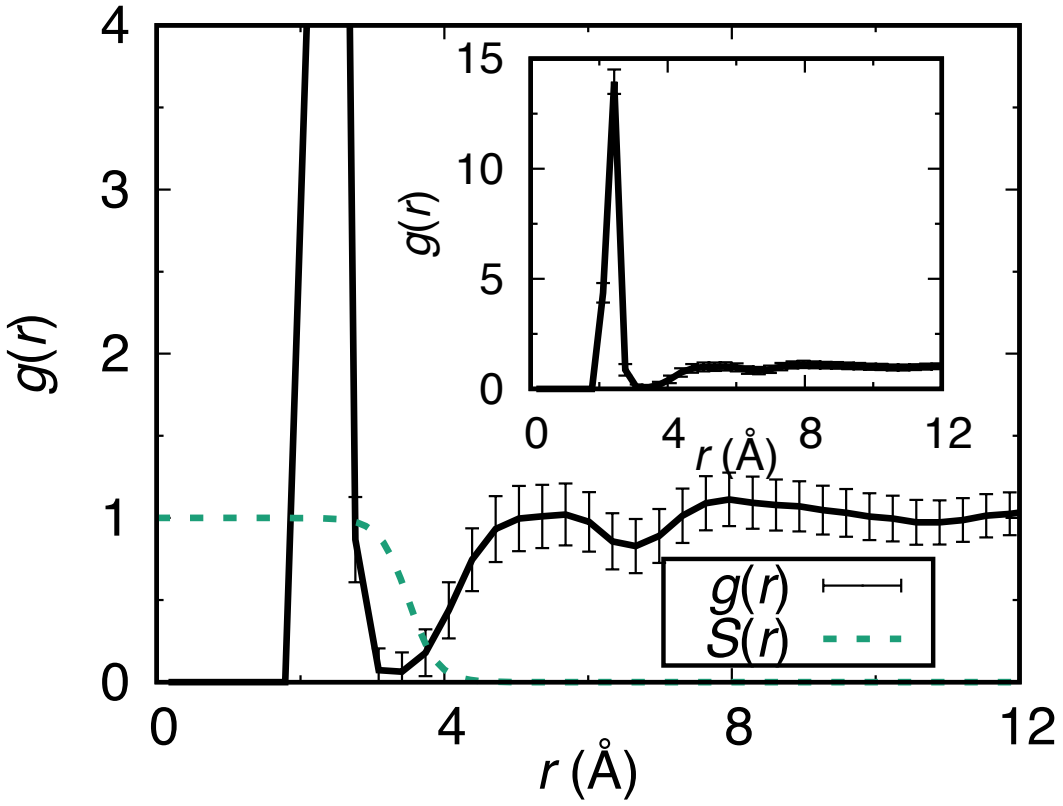

Figure 2.2: Pair distribution function, $g(r)$ (solid black curve), showing the chelation of the Na^+ cores in Na_2 by THF, leading to the formation of metal-oxygen dative bonds. $g(r)$ is averaged over Na^+–THF oxygen site distances for both Na^+ cores. The dashed green curve shows the smooth weighting function, $S(r)$, used to define the THF coordination number around the Na^+ cores. The inset shows $g(r)$ on an expanded scale, revealing the full coordination of the Na^+ cores by THF molecules at the 2.35 Å dative bond distance. The error bars represent 95% confidence intervals. The sharp coordination peak at the 2.35 Å similar to that observed for the Na^+:solvated electron tight-contact pairs formed from bare sodium in liquid THF, reveals that THF molecules displace the Na_2 bonding electron density, exposing both Na^+ cores for chelation.

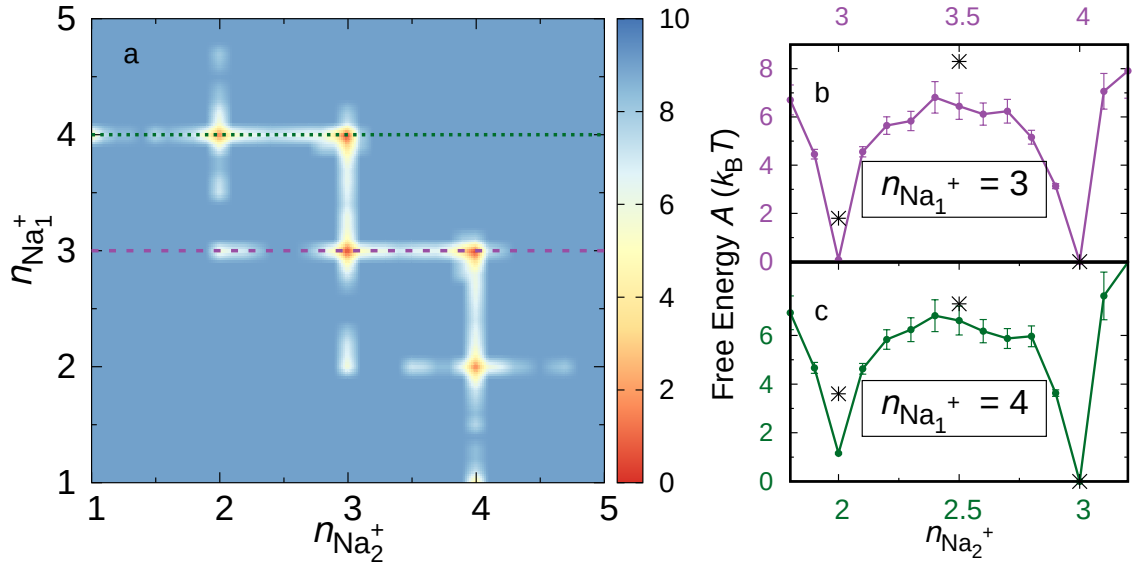

Figure 2.3: The stable coordination states of Na_2 in liquid THF behave as distinct molecules. **a**, The potential of mean force as a function of the Na^+–THF solvent coordinate, n_{Na^+} (generated by summing the number of THF oxygen atoms weighted by $S(r)$ in Fig. 2.2), for each Na^+ core. The data clearly reveal multiple stable states with integer numbers of coordinated THF molecules that are connected by conversion pathways in which the coordination of one Na^+ core changes by a single THF molecule. Slices along **(b)** the $n_{Na_1^+}$ = 3 and **(c)** the $n_{Na_1^+}$ = 4 conversion pathways reveal steep potential barriers of several $k_B T$ that must be overcome to convert between the stable coordination states, much like the energy barriers of a traditional chemical reaction coordinate. Error bars represent 95% confidence intervals. For comparison, the results of fixed-point DFT calculations (see the SI for details) using the range-separated hybrid ωB97M-V functional[104] with implicit solvent are shown as the black asterisks.

$Na(THF)_4 \rightarrow Na(THF)_2$–$Na(THF)_4$ reaction and ∼16 ps for the reverse $Na(THF)_2$–$Na(THF)_4$ $\rightarrow Na(THF)_3$–$Na(THF)_4$ reaction (see SI for details). These 'reaction times' observed during the simulation trajectory match reasonably well with values predicted from transition state theory, as shown in the SI, consistent with the assignment of the interconversion between coordination states as chemical reactions. Clearly, the coordination states at each free energy minimum can be thought of as distinct chemical species, with reactive pathways connecting the different species in equilibrium. Thus, even though each Na^+–THF dative bond has a strength that is similar to that of a hydrogen bond, the collective interaction of the solute with the solvent produces a variety of new chemical species that are in equilibrium, each of which is distinguished only by the involvement of the solvent.

To verify that the solvent-induced changes in molecular identity we see make sense, we used density functional theory (DFT) to calculate the relative energies of the different Na_2/THF coordination states extracted from our MQC simulations, performing calculations on geometry-optimized configurations from our simulations extracted at both the free energy minima and at the tops of the interconversion barriers. Since the coordination states involve relatively weak dative interactions between the THF oxygen and sodium atoms, we used the range-separated hybrid ωB97M-V functional, which includes non-local correlation;[104] the details of how we performed these fixed-point calculations are given in the SI. Indeed, we find, as summarized by the black asterisks in Figs. 2.3b and c, that the relative energetics calculated both directly in the MQC simulations and by DFT, for both the different coordination states and the barriers for their interconversion, agree to within one or two k_BT, an amount that is well within the error of the DFT calculations.

How unique are the Na_2 chemical species that differ only in their local coordination with the solvent? In Fig. 2.4 we compare the potential energy of the gas-phase Na_2 molecule (black curve) to the potentials of mean force (PMFs) for the molecule in liquid Ar (orange curve), in liquid THF on average (purple dotted curve), and for each of the stable THF-solvated coordination states (red, green and blue curves) as a function of the Na–Na bond

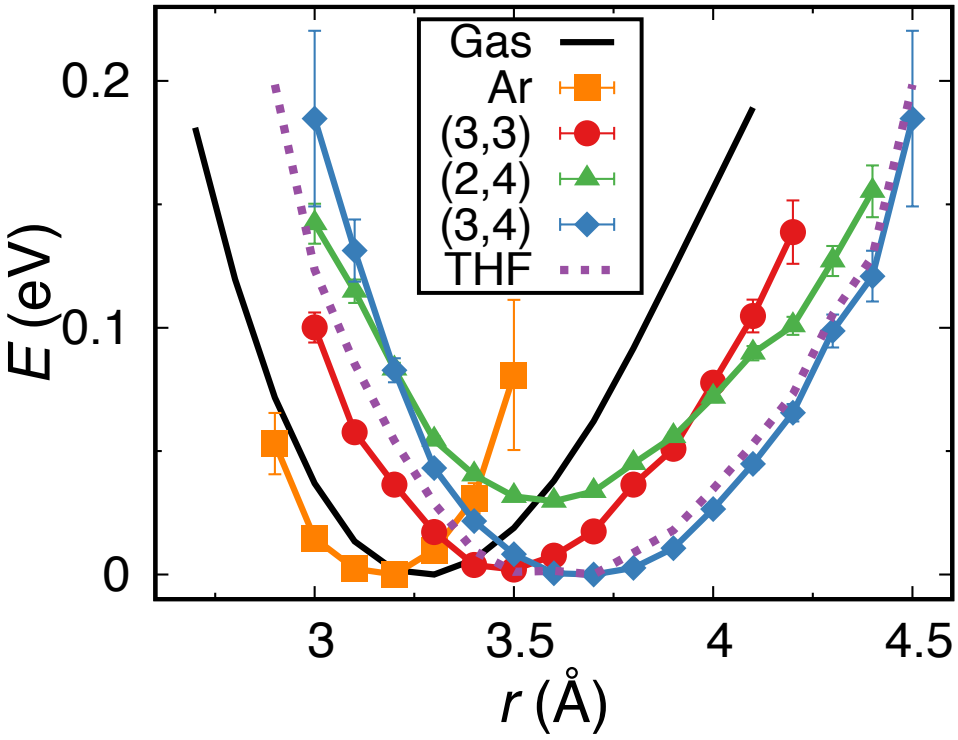

Figure 2.4: Different potentials of mean force for the Na_2 molecule in various environments, including with different local solvent coordination in liquid THF. The gas-phase potential energy surface for Na_2 calculated with our MQC model (as described in Glover *et al.*[46]) is plotted in black with the minimum set to zero for comparison with the condensed-phase PMFs. The PMFs for each Na_2 coordination state in liquid THF are plotted with minima set to the coordination state energies from Fig. 2.3 to illustrate the relative probabilities. The overall PMF in liquid THF (purple dotted line) is not smooth, most notably with wiggles present in the curve bottom, where statistics ought to be high enough to preclude defects, whereas the PMFs of the individual coordination states are quite smooth, highlighting the necessity of thinking of the Na_2/THF system as three discrete molecules in equilibrium rather than an overall average. Error bars represent 95% confidence intervals.

distance; these are the potential energy surfaces that govern how the two Na atoms move in each of the respective environments. The figure shows clearly that the overall PMF for the sodium dimer in liquid THF is not smooth; there are wiggles at the bottom of the well that result from the presence of the different (and distinct) solvent coordination states. Thus, it makes much more sense to think of the Na_2/THF system as three different molecules in equilibrium: as summarized in Table 2.1, each THF-coordination state has a different Na–Na bond length (r_e, the position of the minimum in the PMF) and a different vibrational frequency (ω_e, the curvature of the PMF around the minimum), verifying that each is a unique chemical species.

Figure 2.5a shows the vibrational motions of Na_2 in the different environments, calculated as power spectra (Fourier transforms of the bond velocity autocorrelation function, $C(t) = \langle v(t) \cdot v(0) \rangle$; see the SI for details). The peak in the power spectrum in liquid Ar is blue shifted from that in the gas phase because, on average, Pauli repulsion interactions from the first-shell Ar solvent molecules compress the bonding electrons and shorten the overall bond length, thus raising the Na_2 vibrational frequency.[46] In liquid THF, however, the main Na–Na vibrational peak is lowered in frequency; the purple dotted curve shows that on average the Na atom motions in THF occur at a frequency more than 10 cm^{-1} below that predicted by the curvature of the average PMF for the dimer in THF (Table 2.1). However, the frequencies of the lowered Na–Na vibrational motions in THF match nearly perfectly with those predicted by the curvatures of the individual coordination-state PMFs in (*cf.* Fig. 2.4 and Table 2.1). Figure 2.5a also shows the presence of a sharper blue-shifted-peak near $\sim$200 cm^{-1} that is nearly double that of the gas-phase vibrational frequency. This higher-frequency motion corresponds to the stretching of the Na^+–THF oxygen dative bonds, as verified by tracking the bond velocities of the dative bonds during intervals where the dimer remained in a single coordination state. Like the Na–Na vibrational peak, the dative bond stretching peak shifts with coordination number, with less-coordinated Na^+ cores holding the datively-bound THFs more tightly, resulting in a slightly higher stretching frequency. This

also explains the splitting of the high-frequency peak for the asymmetrically-coordinated states, which have two types of solvent dative bonding interactions in a single molecule. The net result is that the Na atoms move at multiple new frequencies when the dimer is placed in liquid THF, and these frequencies can only be clearly resolved by considering the individual coordination states.

In liquid Ar, we showed previously that solvent collisions push the bonding electrons in Na_2 off-center, creating randomly-oriented instantaneous dipole moments for the non-polar molecule in the non-polar solvent that produce an infrared absorption spectrum.[46] In liquid THF, we see in Table 2.1 that the symmetrically-coordinated $Na(THF)_3$–$Na(THF)_3$ species behaves similarly to that in liquid Ar, although the average value of the instantaneous dipole is somewhat larger in THF. But for the asymmetrically coordinated chelation states, the average net displacement of the Na_2 bonding electronic density from the more-coordinated to the less-coordinated Na^+ core gives rise to a permanent dipole. Thus, even though gas-phase Na_2 has no dipole and is completely IR inactive, in solution the molecule should be at least weakly IR active, and should have a stronger IR absorption for chemical species such as $Na(THF)_2$–$Na(THF)_4$ and $Na(THF)_3$–$Na(THF)_4$ that have permanent dipole moments.

Figure 2.5b shows the calculated IR spectra (Fourier transform of the dipole autocorrelation function; see SI) of Na_2 in each of the various environments considered here. Each spectrum shows a large peak at low frequencies ($\sim$50 cm^{-1} in Ar and $\sim$20 cm^{-1} in THF), resulting from intermolecular rattling motions of the entire coordinated dimer species in the cage of surrounding solvent molecules, a motion that strongly modulates the molecular dipole moment.[28, 46] In THF, the IR spectrum of each coordination state also shows a peak at $\sim$200 cm^{-1}, the stretching frequency of the Na^+–THF oxygen site dative bonds; as the dative bonds become slightly shorter or longer, this pushes (or pulls) the bonding electron density away from (or toward) the Na–Na internuclear space, modulating the overall solute dipole moment. Furthermore, each of the chelated species in THF shows a shoulder in their IR spectrum at $\sim$60 cm^{-1}, which is the vibrational frequency of the fully-chelated Na atoms

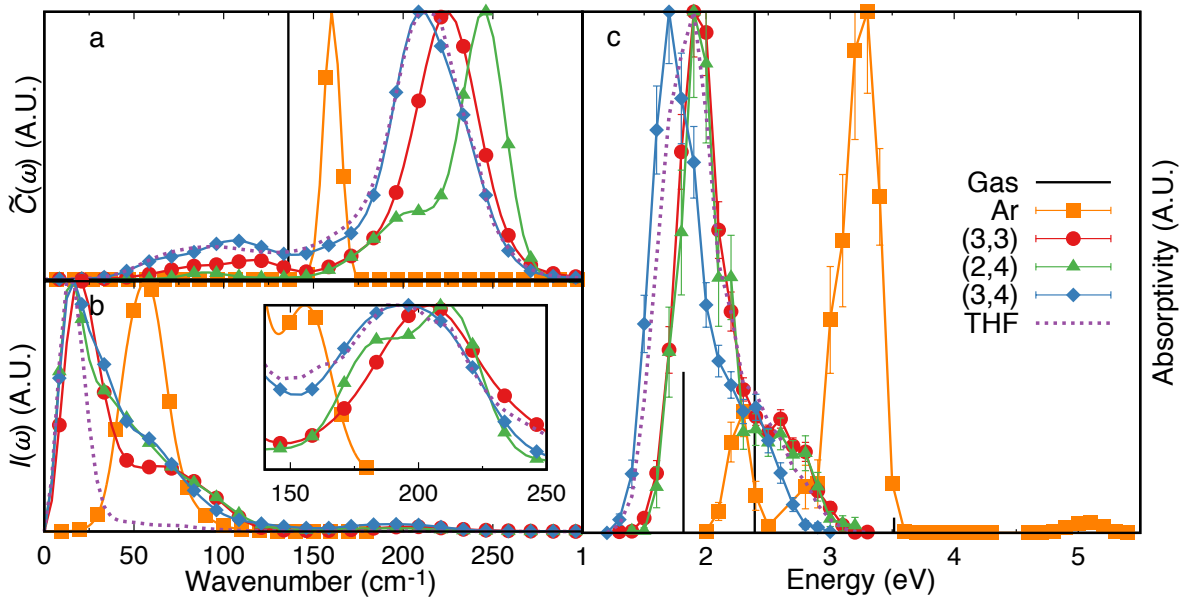

Figure 2.5: Different Na_2 coordination states are spectroscopically distinct. **a**, Vibrational spectra of Na_2 calculated from the Fourier transform of the bond velocity autocorrelation function. The gas phase vibrational frequency is shown as a black line at 136 cm^{-1}. The spectrum in liquid Ar (orange curve) is blue shifted relative to the gas phase, as expected from to the compression of the Na_2 bonding electrons due to Pauli repulsion interactions with the first-shell Ar solvent molecules. In liquid THF (purple dotted curve for overall and blue, green and red curves for individual coordination states), however, the main Na–Na vibrational peak is red-shifted due to elongation of the bond with a second, sharper peak near 200 cm^{-1} from the motions of the Na^+–THF oxygen dative bonds. **b**, Infrared spectra of Na_2 in different solution environments calculated from the Fourier transform of the dipole moment autocorrelation function; the molecule has no IR spectrum in the gas phase. Apart from the large peak at 50 cm^{-1} in Ar and 20 cm^{-1} in THF (intermolecular rattling motions), more subtle features of the dipole motion modulation are present at 60 cm^{-1} for THF coordination states (vibration of fully-chelated sodium atoms), 160 cm^{-1} for Na_2 in Ar (Na_2 vibration), and 200 cm^{-1} for Na_2 in THF (dative bond vibration). **c**, Calculated electronic absorption spectra for the Na_2 molecule in different environments. The gas phase absorbance lines are plotted as vertical black lines scaled to their relative intensities. Similar to the vibrational spectra (**a**), the Na_2 absorption spectrum is blue-shifted in liquid Ar but red-shifted in liquid THF. Error bars represent 95% confidence intervals.

(including their coordinated solvent molecules) moving against each other, also modulating the overall dipole moment. This shoulder does not appear when considering the overall IR spectrum for the dimer in THF (purple dotted curve), indicating that the modulation of the dipole of the sodium dimer in THF cannot be explained without isolating the behavior of the specific individual coordination states.

Not only do the different Na_2 solvent coordination states have different vibrational spectra, they also have different predicted electronic absorptivity. Figure 2.5c shows the calculated UV-Visible absorption spectra for Na_2-based species in different environments; details of how we calculated the spectra are given in the SI but are similar to those in our previous work.[41, 46, 101] In apolar liquid Ar, the electronic absorption spectrum resembles that in the gas phase, although it is somewhat blue shifted, as expected since the valence electrons in Ar are more compressed than in the gas phase. In liquid THF, however, the absorption spectra of the different coordination states are predicted to red shift relative to the gas phase due to the elongation of the Na_2 bond and the displacement of electron density away from the Na^+ cores. The magnitude of the red shift increases with increasing coordination. The $Na(THF)_2$–$Na(THF)_4$ and $Na(THF)_3$–$Na(THF)_3$ states, each with a total coordination number of 6, shift ∼0.4 eV to the red of the gas phase maximum while the $Na(THF)_3$–$Na(THF)_4$ state, with a total coordination number of 7, shifts nearly twice as much. It is worth noting that if one were to ignore the existence of the different coordination states and examine only the average absorption spectrum of Na_2 in THF (purple dotted curve), the main peak would have an unusually broad width, and the presence of the secondary peak due to transitions to higher excited states would be lost, potentially leading to a mis-assignment of the observed spectral features.

Finally, we note that even though all these predictions of solvent control over molecular identity have been made on the basis of computer simulations, it should be possible to verify all of these predictions experimentally. Solvated Na_2 molecules have already been prepared in low-temperature rare gas matrices by co-evaporating Na metal with the solvent, and the

Raman spectrum of the solvated dimers has been measured.[72–78] It should be feasible to create Na_2 in other good evaporatable glass-forming liquids, such as 2-methyl-THF,[79] which ought to show all the same distinct IR and UV-Visible spectroscopic features predicted here for unsubstituted THF. Moreover, if there is some way to prepare Na_2 transiently at room temperature, our simulations suggest that the different chelated species interconvert on a time scale slow compared to the vibration time scale, so that ultrafast spectroscopy techniques should be able to test our predictions. Furthermore, we have performed preliminary simulations of the sodium dimer cation (Na_2^+) in liquid THF, and found that there are similar coordination states, although with slightly higher average coordination numbers. This opens the possibility for preparing mass-selected gas-phase Na_2^+/THF clusters, whose spectroscopy and properties could also be probed directly. Whether prepared as neutral dimers or molecular cations, it should be possible to experimentally confirm the presence of the different solvent-coordinated chemical species in equilibrium by vibrational or electronic spectroscopy.

2.4 Conclusions

In summary, MQC MD simulations of Na_2 in liquid THF reveal that the solvent plays an intimate role in the bond dynamics, electronic properties and indeed, chemical identity of simple solutes. Even though there are only relatively weak local specific interactions between Na atoms and liquid THF, we find that several unique coordination states of Na_2 are stable under equilibrium conditions: $Na(THF)_2$–$Na(THF)_4$, $Na(THF)_3$–$Na(THF)_3$, and $Na(THF)_3$–$Na(THF)_4$. There is no simple way to explain the average properties of Na_2 in THF except by thinking of each coordination state as a different molecule that undergoes a series of equilibrium chemical reactions, crossing free energy barriers of $\sim 8\ k_B T$ to convert from one stable coordination state to another. Indeed, the rates at which the different coordination states interconvert are consistent with simple transition state theory, adding

credence to their identity as separate chemical species. Moreover, each coordination species has a unique bond length, distinct bond dynamics, and different IR and UV-Visible absorption spectra, providing an experimental handle to test the idea that interactions with the solvent can induce changes in solute chemical identity. We close by reiterating that the local specific interactions responsible for this behavior, the formation of Na–THF oxygen dative bonds, are no stronger than the hydrogen bonds that help form the secondary structure of peptides and proteins or lead to clathrate formation in aqueous solutions. This suggests that the concept of solvent participation in chemical identity, with chemical reactions converting between different local coordination states, is likely ubiquitous throughout solution chemistry and biochemistry.

2.5 Methods

2.5.1 Overview of Simulation Details

Our MQC MD simulations consisted of classical solvent molecules, two classical Na^+ cations, and two fully quantum mechanical electrons. Interactions between the classical particles and the quantum mechanical electrons were accounted for using Phillips Kleinmen (PK) pseudopotentials,[88] modified with polarization potentials to correct for the frozen-core approximation implicit in PK formalism.[27, 33, 89] An overview of the classical interactions and pseudopotentials used is given in the SI as well as in our previous work.[27, 39, 41, 86] Simulations in liquid Ar involved 1600 solvent molecules in a cubic simulation cell of side length 43.8 Å, while those in liquid THF used 254 solvent molecules contained in a cubic simulation cell with side length 32.5 Å. The simulation cell lengths were chosen to match the experimental solvent densities at the simulation temperature (1.26 g/mL at 120 K for the Ar simulations and 0.89 g/mL at 298 K for the THF simulations). Periodic boundary conditions were implemented with minimum image convention[87] and all interactions were tapered smoothly to zero at 16 Å over a 2 Å range using a center of mass-based switching

function due to Steinhauser.[105]

We used our two-electron Fourier grid (2EFG) electronic structure algorithm[85] to solve the time-independent Schrodinger equation for the electrons' wave function at every time step (5 fs in Ar and 4 fs in THF). The valence electrons' eigenstates were expanded on a six-dimensional real-space grid. For Ar, we used a basis of 16×16×16 over a 14 Å^3 box, and for THF, we used a basis of 20×20×20 over a 17.5 Å^3 box, for a consistent grid spacing of 0.875 Å. These dimensions were chosen to keep the basis set as small as possible for each system while still capturing both the spatial extent and the solvent-induced distortions of electronic wave function. We centered the grid in the middle of the simulation cell and shifted all classical particles relative to the grid every 500 fs to avoid leakage of the wave function at the edges of the grid basis and so that the wave function was always located roughly in the center of the simulation cell. The classical particles were shifted an integer number of grid spaces to avoid discontinuities in the quantum energy that would prevent total energy of simulation from being conserved. The Ar simulation was equilibrated at 120 K (within the liquid region of the phase diagram)[95, 106] and the THF simulation at 298 K before 500-ps production trajectories were run.

2.5.2 Definition of Coordination Coordinate

To develop the coordination coordinate used to construct our coordination PMF, we first defined a continuous coordination number variable, $n_{\mathrm{Na^+}}$, as

$$n_{\mathrm{Na^+}} = \sum_i S\left(|r_{\mathrm{O},i} - r_{\mathrm{Na^+}}|\right), \tag{2.1}$$

where i runs over every THF oxygen site and $r_{\mathrm{Na^+}}$ and $r_{\mathrm{O},i}$ are the positions of the $\mathrm{Na^+}$ core and the i^{th} oxygen site respectively. The Fermi function $S(r)$ is defined as $S(r) = \frac{1}{\exp[\kappa(r-r_c)]+1}$, where r_c is a cutoff radius that defines when a solvent molecule is coordinated to the $\mathrm{Na^+}$ and κ^{-1} is the width of the transition region where the Fermi function switches

from 1 to 0 around r_c. For this work, we selected $\kappa^{-1} = 0.2$ Å and $r_c = 3.50$ Å, corresponding to the first minimum of the Na^+-THF oxygen site $g(r)$. These values are similar to those used by our group for studies of sodium neutral in THF[86] but have been re-optimized for the Na_2 molecule. Equation 1 was evaluated for each Na^+ core to generate the plots in Figure 2.3.

2.5.3 Potential of Mean Force Calculations

All potential of mean force plots for coordination number were calculated based on the negative natural logarithm of the probabilities of each state. First, we binned up the number of production run configurations in each state, assuming Poisson statistics such that the error for each bin count was simply its square root. Next, we normalized the histogram results by dividing by the maximum bin count. Finally, we generated the PMF free energy values, A, in $k_B T$ by taking the negative natural logarithm of the normalized bin counts. The normalization ensured that the most probable state is plotted at 0 $k_B T$. The free energy error was propagated according to $\sigma = \pm \frac{\sqrt{\text{bincount}}/\text{maxbincount}}{\text{bincount}/\text{maxbincount}}$. Because the proportion of configurations in each Na_2 coordination state accessed at equilibrium in THF are of similar amounts, we did not need to use umbrella sampling to improve statistics (the relative population values for the $Na(THF)_3$-$Na(THF)_3$, $Na(THF)_2$-$Na(THF)_4$, and $Na(THF)_3$-$Na(THF)_4$ were 50:17:54 respectively). We note that in our previous work on the related sodium cation:solvated electron contact pairs, direct sampling of the different coordination states was in excellent agreement with those determined by importance sampling.[101]

2.6 Supplemental Information

2.6.1 Mixed Quantum/Classical Model

In addition to classical solvent molecules, our mixed quantum/classical (MQC) molecular dynamics (MD) simulations, performed in the microcanonical ensemble, consisted two classical

Na^+ cations and two fully quantum mechanical electrons. For simulations in liquid Ar, we used a simulation cell of side length 43.8 Å and 1600 solvent molecules, while our simulations in liquid THF used a simulation cell of side length 32.5 Å and 254 solvent molecules. The choice of cell size reproduced appropriate solvent densities at the simulation temperatures (1.26 g/mL at 120 ± 2 K for Ar simulations and 0.89 g/mL at 298 ± 6 K for THF simulations). The THF molecules were treated as rigid, planar five-membered rings following the work of Chandrasekar and Jorgensen.[103] The rigid planarity of the molecules was enforced using the RATTLE algorithm, as in our previous MQC MD work in this solvent.[86] Periodic boundary conditions were implemented with minimum image convention[87] and all interactions were tapered smoothly to zero at 16 Å over a 2 Å range with a center of mass-based switching function due to Steinhauser.[105]

All interactions were taken to be pair-wise additive. Thus, the full Hamiltonian of the system is $\hat{H} = H^{\mathrm{cl}} + \hat{H}^{\mathrm{qm}}$. In atomic units, the classical portion of the Hamiltonian is given by

$$H^{\mathrm{cl}} = \frac{1}{2} m_{\mathrm{Na^+}} \sum_{i=1}^{2} v_{\mathrm{Na^+}_i}^2 + \frac{1}{2} m_{\mathrm{solv}} \sum_{i=1}^{n_{\mathrm{solv}}} v_{\mathrm{solv}_i}^2 + U^{\mathrm{Na^+-Na^+}}(|\boldsymbol{R}_{\mathrm{Na^+}_1} - \boldsymbol{R}_{\mathrm{Na^+}_2}|) + \sum_{i=1}^{n_{\mathrm{solv}}} \sum_{j>i}^{n_{\mathrm{solv}}} U^{\mathrm{solv-solv}}(|\boldsymbol{R}_{\mathrm{solv}_i} - \boldsymbol{R}_{\mathrm{solv}_j}|) + \sum_{i=1}^{2} \sum_{j=1}^{n_{\mathrm{solv}}} U^{\mathrm{Na^+-solv}}(|\boldsymbol{R}_{\mathrm{Na^+}_i} - \boldsymbol{R}_{\mathrm{solv}_j}|) \quad (2.2)$$

where v_{χ_i} is the velocity of the i^{th} sodium ($\chi = \mathrm{Na^+}$) or solvent molecule ($\chi = \mathrm{solv}$) at position $\boldsymbol{R}_{\chi_i}$ and mass m_χ and $U^{\chi-\gamma}$ is a classical potential between atom types χ and γ ($\chi, \gamma = \mathrm{Na^+}$ or solv). The quantum Hamiltonian is given by

$$\hat{H}^{\mathrm{qm}} = \sum_{i=1}^{2} \frac{\hat{\boldsymbol{p}}_i^2}{2} + \sum_{i=1}^{2} \sum_{j=1}^{2} V^{\mathrm{Na^+}}(|\boldsymbol{R}_{\mathrm{Na^+}_j} - \hat{\boldsymbol{r}}_i|) + \sum_{i=1}^{2} \sum_{j=1}^{n_{\mathrm{solv}}} V^{\mathrm{solv}}(|\boldsymbol{R}_{\mathrm{solv}_j} - \hat{\boldsymbol{r}}_i|) + \hat{r}_{12}^{-1} \quad (2.3)$$

where $\hat{\boldsymbol{p}}_i$ and $\hat{\boldsymbol{r}}_i$ are the momentum and position operators for electron i, respectively, V^χ is the pseudopotential representing the interaction between an electron and atom type χ, and

$\hat{r}_{12}^{-1}$ is the Coulomb operator for the two valence electrons.

We modeled the classical interactions between the two Na^+ cations through a point-charge Coulomb potential, $U^{Na^+-Na^+}(R) = 1/R$, since the short-range repulsion between the cores is negligible around the internuclear separation of Na_2. The Na^+-Ar interaction was taken from a fit to the *ab initio* calculations of Ahmadi, Almlöf, and Røeggen[107]:

$$U^{Na^+-Ar}(R) = \frac{a_1 \exp(-a_2 R)}{R} - \frac{2}{1 + a_1 \exp(a_3/R)} \left(\frac{C_6}{R^6} + \frac{C_8}{R^8} \right) \tag{2.4}$$

where $a_1 = 242.32$ Hartree, $a_2 = 1.67$ bohr^{-1}, $a_3 = 5.6$ bohr, $C_6 = 255$ bohr^5, and $C_8 = 4410$ bohr^7. Following Gervais et al,[92] we have subtracted the charge-dipole term, which goes as $-0.5\alpha_{Ar}/R^4$, where α_{Ar} is the dipole polarizability of Ar, since Ar is interacting with a net neutral Na_2 species. All other classical interactions were modeled with Lennard-Jones potentials:[87]

$$u_{ij}(r_{ij}) = \frac{1}{4\pi\epsilon_0} \frac{q_i q_j}{r_{ij}} + 4\epsilon_{ij} \left[\left(\frac{\sigma_{ij}}{r_{ij}} \right)^{12} - \left(\frac{\sigma_{ij}}{r_{ij}} \right)^{6} \right] \tag{2.5}$$

where r_{ij} is the distance between the i^{th} and j^{th} solvent/Na^+ site, q_i is the charge on the i^{th} site, ϵ_{ij} is the potential well depth, and σ_{ij} is the finite distance at which the inter-particle potential is zero. The Lennard-Jones parameters used in this study are listed in Table 2.2. The standard Lorentz-Berthelot combining rules were used to calculate the solute-solvent site and solvent site-solvent site interactions in THF.[87]

	σ (Å)	ϵ (kJ/mol)	q (e)
Argon	3.405	0.996	0.0
THF-oxygen	3.0	0.71	–0.5
THF-α-methyl	3.8	0.49	+0.25
THF-β-methyl	3.905	0.49	0.0
Na^+	1.67	22.07	+1.0

Table 2.2: Lennard-Jones and coulomb potential parameters for Na_2, Ar, and THF.

Interactions between the classical particles and the quantum mechanical electrons were accounted for using Phillips Kleinman (PK) pseudopotentials[88] modified with polarization

potentials to correct for the frozen-core approximation implicit in PK formalism.[27, 33, 89] For the electron-argon interaction, $V^{e^- - \mathrm{Ar}}$ we used a modified version of the pseudopotential developed by Gervais *et al*,[92] described in detail in our previous work.[46] For $V^{e^- - \mathrm{Na}^+}$ and $V^{e^- - \mathrm{THF}}$, we used rigorously-derived psedopotentials previously developed by our group, the details of which can be found in Refs. 39 and 27, respectively. The final pseudopotential fits are presented here Tables 2.3 and 2.4.

i	c_i (a.u.)	α_i (a.u.)
1	-0.103 055 903	0.189 844 564
2	0.436 627 83	0.069 933
3	0.541 733 81	0.032 893
4	0.134 538 22	0.016 122

Table 2.3: Parameters used in the construction of the sodium-electron pseudopotential for use in Na_2 simulations, $\phi(r) = \sum_{i=1}^{4} c_i e^{-\alpha_i r^2}$. Further details of the sodium-electron pseudopotential can be found in Ref 39.

2.6.2 Two-Electron Fourier Grid Method for Solving for the Valence Electrons' Wave function

The details of our two-electron Fourier grid (2EFG) method for solving for the valence electrons' wave function are described extensively in our previous work,[85] but are briefly outlined here for completeness. In our 2EFG method, the valence electrons' wave function is expanded on a six-dimensional real-space grid according to

$$|\Psi\rangle = \sum_{i=1}^{N^3} \sum_{j=1}^{N^3} \Psi_{i,j} \, |\boldsymbol{r}_i \boldsymbol{r}_j\rangle \tag{2.6}$$

where $|\boldsymbol{r}_i \boldsymbol{r}_j\rangle$ is the basis point of the six-dimensional regular, real-space grid at 6-dimensional position $(\boldsymbol{r}_i, \boldsymbol{r}_j)$, N is the number of grid points in each dimension, and $\Psi_{i,j}$ are the real-valued expansion coefficients in this basis. We enforce spin-singlet symmetry in the expansion coefficients by restricting $\Psi_{i,j} = \Psi_{j,i}$. Constructing the basis in this manner is advantageous

$$U_{fit}(\mathbf{r}) = \left\{ \begin{array}{ccccccccccc} & U_o & + & U_{c\alpha 1} & + & U_{c\alpha 2} & + & U_{c\beta 1} & + & U_{c\beta 2} \\ + & U_{h\alpha 1} & + & U_{h\alpha 2} & + & U_{h\alpha 3} & + & U_{h\alpha 4} & + & U_{h\beta 1} \\ + & U_{h\beta 2} & + & U_{h\beta 3} & + & U_{h\beta 4} & + & U_{ao} & + & U_{ao} \\ + & U_{ac} & + & U_{ac} & + & U_{aa} & + & U_{af} & & \end{array} \right.$$

$$U_o(\mathbf{r}-\mathbf{r_o}) = \begin{array}{cl} & \left(o_1(x-x_o)^4 + o_2(y-y_o)^4 + o_3(z-z_o)^4 - o_4\right) \\ \times & exp\left(-\left[o_5(x-x_o)^2 + o_6((y-y_o)^2 + (z-z_o)^2)\right]\right) \\ + & o_7 \frac{e^{-o_8(\mathbf{r}-\mathbf{r_o})^2}}{|\mathbf{r}-\mathbf{r_o}|} \end{array}$$

$o_1 = 2.8926$	$o_2 = 0.1017$	$o_3 = 1.9379$	$o_4 = 4.1887$
$o_5 = 1.0552$	$o_6 = 1.2853$	$o_7 = 9.4147$	$o_8 = 23.4135$

$$U_{c\alpha}(\mathbf{r}-\mathbf{r_{c\alpha}}) = \begin{array}{cl} & c_1^\alpha\left[(y-y_{c\alpha}) + c_2^\alpha(z-z_{c\alpha})\right] \\ \times & exp\left(-\left[c_3^\alpha(x-x_{c\alpha})^2 + c_4^\alpha((y-y_{c\alpha})^2 + (z-z_{c\alpha})^2)\right]\right) \\ - & c_5^\alpha \frac{1}{|\mathbf{r}-\mathbf{r}_{c\alpha}|} + c_6^\alpha exp\left[-c_7^\alpha(\mathbf{r}-\mathbf{r}_{c_\alpha})^4\right] \end{array}$$

$c_1^\alpha = 62.6462$	$c_2^\alpha = 0.1426$	$c_3^\alpha = 7.9044$	$c_4^\alpha = 7.9516$
$c_5^\alpha = 0.3147$	$c_6^\alpha = 6.3821$	$c_7^\alpha = 34.2773$	

$$U_{c\beta}(\mathbf{r}-\mathbf{r_{c\beta}}) = \begin{array}{cl} & c_1^\beta\left[(y-y_{c\beta}) + c_2^\beta(z-z_{c\beta})\right] \\ \times & exp\left[-\left(c_3^\beta(x-x_{c\beta})^2 + c_4^\beta((y-y_{c\beta})^2 + (z-z_{c\beta})^2)\right)\right] \\ - & c_5^\beta \frac{1}{|\mathbf{r}-\mathbf{r}_{c\beta}|} + c_6^\beta e^{-c_7^\beta(\mathbf{r}-\mathbf{r}_{c\beta})^4} \end{array}$$

$c_1^\beta = 13.3107$	$c_2^\beta = 1.3455$	$c_3^\beta = 5.3624$	$c_4^\beta = 4.4085$
$c_5^\beta = 0.3033$	$c_6^\beta = 1.4495$	$c_7^\beta = 7.8897$	

$$U_{h\alpha}(\mathbf{r}-\mathbf{r_{h\alpha}}) = -h_1^\alpha \frac{exp\left[-h_2^\alpha(\mathbf{r}-\mathbf{r}_{h\alpha})^2\right]}{|\mathbf{r}-\mathbf{r}_{h\alpha}|} + h_3^\alpha exp\left[-h_4^\alpha(\mathbf{r}-\mathbf{r}_{h\alpha})^2\right]$$

$h_1^\alpha = 0.8357$	$h_2^\alpha = 0.8769$	$h_3^\alpha = 0.2657$	$h_4^\alpha = 0.0852$

$$U_{h\beta}(\mathbf{r}-\mathbf{r_{h\beta}}) = -h_1^\beta \frac{exp\left[-h_2^\beta(\mathbf{r}-\mathbf{r}_{h\beta})^2\right]}{|\mathbf{r}-\mathbf{r}_{h\beta}|} + h_3^\beta exp\left[-h_4^\beta(\mathbf{r}-\mathbf{r}_{h\beta})^2\right]$$

$h_1^\beta = 0.7861$	$h_2^\beta = 0.9584$	$h_3^\beta = 0.1362$	$h_4^\beta = 0.0359$

$$U_{ao}(\mathbf{r}-\mathbf{r_{ao}}) = a_1^o exp\left[-\left(a_2^o(x-x_{ao})^2 + a_3^o(y-y_{ao})^2 + a_4^o(z-z_{ao})^2\right)\right]$$

$a_1^o = 2.7673$	$a_2^o = 1.0552$	$a_3^o = 0.5211$	$a_4^o = 0.7436$

$$U_{ac}(\mathbf{r}-\mathbf{r_{ac}}) = a_1^c exp\left[-\left(a_2^c(x-x_{ac})^2 + a_3^c((y-y_{ac})^2 + (z-z_{ac})^2)\right)\right]$$

$a_1^c = 0.9996$	$a_2^c = 0.6810$	$a_3^c = 0.3058$	

$$U_{aa}(\mathbf{r}-\mathbf{r_{aa}}) = \begin{array}{cl} & a_1^a exp\left[-\left(a_2^a(x-x_{aa})^2 + a_3^a((y-y_{aa})^2 + (z-z_{aa})^2)\right)\right] \\ - & a_4^a exp\left[-\left(a_5^a(x-x_{aa})^2 + a_6^a((y-y_{aa})^2 + (z-z_{aa})^2)\right)\right] \end{array}$$

$a_1^a = 11.7043$	$a_2^a = 0.5978$	$a_3^a = 0.1703$	
$a_4^a = 10.7099$	$a_5^a = 0.5994$	$a_6^a = 0.1597$	

$$U_{af}(\mathbf{r}-\mathbf{r_{af}}) = a_1^f exp\left[-\left(a_2^f(x-x_{af})^2 + a_3^f(y-y_{af})^2 + a_4^f(z-z_{af})^2\right)\right]$$

$a_1^f = 0.4472$	$a_2^f = 0.0443$	$a_3^f = 0.0379$	$a_3^f = 0.2579$

Table 2.4: Functional form and parameters of the fit to the exact e^-–THF effective potential. The 47-parameter fit has functional contributions centered on 19 different sites. The functional and parameter notations are explained in Ref 27. For the parameters given here, the distances are in Bohr radii and the energies are in Hartrees.

because all of the various potential energy operators have a diagonal matrix representation, including the electron–electron Coulomb operator. Furthermore, transforming the real-space wave function to reciprocal-space through fast Fourier transforms also gives the kinetic energy operator a diagonal matrix representation, allowing for rapid construction of the quantum Hamiltonian operator matrix.

2.6.3 MQC Simulations of Na_2 in the Condensed Phase

For simulations in liquid Ar, we used a basis of 16×16×16 grid points distributed over a cubic box with 14 Å sides for the valence electrons, and for simulations in liquid THF, we used a basis of 20×20×20 grid points distributed over a cubic box with 17.5 Å sides, giving a consistent grid spacing of 0.875 Å. These dimensions were chosen to keep the basis set as small as possible for each system while still capturing the spatial extent of electronic wave function, which was larger in THF than Ar. We centered the grid in the middle of the simulation cell and shifted all classical particles relative to the grid every 500 fs to avoid leakage of the wave function off the edges of the grid basis, so that the wave function was always located roughly in the center of the simulation cell. The classical particles were shifted an integer number of grid spaces to avoid discontinuities in the quantum energy that would prevent total energy of simulation from being conserved.[39] We used the velocity Verlet algorithm[87] to propagate the classical degrees of freedom ($\boldsymbol{v}_{\mathrm{Na^+}_i}$, $\boldsymbol{v}_{\mathrm{solv}_i}$, $\boldsymbol{R}_{\mathrm{Na^+}_i}$, and $\boldsymbol{R}_{\mathrm{solv}_i}$) of the Hamiltonian in Eqs. 1 and 2 in the microcanonical (N, V, E) ensemble. We determined the forces from the sum of the classical-classical and classical-quantum interactions described above. We used the implicit restart Lanczos method to iteratively solve the TISE for the ground state wavefunction at every time step (5 fs in Ar and 4 fs in THF).[108] The quantum forces on the classical particles were then found using the Hellman-Feynman theorem:

$$\boldsymbol{F}_i^Q = -\langle\Psi|\,\boldsymbol{\nabla}_{\boldsymbol{R}_i}\hat{H}\,|\Psi\rangle \tag{2.7}$$

where, $\boldsymbol{F}_i^Q$ is the quantum force on classical particle i at position $\boldsymbol{R}_i$. Because the wave function is expanded in a basis that does not functionally depend on the position of the classical particles, Eq. 6 is exact (in other words, there are no issues with Pulay forces from the basis functions changing with time).[85]

For Ar, the initial conditions were taken from a classical simulation of LJ Ar at 120 ±2 K, yielding a reduced density of 0.75 that falls within the liquid region of the LJ phase

diagram.[106] A solute cavity was carved out by two LJ spheres of an appropriate size to represent the Na_2 solute. The two classical Na^+ cations were then placed in this cavity and particles were shifted such that the Na^+ cations and solute cavity was in the center of the quantum grid. We propagated the MQC system for an equilibration period of 50 ps during which the classical particle velocities were occasionally rescaled to adjust the average temperature to 120 K before a 500-ps production run without velocity rescaling. For THF, we first removed a solvent molecule from an equilibrated snapshot of our previous work with Na^- in THF to make room for the second Na^+ core. We then propagated the MQC system for several hundred picoseconds with velocity rescaling to adjust the average temperature to 298 K before the 500-ps production run.

2.6.4 Coordination Number Interconversion

We extracted interconversion times between coordination states from our THF simulation trajectory by binning up the times the Na_2 molecule spent in each coordination state before converting to another. From this analysis, we determined conversion times of 32 ± 10 ps and 37 ± 19 ps for the $Na(THF)_3$–$Na(THF)_3$ → $Na(THF)_3$–$Na(THF)_4$ and $Na(THF)_3$–$Na(THF)_4$ → $Na(THF)_3$–$Na(THF)_3$ transitions and 16 ± 7 ps and 38 ± 18 ps for the $Na(THF)_2$–$Na(THF)_4$ → $Na(THF)_3$–$Na(THF)_4$ and $Na(THF)_3$–$Na(THF)_4$ → $Na(THF)_2$–$Na(THF)_4$ chemical reactions.

To further support the concept that these conversions occur as chemical reactions, we performed an analysis of our data using transition state theory, similar to the method described in our previous work,[101] briefly outlined here. According to transition state theory, inverse rates, τ, can be predicted according to $\tau = \tau_0 \exp\left(\frac{\Delta A^\ddagger}{k_B T}\right)$, where $\Delta A^\ddagger$ is the free energy barrier height for the interconversion and τ_0 is an inverse attempt frequency. We took $\Delta A^\ddagger$ to be the barrier height between coordination states, extracted from Fig. 2.3. With τ_0 set to 0.05 ps, conversion times of 32 ps and 35 ps for the $Na(THF)_3$-$Na(THF)_3$ → $Na(THF)_3$-$Na(THF)_4$ and $Na(THF)_3$-$Na(THF)_4$ → $Na(THF)_3$-$Na(THF)_3$ transitions and 16 ps and

40 ps for the $Na(THF)_2$-$Na(THF)_4$ $\rightarrow$ $Na(THF)_3$-$Na(THF)_4$ and $Na(THF)_3$-$Na(THF)_4$ $\rightarrow$ $Na(THF)_2$-$Na(THF)_4$ chemical reactions. Presumably the free energy barriers to other coordination states are too high to enable access during equilibrium dynamics but could be explored using umbrella sampling.

2.6.5 Potential of Mean Force Calculations

All potential of mean force plots along the coordination number coordinate were calculated as the negative natural logarithm of the occurance probability of each state. First, we binned up the number of production run configurations in each state, assuming Poisson statistics such that the error was simply its square root of the number of counts in each bin. Next, we normalized the histogram results by dividing by the maximum bin count. Finally, we generated the PMF free energy values, A, in $k_B\,T$ by taking the negative natural logarithm of the normalized bin counts. The normalization ensured that the most probable state is plotted at 0 $k_B\,T$. The free energy error was propagated according to $\sigma = \pm\frac{\sqrt{\text{bincount}}/\text{maxbincount}}{\text{bincount}/\text{maxbincount}}$. Because the number of configurations in each Na_2 coordination state accessed at equilibrium in THF were similar, we did not need to use umbrella sampling to improve statistics (the relative population values for the $Na(THF)_3$-$Na(THF)_3$, $Na(THF)_2$-$Na(THF)_4$, and $Na(THF)_3$-$Na(THF)_4$ were 50:17:54 respectively). We also performed a similar analysis with bins along a coordinate consisting of the Na^+–Na^+ for each solvated configuration state.

The results of this analysis for the Na_2 coordination state and bond length are shown in Figures 2.3 (coordination state) and 2.4 (bond length). The free energy values for Figure 2.4 were converted to eV for better comparison between the results in liquid Ar and THF with the gas-phase potential energy surface. We also calculated PMFs for the dipole moment magnitudes, angles, and projections along the bond axis for each Na_2 condensed phase state to further reveal the differences between each of these unique coordination states, shows in Figs. 2.6–7 below.

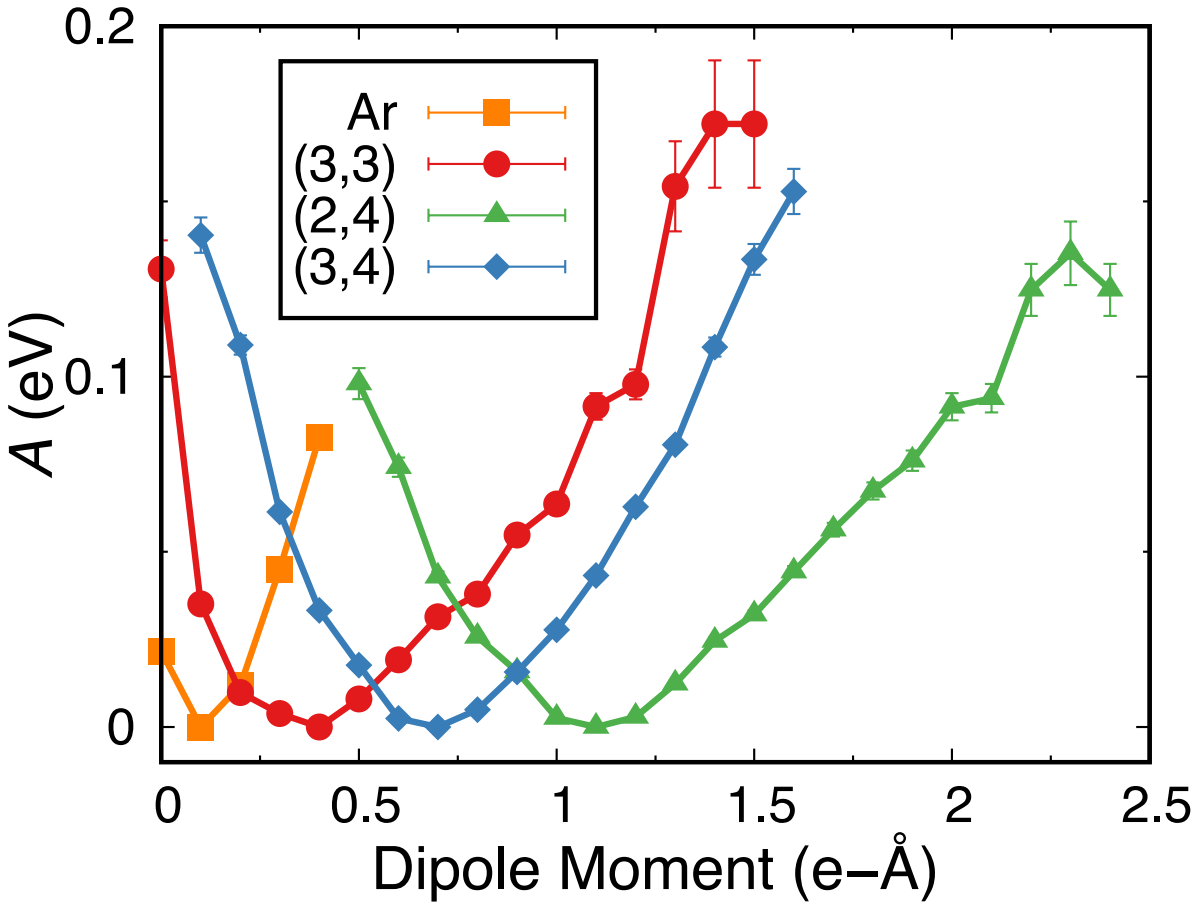

Figure 2.6: Potential of mean force for the magnitude of the dipole moment for Na_2 in various environments

Figure 2.6 shows that the asymmetrically-coordinated solvation states in THF have, on average, higher dipole moments than symmetrically coordinated states, with the $Na(THF)_2$–$Na(THF)_4$ state (green curve) producing the largest average dipole moment of 1.1 *e*-Å. However, even the symmetrically coordinated $Na(THF)_3$–$Na(THF)_3$ state (red curve) has significant instantaneous dipole moments, on average around 0.4 e-Å (which is significantly larger than that seen in liquid Ar). And even though the average dipole values induced in Na_2 in liquid Ar are small compared to those in liquid THF, the dipole moment magnitudes in liquid Ar are still significant compared to the gas phase.[46]

Figure 2.7 shows calculated PMFs of the angle the dipole moment makes with the Na_2 bond axis, revealing that in liquid Ar, the dipole moments are truly randomly oriented, with almost equal probability for the dipole to face in any direction. In liquid THF, however, we

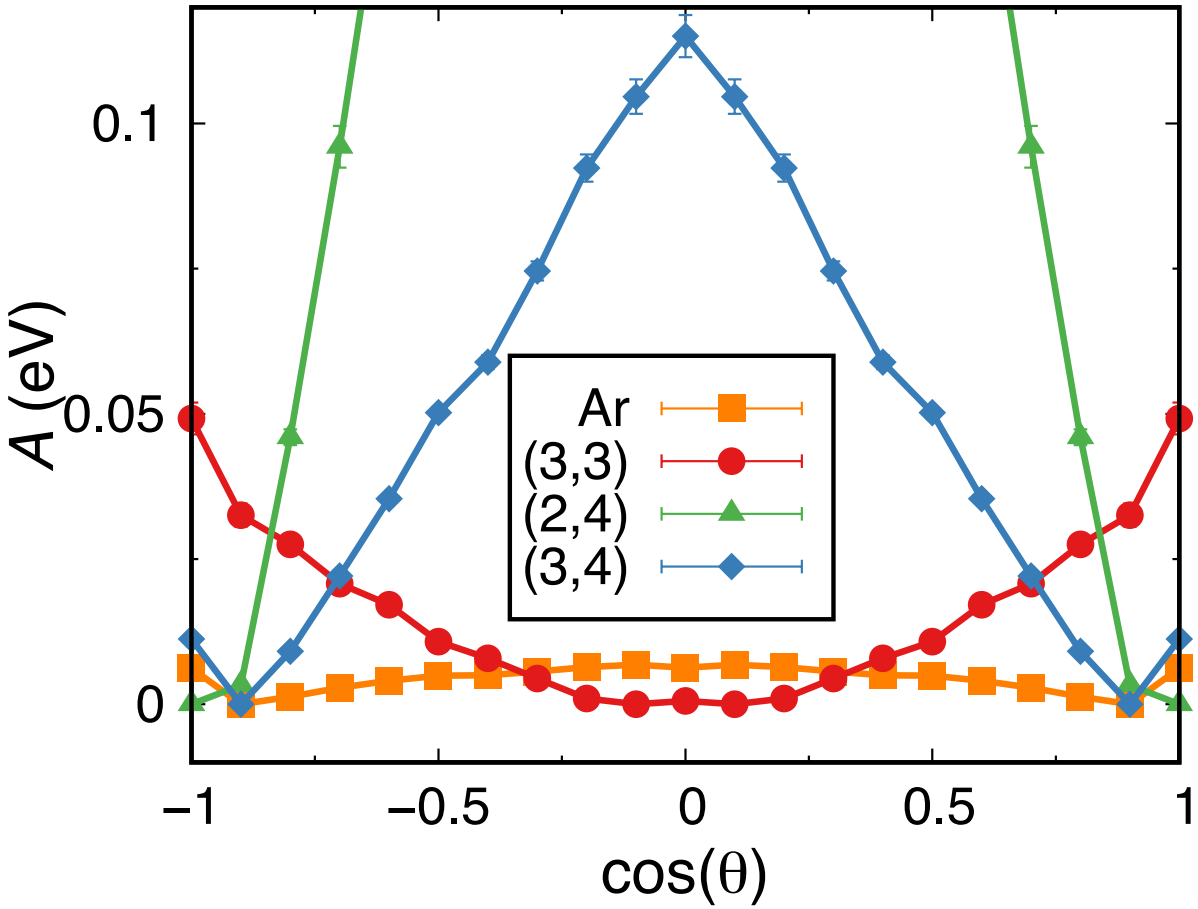

Figure 2.7: Potential of mean force for the angle between the dipole moment vector and the bond axis for Na_2 in various environments. A value of $\cos(\theta) = 0$ means the dipole moment is oriented perpendicular to the bond axis while a value of ± 1 means the dipole moment is oriented along the bond axis.

see two vastly different scenarios. Asymmetrically-coordinated solvation states have dipole moments that prefer to point nearly directly along the bond axis. Symmetrically-coordinated solvation states, on the other hand, prefer to point nearly perpendicular to the bond axis, likely because the presence of equal numbers of coordinating solvent molecules on each Na atom make charge fluctuations along the bond axis less likely than those off-axis.

Perhaps most tellingly, Figure 2.8 shows PMFs of the dipole moment projected along the bond axis, which reveal that asymmetrically coordinated Na_2 in THF have permanent dipole moments along the bond axis while symmetrically coordinated states and Na_2 in Ar have no permanent dipole moment, instead simply picking up instantaneous dipole moments around

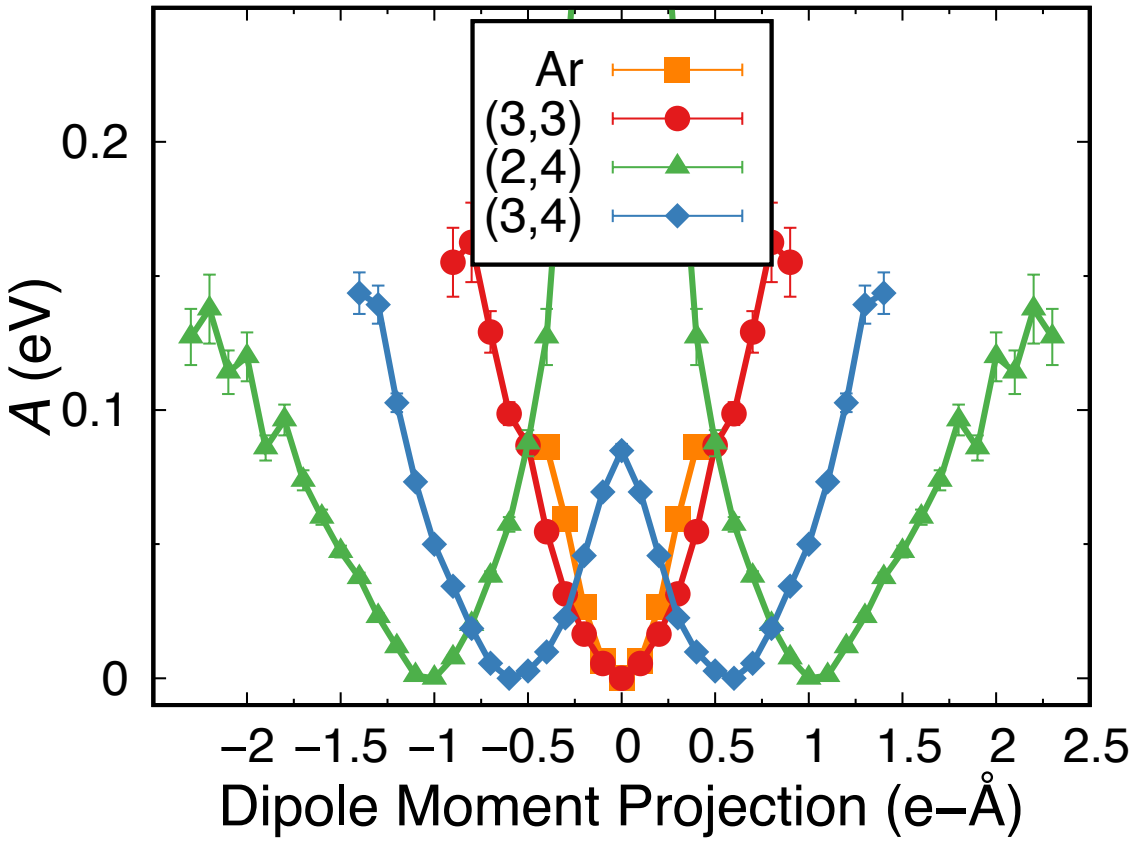

Figure 2.8: Potential of mean force for the projection of the dipole moment vector onto the bond axis for Na_2 in various environments

a zero average due to local solvent fluctuations.

2.6.6 Simulated Spectra Calculations

To produce calculated power and infrared (IR) spectra of Na_2, we first investigated the time dependence of the instantaneous bond velocity and dipole moment of Na_2 by calculating autocorrelation functions for each of these parameters, $C(t) = \langle X(t) \cdot X(0) \rangle$, where $X(t)$ is the bond velocity/dipole moment at time t. Since the Na_2 molecule interconverts between multiple stable coordination states in liquid THF, we selected segments from the equilibrium trajectory where the Na_2 remained in one coordination state for several picoseconds and then averaged the autocorrelation functions for each unique coordination state to improve statistics. The corresponding power/IR spectra were determined as the Fourier transform of

$C(t)$. Further details of these calculations can be found in Glover *et al.*[46]

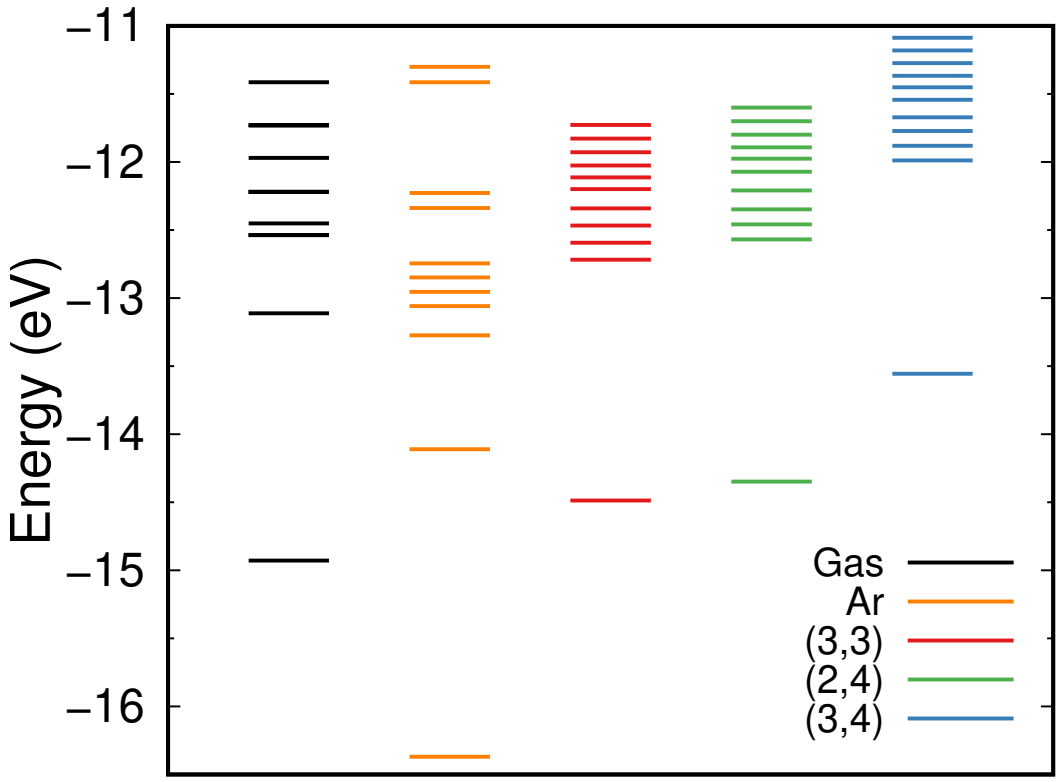

Figure 2.9: Energy eigenvalues for the ground state and first ten excited states of Na_2 in the gas phase and condensed phase environments.

Our 2EFG method was used to calculate the eigenstates for the ground state and first ten electronic excited states for Na_2 in the gas phase, in liquid Ar, and in each equilibrium coordination state in liquid THF. Comparing the eigenvalues in these different environments, Fig. 2.9 reveals the striking effects of the condensed phase on the electronic structure of Na_2. In Ar, the ground state is stabilized by almost 2 eV while the spacing between eigenstates is increased due to the compression of the Na_2 valence electrons by the cage of Ar atoms. The ground state of Na_2 in all THF environments is destabilized with an increasing destabilization associated with increased coordination. Interestingly, the most stable Na_2 coordination state in THF (that with the lowest free energy), $Na(THF)_3$–$Na(THF)_4$, is the most electronically destabilized of the equilibrium states. This indicates that the free energetic gain acquired

from the addition of one more coordinating THF (relative to $Na(THF)_3$–$Na(THF)_3$ and $Na(THF)_2$–$Na(THF)_4$) is sufficient to offset the electronic destabilization. Also of note is the fact that the $Na(THF)_3$–$Na(THF)_3$ and $Na(THF)_2$–$Na(THF)_4$ species have similar degrees of electronic destabilization and eigenvalue spacings. This explains why these two coordination states have very similar absorption spectra, as seen in Figure 2.5c.

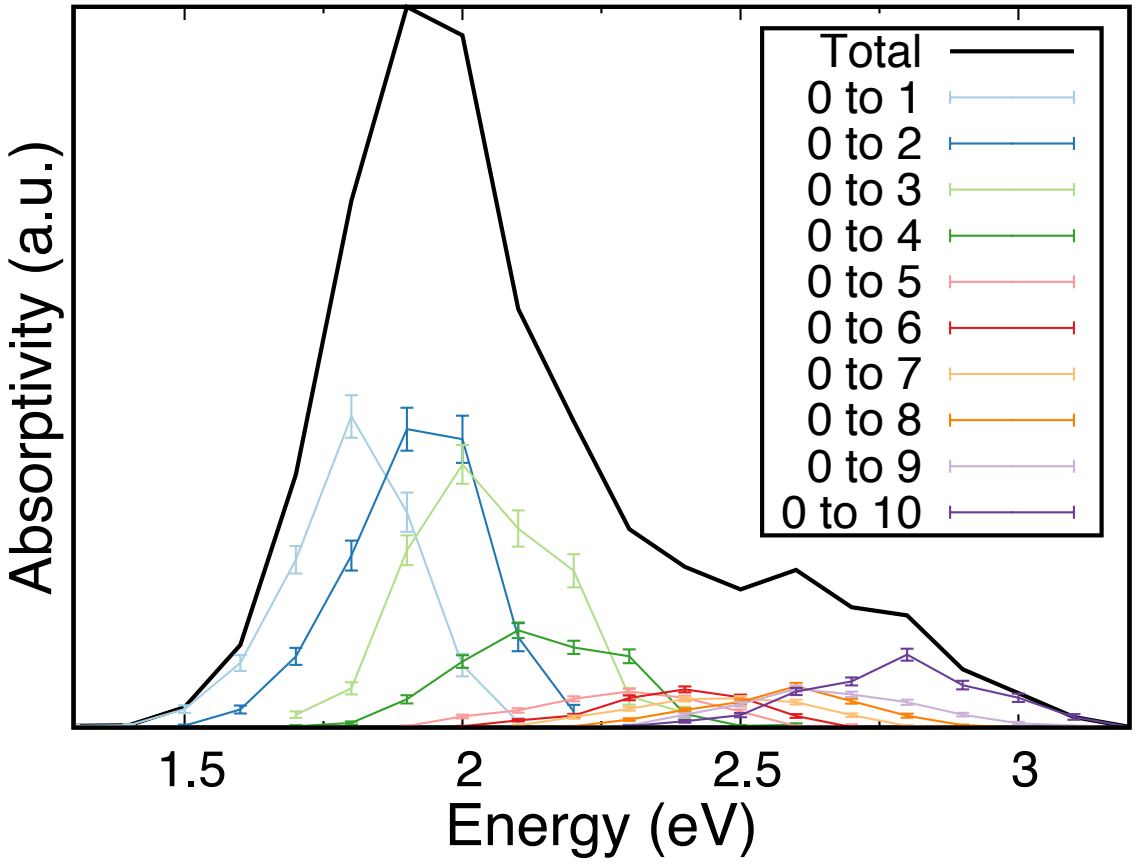

Figure 2.10: Absorbance spectrum of the $Na(THF)_3$-$Na(THF)_3$ coordination state showing the individual inhomogeneous contributions from the transitions from the ground state to each of the first ten excited states.

By determining the transition dipoles between the Na_2 valence electronic ground state and the first ten excited states, we calculated the absorption spectrum of each coordination state in the inhomogeneous broadening limit according to

$$I(E) \propto \left\langle \sum_j \left|\boldsymbol{\mu}_{0j}\right|^2 \Delta E_{0,j} \delta\left(E - \Delta E_{0j}\right) \right\rangle \tag{2.8}$$

where j runs over the excited states and $\Delta E_{0,j}$ and $\boldsymbol{\mu}_{0j}$ are respectively the energy difference and transition dipole between the ground and jth state.[86, 101] We used a histogram bin width of 0.1 eV. An example of the individual contributions of the transition from the ground to each excited state to the overall absorption spectrum is given in Figure 2.10 for the $Na(THF)_3$-$Na(THF)_3$ coordination state.

2.6.7 Verification of Results with Density Functional Theory (DFT) Calculations

As a means to verify the accuracy of our theoretical model (chosen pseudopotentials, CISD grid solver, etc.), we performed DFT calculations on representative coordination states (and some transition states) of Na_2 in THF. First, we selected configurations of each coordination state at the minimum of its potential of mean force – i.e., its equilibrium bond distance. Because our model uses planar THF with CH_2 groups treated as a united atom, we first explicitly added the hydrogen atoms and then optimized the overall structure with DFT using the B3LYP functional with the 6-31+G* basis set as implemented in QCHEM 5.0. With B3LYP, the optimized structures had Na–Na bond lengths of 3.68, 3.57, and 3.81 Å for the $Na(THF)_2$–$Na(THF)_4$, $Na(THF)_3$–$Na(THF)_3$, and $Na(THF)_3$–$Na(THF)_4$ states, respectively. The Na–THF oxygen site dative bond length were, on average, 2.45 ± 0.03 Å. We then performed single-point calculations of each geometrically-relaxed coordination state to determine the relative energies using the range-separated hybrid ωB97M-V functional, which includes non-local correlation. To compare the energies of coordination states with different total numbers of THF molecules (e.g., (3,4) vs. (3,3) and (2,4), we added or subtracted the energy of an isolated THF molecule calculated at the same level of theory. The ωB97M-V calculations predicted that, in agreement with our MQC calculations, the $Na(THF)_3$–$Na(THF)_4$ was the most stable coordination state, with the $Na(THF)_3$–$Na(THF)_3$ being next stable (110 meV or $\sim$4.3 k_BT higher) and $Na(THF)_2$-$Na(THF)_4$ being least stable (160 meV or $\sim$6.2 k_BT higher). We then tested the barrier heights, approx-

imated as the energy needed to pull one THF from $Na(THF)_3$–$Na(THF)_4$ to form either $Na(THF)_3$–$Na(THF)_3$ or $Na(THF)_2$–$Na(THF)_4$. These values were 454 meV ($\sim$17.7 k_BT) for the $Na(THF)_3$–$Na(THF)_3$ $\rightarrow$ $Na(THF)_3$–$Na(THF)_4$ transition and 291 meV ($\sim$11.4 k_BT) for the $Na(THF)_2$–$Na(THF)_4$ $\rightarrow$ $Na(THF)_3$–$Na(THF)_4$ transition.

Interestingly, if B3LYP was used instead of ωB97M-V, $Na(THF)_3$–$Na(THF)_3$ was predicted to be the most stable state, $Na(THF)_3$-$Na(THF)_4$ next most stable (81 meV or $\sim$3.2 k_BT higher) and $Na(THF)_2$–$Na(THF)_4$ the least stable (121 meV or $\sim$4.7 k_BT higher). The calculated energy barriers were 356 meV ($\sim$13.9 k_BT) for the $Na(THF)_3$–$Na(THF)_3$ $\rightarrow$ $Na(THF)_3$–$Na(THF)_4$ transition and 269 meV ($\sim$10.5 k_BT) for the $Na(THF)_2$–$Na(THF)_4$ $\rightarrow$ $Na(THF)_3$–$Na(THF)_4$ transition. This shows that the assumptions and details of the DFT functional chosen has an effect on the prediction of the most stable coordination state and the relative energies of each state. However, the more accurate ωB97M-V shows better agreement with our MQC model.

Of course, our MQC model includes the presence of other THFs that help to solvate the different coordination states. To account for this, we ran the ωB97M-V, calculations with implicit THF solvent using a PCM dielectric continuum with THF's dielectric constant of 7.6. With the implicit solvent, all of the coordination-state energies stabilized slightly and the energy barriers lowered relative to the energies of the coordination states. Again, $Na(THF)_3$–$Na(THF)_4$ was the most stable species, followed by $Na(THF)_3$–$Na(THF)_3$ at just 47 meV ($\sim$1.8 k_BT) and $Na(THF)_2$–$Na(THF)_4$ at 93 meV ($\sim$3.6 k_BT). The energy barriers were reduced to 218 meV ($\sim$8.5 k_BT) for the $Na(THF)_3$–$Na(THF)_3$ $\rightarrow$ $Na(THF)_3$–$Na(THF)_4$ transition and 201 meV ($\sim$7.8 k_BT) for the $Na(THF)_2$–$Na(THF)_4$ $\rightarrow$ $Na(THF)_3$–$Na(THF)_4$ transition. These values are all within one-to-two k_BT of what we calculated in the MQC simulations, and given the accuracy of DFT, we consider the agreement to be excellent. The energy values for the latter calculations including implicit solvent are what is plotted as the black asterisks in Figs. 2.3b and c.

2.6.8 Representative Snapshots of Na_2 in Liquid Tetrahydrofuran

Figure 2.1b and c of the main text show representative snapshots of the simulations of Na_2 in liquid Ar and THF (in the (3,4) coordination state), respectively. Additional simulation snapshots and discussion are provided here to give a more comprehensive picture of the distortion of the Na_2 valence electron cloud for each coordination state. The Na^+ cores are plotted as black spheres (scaled to their ionic radius) while the valence electrons' density is represented as a transparent blue surface with a blue wire mesh coating enclosing 90% of the charge density. THF molecules are plotted as light-blue sticks with red oxygen atoms. The dative bonds between Na^+ and THF oxygen sites within 3.5 Å are drawn with thin black lines.

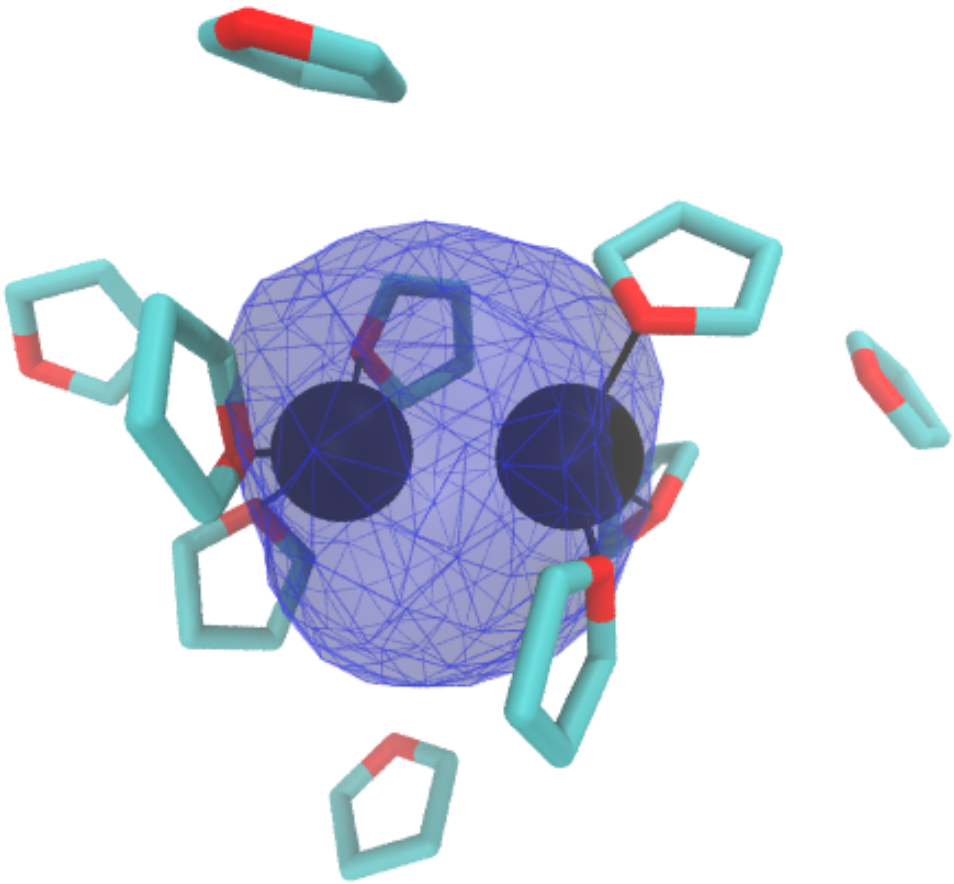

Figure 2.11: A representative snapshot of the $Na(THF)_3$–$Na(THF)_3$ coordination state at its equilibrium bond length of 3.48 Å. Because the $Na(THF)_3$–$Na(THF)_3$ is a symmetrically coordinated state, the electron density is not shoved dramatically more toward either Na^+ cation core. Instead, the electron density primarily spills above and below the bonding axis, and although instantaneous dipole moments along the bond axis can occur due to interactions from uncoordinated solvent molecules, the average dipole moment is zero.

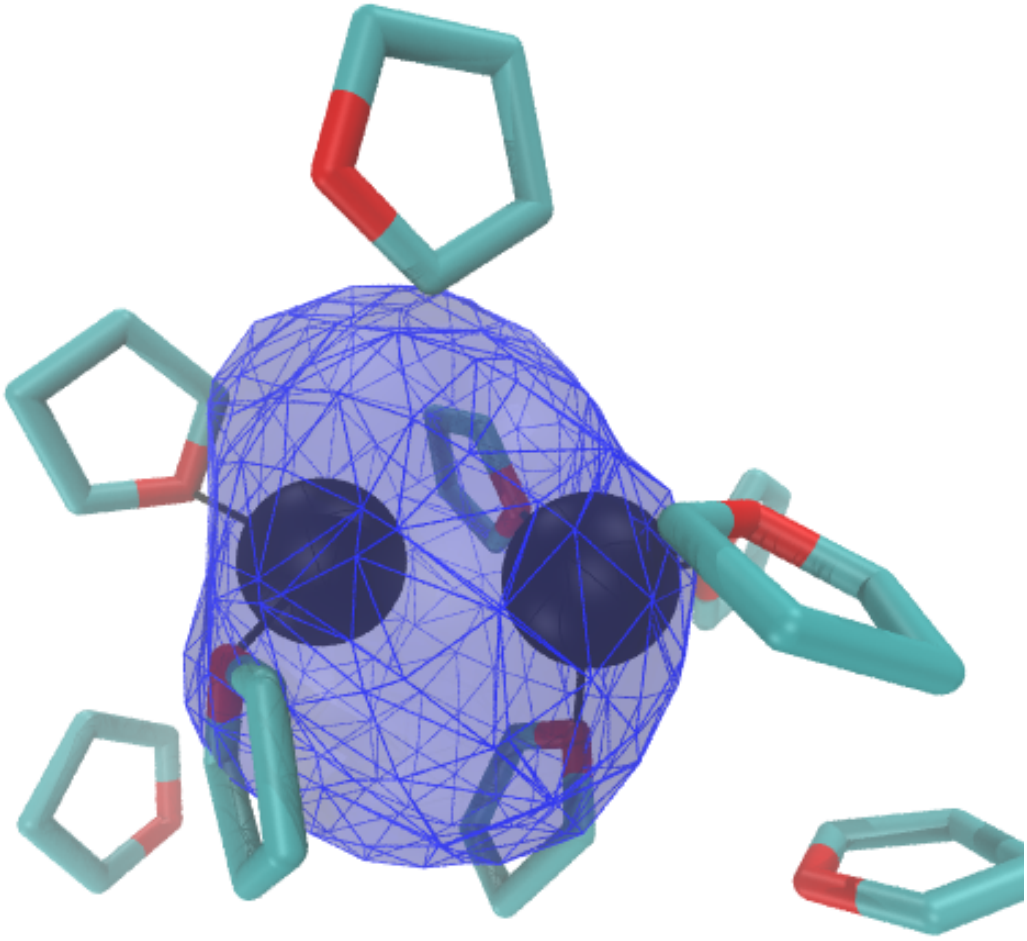

Figure 2.12: A representative snapshot of the $Na(THF)_2$–$Na(THF)_4$ coordination state at its equilibrium bond length of 3.65 Å Two THF molecules coordinate the left Na^+ core while four coordinate the right core. The electron density is highly distorted in this asymmetric coordination state, with more density pushed toward the left, away from the more highly-coordinated core, leading to a permanent average dipole moment. In addition, there is clearly still some distortion of the electron density around the less coordinated Na^+ as the two coordinating THF molecules need to push electron density aside to form their dative bonds to the core.

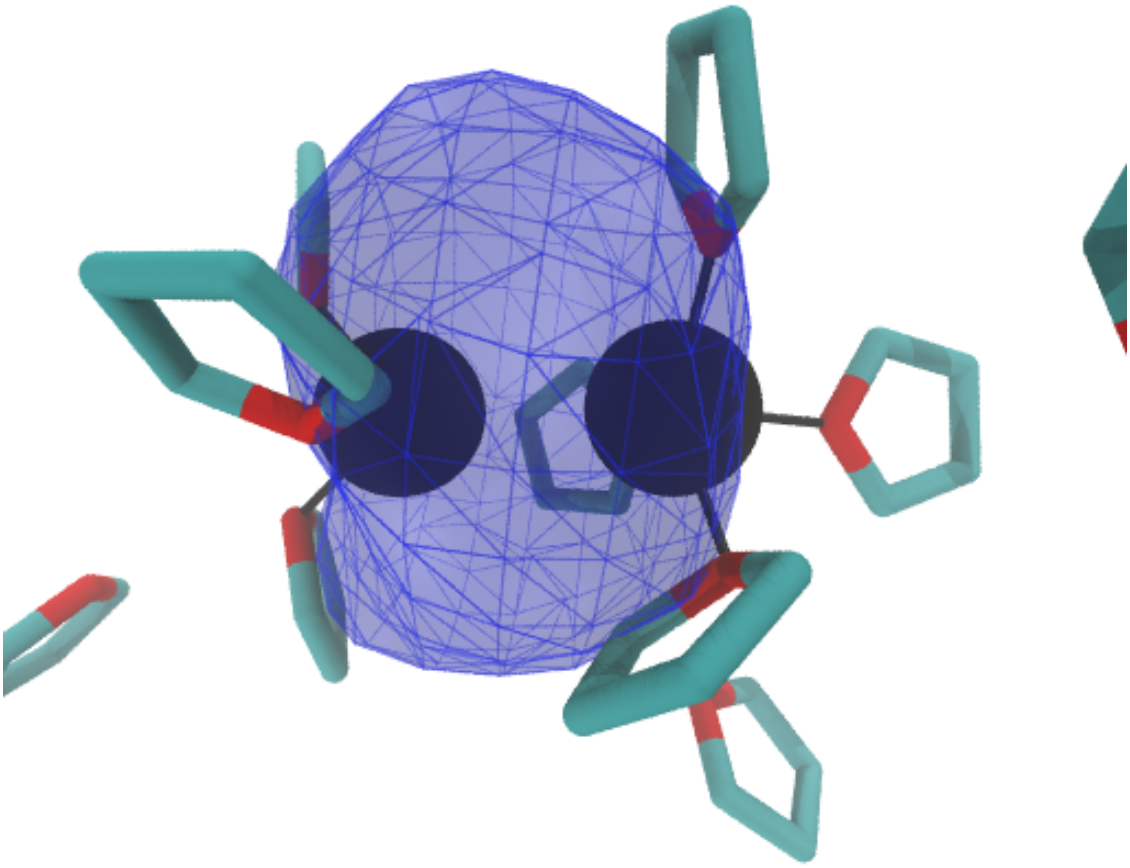

Figure 2.13: A representative snapshot of the $Na(THF)_3$–$Na(THF)_4$ coordination state at its equilibrium bond length of 3.70 Å. In this configuration, three THF molecules have formed dative bonds with the left-hand Na^+ cation core while four have formed dative bonds with the right-hand core. Due to the crowding of so many THF molecules around each core, the bonding electron density spills out significantly above and below the bonding axis. However, slightly more density shifts toward the less coordinated core to compensate for the extra crowding around the right-hand core, leading to a small permanent dipole moment for the $Na(THF)_3$–$Na(THF)_4$ coordination state.

Chapter 3

The Role of the Solvent in the Condensed-Phase Dynamics and Identity of Chemical Bonds: The Case of the Sodium Dimer Cation in THF

3.1 Abstract

When a solute molecule is placed in solution, is it acceptable to presume that its electronic structure is essentially the same as in the gas phase? In this paper, we address this question from a simulation perspective for the case of the sodium dimer cation (Na_2^+) molecule in both liquid Ar and liquid tetrahydrofuran (THF). In previous work, we showed that when local specific interactions between a solute and solvent are energetically on the order of a hydrogen bond, the solvent can become part of the chemical identity of the solute. Here, using mixed quantum/classical molecular dynamics simulations, we see that for the Na_2^+ molecule, solute–solvent interactions lead to two stable, chemically-distinct coordination states ($Na(THF)_4{-}Na(THF)_5^+$ and $Na(THF)_5{-}Na(THF)_5^+$) that are not only stable

themselves as gas-phase molecules but that also have a completely new electronic structure with important implications for the excited-state photodissociation of this molecule in the condensed phase. Furthermore, we show through comparative classical simulations that treating the solute's bonding electron explicitly quantum mechanically is necessary to understand even the ground-state dynamics of this simple diatomic molecule.

3.2 Introduction

Solvent molecules, although usually assumed to be mere spectators in condensed-phase chemical reactions, can not only dictate a solute's bond dynamics, thus playing a key role in the solute's reactivity, but they are also capable of helping to form new chemical species that are distinct both in behavior and reactivity compared to the original solute.[109] The effects of solvent interactions on the electronic structure of solutes go beyond well-studied cases where the solvent is known to create the solute's electronic structure, such as for solvated electrons[38] or the charge-transfer-to solvent transitions of simple anions.[2] For example, in electron transfer reactions, the reorganization of the solvent is usually the driving force that moves the electron from donor to acceptor.[3–5] And in photodissociation reactions, the 'cage' of solvent molecules that surrounds around any given solute prevent the breaking of a chemical bonds by trapping the geminate photofragment pair. This forces the bond to re-form if the fragments are unable to escape the solvent cage.[1] In previous work, our group showed that the solvent can affect chemical bonds in yet another way: Pauli repulsion interactions from the surrounding solvent can compress a solute's bonding electrons, decreasing the bond length, increasing the bond vibrational frequency, blue-shifting the electronic absorption and inducing inducing relatively large instantaneous dipole moments, even without electrostatic forces.[46]

Beyond these general solute-solvent interactions, when there are local specific interactions between a solute and solvent that are energetically on the order of that of a hydrogen bond,

an entirely new chemical effect can occur: solvent molecules can incorporate themselves as an integral part of the solute's chemical identity. We identified an example of this phenomenon in a previous study of the sodium dimer (Na_2) in liquid tetrahydrofuran (THF).[109] We found that dative bonds formed between the sodium cation cores within the molecule and the lone pairs on the THF oxygen atoms. These interactions produced three discrete new solutes, $Na(THF)_2$–$Na(THF)_4$, $Na(THF)_3$–$Na(THF)_3$, and $Na(THF)_3$–$Na(THF)_4$, due to different degrees of solvent coordination. These stable coordination states interconverted by overcoming an energy barrier of $\sim 8\ k_B T$. In other words, the equilibrium involving breaking and/or formation of a Na^+–THF dative bond constitutes a chemical reaction that converts one unique chemical species into another.[109]

In this work, we have chosen to further explore how solvents with modest local specific interactions influence the electronic structure and chemical identity of solutes by studying the Na_2^+ molecule. We make this choice for several reasons. First, Na_2^+ has a relatively simple electronic structure that can be well described in mixed quantum/classical (MQC) molecular dynamics (MD) simulations. This provides an excellent point of comparison to our previous work on the behavior of the solvated Na_2 molecule,[109] allowing us to explore what differences a single electron can make in terms of solvent interactions with solutes. Second, unlike neutral Na_2 in solution, solvated Na_2^+ could be created experimentally. Not only should it be straightforward to prepare $Na_2(THF)_n^+$ clusters in mass-selected supersonic expansions, but Na_2^+ could be prepared in bulk liquid THF at room temperature via pulse radiolysis of solutions containing high concentrations of sodium salts. This will allow us to make a series of predictions about solvent-induced changes in chemical identity that can be directly tested experimentally. Finally, also unlike neutral Na_2, for which the lowest several excited states are bound, the first excited state of the Na_2^+ molecule is dissociative in the gas phase.[110–113] Therefore, this study provides a launching point to understand the effects of solvation on excited states, paving the way for future studies of the photodissociation dynamics of the Na_2^+ species in a variety of solvent environments.

Thus, this paper focuses on understanding solvent effects on the electronic structure of Na_2^+ using MQC MD simulations. We find that when Na_2^+ is placed inside liquid argon, Pauli repulsion interactions between argon atoms and the Na_2^+ bonding electron result in distortion of the bonding electron density, an effect that induces infrared (IR) activity in what would otherwise be a perfectly symmetric solute with no expected IR absorption. We also see an increase in vibrational frequency and decrease in bond length as confinement of the bonding electron by the surrounding solvent strengthens the Na–Na bond. In contrast, in liquid THF, we find that the sodium dimer cation molecule forms two distinct coordination states due to the dative bonding interactions between the Na atom cores of Na_2^+ and the THF oxygen-sites. Both of these coordination states display opposite trends from Na_2^+ in liquid Ar, with a dramatic lengthening of the bond and decrease in vibrational frequency. By running all-classical simulations of the same system, we find that all of these features are entirely quantum mechanical effects: although classical simulations do exhibit dative-bonding interactions between the solute and the solvent, classical mechanics entirely misses the decrease in vibrational frequency and lengthening of the Na_2^+ bond. Instead, classical simulations of Na_2^+ in THF behave much like quantum simulations of Na_2^+ in Ar, emphasizing the importance of a quantum treatment of the local specific interactions that can alter chemical identity. When quantum mechanics is considered, even though the dative bonding interactions are individually weak, the electronic structure of Na_2^+ is modified to such an extent that each of the solvent-coordinated states should be described as unique molecules with properties independent of the original Na_2^+ solute: each of the two stable coordination states has a unique Na–Na bond length, vibrational frequency, spectroscopic signatures, and electronic structure.

To isolate the effects of the weak solvent complexation that changes the chemical identity from more typical solvation, we also show that the THF-coordinated species are stable in the gas phase, highlighting the necessity of treating these species as discrete molecules. The first excited state of the THF-coordinated species is dramatically altered compared to un-

coordinated Na_2^+ in the gas phase or in liquid Ar. Gas-phase Na_2^+ has a first excited state with a node perpendicular to the Na–Na bond (a σ^* antibonding orbital), as expected from molecular orbital theory.[95, 96] But the lowest excited state of the coordinated $Na_2(THF)_n^+$ molecules places electron density above and below the bond axis, resembling a π molecular orbital. This means that the electronic properties and excited-dynamics of these complexes are entirely different from the uncomplexed molecule: not only is the absorption spectrum of the complexed molecule completely changed from the uncomplexed molecule, but photoexcitation of the complexed molecule will not break the chemical bond in the same way as the uncomplexed molecule. All of the results highlight the importance of including the solvent as part of the chemical identity of the solute when there are local specific interactions that are about the same strength as an H-bond in water.

3.3 Computational Methods

For our MQC MD simulations, we consider the Na_2^+ molecule as two classical Na^+ cores held together by a single quantum-mechanically-treated valence bonding electron. Thus, our simulations consisted of hundreds of classical solvent molecules (either Ar or THF), two classical Na^+ cations and one fully quantum mechanical bonding electron. For the interactions between the classical particles and the quantum mechanical electron, we utilized Phillips-Kleinman (PK) pseudopotentials,[88] modified with polarization potentials to correct for the frozen-core approximation implicit in PK formalism; these are the same PK pseudopotentials used in our previous work.[27, 39, 46, 89, 109] For our all-classical simulations, we approximated the Na_2^+ molecule as two Na cores each carrying a half charge with Lennard-Jones parameters intermediate between those of a Na^+ and neutral Na. The Na–Na potential was then constructed by fitting the gas phase Na–Na potential energy curve to a Morse potential while the Na–THF interactions remained the same as in the MQC simulations, described below.

Our simulations of Na_2^+ in THF contained 254 solvent molecules inside a cubic simulations cell with a side length of 32.5 Å. The length of the simulation cell was chosen to match the experimental density of THF at the simulation temperature (0.89 g/mL at ∼298 K). The simulations were performed in the microcanonical ensemble and utilized periodic boundary conditions[87] with the minimum image convention. The classical interactions between the Na^+ cations and the THF solvent molecules were modeled with Lennard-Jones potentials. The THF molecules were treated as rigid, planar five-membered rings following the work of Chandrasekar and Jorgensen.[103] The rigid planarity of the molecules was enforced using the RATTLE algorithm.[85] All interactions in the cells were tapered smoothly to zero at 16 Å over a 2-Å range using a center-of-mass-based switching function developed by Steinhauser.[105] For the quantum mechanical electron, the electronic eigenstates were expanded in a basis of 64 × 64 × 64 plane waves that spanned the cubic simulation cell, and the single-electron Hamiltonian was diagonalized at every MD time step using the implicitly-restarted Lanczos method as implemented in ARPACK.[108] The MD trajectory was propagated adiabatically on the electronic ground-state surface using the velocity Verlet algorithm[87] with a 4-fs time step. The simulation was subjected to velocity rescaling[87] and then equilibrated for several ps at 298 K before running a 1-ns production trajectory.

Simulations of Na_2^+ in Ar were conducted in the same manner as those in THF with the obvious exception of how the solvent was treated. The Na^+–Ar interaction was taken from a fit to the *ab initio* calculations of Ahmadi, Almlöf, and Røeggen.[107] The cubic simulation cell for simulations in Ar had a side length of 43.8 Å and contained 1,600 solvent atoms to match the experimental solvent density of Ar at 120 K (1.26 g/mL). For simulations in Ar, the electronic eigenstates were expanded on a basis of 32 × 32 × 32 plane waves spread over a 25-Å box and the MD trajectory was propagated with a 5-fs time step. The Ar simulation state point is well within the liquid region of simulated Ar's phase diagram.[106]

3.4 Results and Discussion

Previous work from our group studying Na_2 in liquid Ar found that all-classical simulations failed to capture solvent-induced changes to the Na_2 bonding electrons due to local Pauli repulsion interactions and therefore could not reproduce the important features to the solute's dynamics in the condensed phase.[46] For instance, although the physical confinement of the Na_2 solute by the surrounding cage of Ar solvent atoms led to an increased vibrational frequency in the all-classical simulations, the effect was underestimated by a factor of $\sim$4, indicating that the solvent-induced quantum effects were a much more important factor in determining the changes to a solute's bond vibrational frequency.[46]

Since simulations of a symmetric dimer molecule solvated in an apolar solvent require explicit quantum treatment of the solute's bonding electron to capture the bond dynamics, how well can all-classical simulations hope to capture the complex behavior of a solute in an environment with locally-specific solute–solvent interactions? After all, it is well known that ethers like THF readily chelate metal cations like Na^+ in solution. For a bare Na^+ in THF, classical simulations predict that the oxygen atoms from six surrounding THFs form dative bonds, with the THF molecules arranged roughly at the corners of an octahedron. In previous work, we performed mixed quantum/classical simulations of neutral Na atoms in THF, and found that the solvent pushes the quantum electron density off-center, so that the neutral sodium species in THF solution is best thought of as a Na^+–solvated electron tight contact pair, with the cation end of the contact pair making dative bonds with four THFs on average.[85] Similarly, in our previous studies of Na_2 in THF, we observed that the Na_2 molecule distorts to allow two-to-four THF oxygen-sites to chelate the Na^+ cores on each side of the molecule, for an average coordination of 3.25 THFs per Na^+.[109]. In the next section, we explore how well classical mechanics can do in describing these effects for the Na_2^+/THF system.

3.4.1 Chelation of Na_2^+ by THF Oxygen-sites Gives Rise to Multiple Stable Coordination States: Comparison Between All-Classical and MQC Simulations

We begin our exploration of the behavior of the Na_2^+ molecule in liquid THF by making a direct comparison between simulations where the bonding electron is treated quantum mechanically and those where the entire system is treated classically.

The most important difference between Na_2^+ dissolved in liquid Ar and dissolved in liquid THF is the presence of Na^+-core–THF dative bonds. The dative bonds between the THF oxygen-sites and Na^+ core(s) in THF-solvated Na_2^+ are most readily seen in the Na–O pair distribution function, which is shown in Fig. 3.1 for both all-classical (dashed red curve) and MQC (solid black curve) simulations of Na_2^+ in THF. For Na_2^+, both the all-classical and MQC pair distribution functions show a large, sharp peak indicative of the Na–THF oxygen site dative bonding interaction. However, the height, width, and location of this peak varies between the two simulations. For the MQC simulations, the sharp, narrow peak appears at 2.35 Å, which is the same position that the dative-bonding peak appears in MQC simulations of THF-solvated Na^+–e^- tight-contact pairs[85] and THF-solvated Na_2.[109] Integration of the dative-bonding peak for Na_2^+ reveals an average of 4.88 dative bonds per Na^+ core for the MQC simulation and 4.46 for the all-classical simulation.

Despite having a similar average number of dative bonds, however, the all-classical simulations show a dative bonding peak that is broader and shallower, suggesting that the coordinating THF molecules are held more loosely. This makes sense because each sodium core in the all-classical simulation carries only half a positive charge rather than the full positive charge in the MQC simulation. Furthermore, the dative bond distance between each Na^+ core and the oxygen sites of the chelating THFs is larger for the all-classical simulation because the sodium cores are larger to account for the extra half-electron assumed to reside on each. In other words, the all-classical model has no polarizability of the bonding electron;

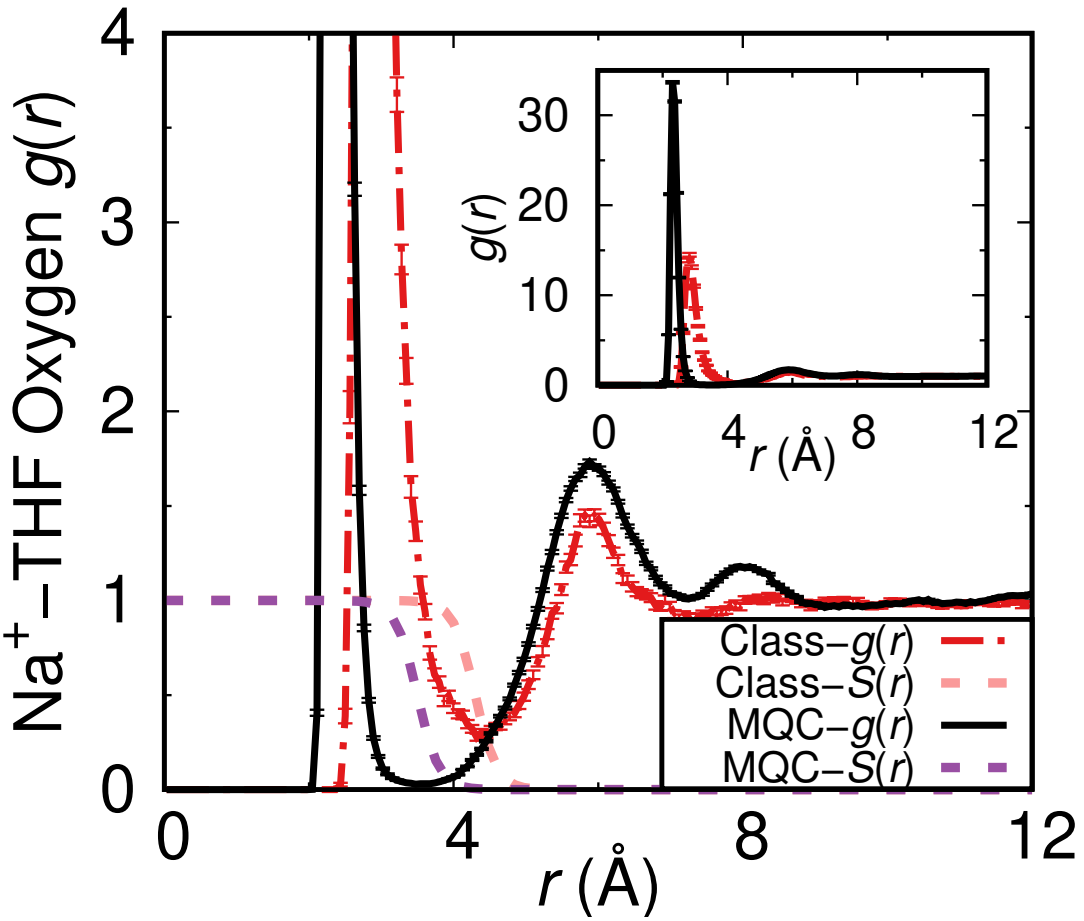

Figure 3.1: The pair distribution function, $g(r)$, shows the chelation of the Na^+ cores in Na_2^+ by THF oxygen sites, leading to the formation of metal-oxygen dative bonds for both all-classical (red dot-dashed curve) and mixed quantum/classical (black solid curve) simulations. In both sets of simulations, $g(r)$ is averaged over the Na^+–THF oxygen site distances for both Na^+ cores. The smooth weighting functions, $S(r)$ (dashed curves) were used to define the solvent coordination number around each Na^+ core, as plotted below in Figs. 3.2 and 3.3. The inset shows $g(r)$ on an expanded scale to reveal the full peak at the ∼2.35 Å dative-bonding distance in the MQC simulations. The error bars shown represent 95% confidence intervals.

it's rigid, fixed electronic geometry is not reflective of the molecule when treated quantum mechanically.

To analyze the coordination on each Na^+ core for Na_2^+ in THF, we utilized a continuous coordination number, which was defined for both the MQC and all-classical simulations by counting the number of THF oxygen sites that reside within a given distance of the center of each sodium core; see the SI for details. Using this coordinate, whose counting functions $S(r)$ are plotted in Fig. 3.1, we calculated the free energy, or potential of mean force (PMF) of the system as a function of n, the number of coordinating solvent molecules on each sodium core, labelled Na_a^+ and Na_b^+, which is shown in Fig. 3.2a for the MQC simulation and Fig. 3.3a for the all-classical simulation.

For the MQC simulation in Fig. 3.2a, several energetic minima are apparent, all at integer values of coordination, revealing two main stable coordination states: $Na(THF)_4$-$Na(THF)_5^+$ and $Na(THF)_5$-$Na(THF)_5^+$. Slices along the coordination PMF for restricted values of either four ($n_{Na_a^+} = 4$) or five ($n_{Na_a^+} = 5$) THFs coordinated to one of the two sodium cores for the MQC simulation are plotted in Figs. 3.2b and c, respectively. These figures show that the stable energetic coordination minima are separated by energy barriers of many k_BT. The height of the barrier is larger than the direct strength of one of the dative bonds (which is only ~4 kcal/mol, about the strength of a typical H-bond) because of the solvent reorganization required to change the coordination number. This means that to break or make a THF–Na core dative bond, i.e., to convert from one coordination state to another, the Na_2^+ molecule must undergo a chemical reaction. Analysis of the 1-ns MQC Na_2^+ in THF trajectory reveals reaction times of approximately 32 ± 11 ps for the $Na(THF)_5{-}Na(THF)_5^+ \rightarrow Na(THF)_4{-}Na(THF)_5^+$ reaction and 15 ± 10 ps for the $Na(THF)_4{-}Na(THF)_5^+ \rightarrow Na(THF)_5{-}Na(THF)_5^+$ reaction, times that are consistent with transition state theory, as shown in the SI. Thus, just as we saw with previous work of Na_2 in THF, when Na_2^+ is placed in liquid THF, the solvent integrates as part of the chemical identity of the solute.[109] Furthermore, the $Na_2(THF)_n^+$ complexes have higher coordination

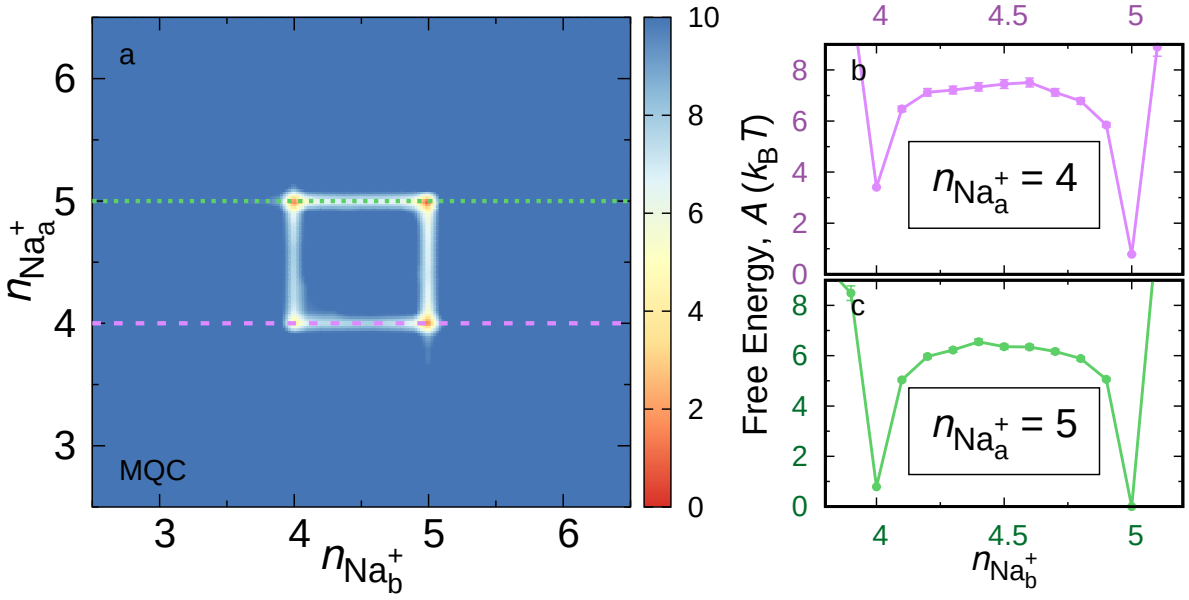

Figure 3.2: Potential of mean force as a function of the number of Na^+ core–THF oxygen dative bonds on each Na^+ core for MQC simulations; since the Na_a^+ and Na_b^+ cores are identical, the plot is symmetric around the diagonal. The number of dative bonds was determined by summing THF oxygen atoms at each distance weighted by the S(r) function plotted in Fig. 3.1 for each Na^+ core. The energetic minima, shown as red/orange colors in panel (a), occur at the integer values of four and five, revealing stable coordination states that are connected by interconversion pathways where a single dative bond is made or broken. Slices along the $n_{Na_b^+}$ coordinate with $n_{Na_a^+} = 4$, panel (b), and $n_{Na_a^+} = 5$, panel (c), show more detail on the heights of the different minima and the barriers between them. A barrier of several $k_B T$ must be surmounted to convert from one stable coordination state to another, indicating that these states are different chemical species. A third coordination state, $Na(THF)_4$-$Na(THF)_4^+$, also can be accessed, but its higher free energy minimum means that it has little Boltzmann weight at equilibrium. The error bars represent 95% confidence intervals.

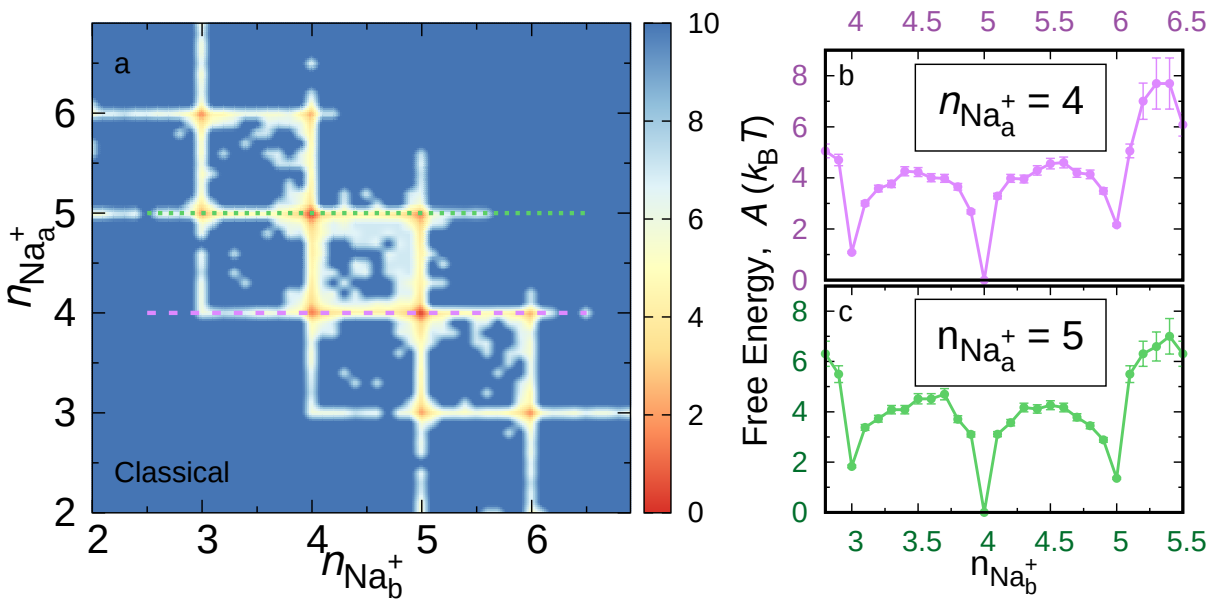

Figure 3.3: Potential of mean force as a function of the number of Na^+ core–THF oxygen dative bonds on each Na^+ core for all-classical simulations, calculated in the same manner as with Fig. 3.2. Although classical mechanics still shows that Na_2^+ in liquid THF exhibits energetic minima at integer values of coordination, the looser classical Na^+–THF oxygen-site dative-bonding interactions allow more coordination states to be accessed, and the individual coordination states are energetically less stable. Panels (b) and (c) show slices along the $n_{Na_b^+}$ coordinate with $n_{Na_a^+} = 4$ in panel (b) and $n_{Na_a^+} = 5$ in panel (c). The error bars shown represent 95% confidence intervals.

numbers than the previously observed $Na_2(THF)_n$ complexes, revealing that even though the single electron of Na_2^+ is more tightly bond, it is easier to push a single electron out of the way to expose the cation core for coordination than it was to distort the two electrons of Na_2.

The all-classical simulation captures some of the coordination effects seen in the MQC simulation, as shown in Fig. 3.3a; however, due to the looser Na^+–THF-oxygen-site dative bonds, the degree of interaction fluctuates more wildly, accessing a wider variety of coordination states. The barriers between coordination states are also lower, so that the system stays in an individual state for less time (about a picosecond versus a few tens of picoseconds for the MQC simulation, as consistent with transition state theory). Yet, the energetic barriers between coordination states, shown in the energy slices in Figs. 3.3b and c, are still

sufficiently large that the molecule prefers integer-valued coordination states, even though the looser dative bonds allow the system to more frequently 'slip' off of the reaction pathways, as evidenced by the splotchy regions of lower free energy seen in Fig. 3.3a. Thus, even though classical simulations can qualitatively capture some of the behavior of this system, it's clear that a quantum mechanical description is necessary for a complete understanding, as we elaborate in the next section.

3.4.2 Quantum Treatment of the Bonding Electron is Essential to Understand Condensed-Phase Bond Dynamics

To further assess the ability of classical simulations to capture the correct behavior of a solute in an environment with locally-specific solute–solvent interactions, we compare several key factors in the solute's dynamics in a variety of environments in Figure 3.4. Table 3.1 summarizes the average bond length, vibrational frequency, and instantaneous dipole moment for Na_2^+ in these various environments as well as the corresponding values for Na_2 from our previous studies.[109]

The bonding electron of gas-phase Na_2^+ forms a cylindrically-symmetric ovoid around the molecule's center of mass, essentially a σ molecular orbital,[95, 96] as can be seen in panel (a) of Fig. 3.4. However, when Na_2^+ is put in the condensed phase, interactions with solvent molecules deform the bonding electron density. In liquid Ar, Fig. 3.4b, Pauli repulsion interactions with the surrounding cage of argon atoms compress the electron density: the normal exponential decay of the gas-phase wavefunction out to infinity is curtailed because of Pauli repulsion from the nearby argons, confining the bonding electron via disorder-induced localization. In other words, the bonding electron in liquid Ar is confined both by coulomb attraction to the Na^+ nuclei and by the irregular, dynamically changing box of the solvent cage. The fact that this confinement produces increased electron density between the nuclei explains the shorter average bond length and the higher vibrational frequency.

Furthermore, the fact that the surrounding solvent cage is asymmetric means that the

System	r_e Å	ω_e (cm^{-1})	$\bar{\mu}$ (e-Å)
Gas-phase Na_2^+	3.841 ± 0.010	113 ± 29	none
Na_2^+ in Argon	3.747 ± 0.007	134 ± 29	0.31 ± 0.10
Na_2^+ in THF^{MQC}	5.237 ± 0.008	42 ± 3	0.9 ± 0.4
Na_2^+ in THF^{CL}	3.605 ± 0.003	154 ± 17	none
$Na(THF)_4$−$Na(THF)_5^+{}_{THF}$	4.901 ± 0.013	68 ± 7	1.0 ± 0.4
$Na(THF)_5$−$Na(THF)_5^+{}_{THF}$	5.65 ± 0.04	56 ± 5	0.8 ± 0.4
$Na(THF)_4$−$Na(THF)_5^+{}_{Gas}$	4.95 ± 0.004	62 ± 6	0.9 ± 0.3
$Na(THF)_5$−$Na(THF)_5^+{}_{Gas}$	5.702 ± 0.006	51 ± 4	0.7 ± 0.3
Gas-Phase Na_2	3.270 ± 0.004	136 ± 23	none
Na_2 in Argon	3.167 ± 0.005	161 ± 48	0.11 ± 0.05
Na_2 in THF^{MQC}	3.617 ± 0.002	112 ± 15	0.6 ± 0.4
$Na(THF)_3$−$Na(THF)_{3THF}$	3.472 ± 0.008	119 ± 33	0.4 ± 0.2
$Na(THF)_2$−$Na(THF)_{4THF}$	3.66 ± 0.01	108 ± 20	1.2 ± 0.3
$Na(THF)_3$−$Na(THF)_{4THF}$	3.692 ± 0.007	113 ± 24	0.7 ± 0.2

Table 3.1: Average bond length, vibrational frequency,and instantaneous dipole moment for Na_2^+ and Na_2 in the gas phase and in various solution environments. The data for Na_2 is taken from Ref. 109.

bonding electron density is not instantaneously centered on the Na–Na bond, creating a fairly large average instantaneous dipole moment of ∼0.3 e-Å, nearly three times the value of the instantaneous dipole moment of Na_2 in Ar.[109][46] This shows that the single bonding electron of Na_2^+ is much more polarizable in Ar than the two bonding electrons of Na_2, likely because the Na_2^+ bond is weaker and thus its electron has a larger surface area with which the Ar solvent atoms can collide. The presence of an instantaneous dipole moment means that even though Na_2^+ is a non-polar homonuclear diatomic molecule and Ar is an entirely apolar solvent, the solvated molecule has a changing dipole moment and thus an infrared spectrum. This is an entirely quantum mechanical effect that could not be properly described without a wavefunction treatment of the bonding electron and its interaction with the surrounding solvent atoms. Thus, even though the structure of the bonding electron for Na_2^+ solvated in Ar bears a general resemblance to the gas-phase Na_2^+, the quantum mechanical interactions with the solvent cause chemically interesting changes to the molecule.

When Na_2^+ is dissolved in liquid THF, in contrast, Fig. 3.4c shows that the system now behaves entirely differently from that in either the gas phase or liquid Ar. The bond length

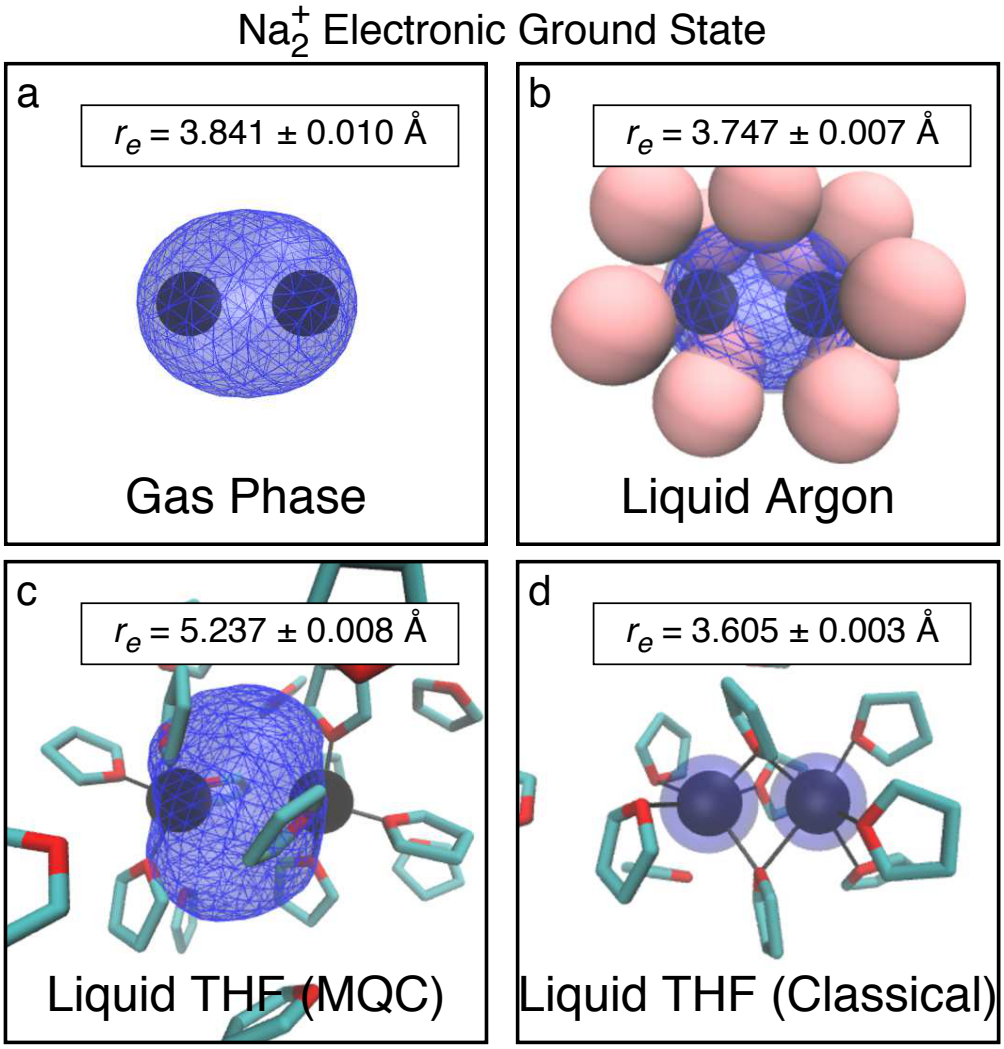

Figure 3.4: Representative simulation snapshots of Na_2^+ reveal how the presence of solvent molecules deforms the bonding electron density in the condensed phase (b-c) relative to the gas phase (a). The Na^+ cores have been plotted as black spheres scaled to the Na^+ ionic radius and the valence electron is displayed as a blue wire mesh which contains 90% of the electron density. In panel (b), the nearest argon solvent atoms are plotted as pink spheres scaled to argon's van deer Waals radius (with a window to allow viewing of the Na_2^+ molecule) while in panel (c), the nearest THF solvent molecules are plotted as turquoise sticks with red oxygen atoms. For THF, the specific configuration shown is in the (4,5) dative bonding coordination state with four THF molecules forming dative bonds between their oxygen sites and the left most Na^+ core and five THF molecules forming dative bonds with the right most Na^+ core. These dative bonds are shown with black lines connecting the THF oxygen site to the Na^+ core. Note that one dative-bonding THF molecule is partially behind each Na^+ core. Panel (d) shows a snapshot of the all-classical simulation of Na_2^+ in THF. The additional radius used to account for the extra half valence electron on each sodium core is plotted as a blue transparent sphere.

increases significantly and the vibrational frequency decreases, showing that not all liquids have the same general effect on the electronic structure of this solute. As with our previous work on Na_2 in liquid THF,[109] we see that the solvent forces a dramatic distortion of the bonding electron wavefunction so as to expose the Na^+ cores in the molecular interior. This pushes the bonding electron density away from the ends of the internuclear axis, leading to relatively large instantaneously induced dipole moments as well as a permanent molecular dipole moment for the asymmetrical coordinated state. Even though this distortion of the bonding electron is energetically unfavorable in the gas phase, in the condensed phase the distortion is driven by the fact that it allows for better solvation by the surrounding THF molecules in two ways. First, the distortion allows for the creation of dative bonds between the THF oxygen atoms and the cation cores on the molecule; Figure 3.4c shows a configuration with four THFs datively bonded to one core and five to the other, labelled $Na(THF)_4{-}Na(THF)_5^+$ or simply (4,5). Second, the complexed molecule is asymmetric and has a large dipole and quadrupole moment, providing a handle for the non-datively-bonded THFs to use their dipoles to provide extra solvation stabilization. For Na_2, this lead to a bond length that was, on average, $\sim$0.35 Å longer than gas phase Na_2. Without the extra valence electron to help hold the molecule together, Na_2^+ in THF is stretched even further, with an average bond length that is nearly 1.4 Å longer than gas-phase Na_2^+.

Figure 3.4d shows that for Na_2^+ in THF, failure to treat the solute's bonding electron explicitly quantum mechanically leads to an entirely incorrect picture of the Na_2^+ bond dynamics. In fact, the all-classical and MQC simulations have opposite predictions for the Na_2^+ molecule in THF, with the all-classical simulation showing a decreased bond length and increased bond vibrational frequency, much like the MQC simulations of Na_2^+ in Ar. This is because in the classical simulation, the interactions that affect the Na_2^+ bond are those of the solvent molecules with the half-charged sodium cores; it is not possible to distort the bonding electron density or change the electronic structure of the molecule. In fact, without electron density blocking solvent molecules from the center of the bond, THF molecules are

sometimes able to "bridge" the Na_2^+ molecule by forming dative bonds with each half-charged sodium core, something that never happens when the quantum mechanical bonding electron density occupies this region. Therefore, the predictions of the all-classical simulation are simply unphysical for this particular system: classically, there's little difference between Ar and THF, even with the presence of dative bonds in THF. Quantum mechanically, the local specific interactions between the THF oxygens and Na cation cores make all the difference in the behavior and identity of the solute.

3.4.3 $Na_2(THF)_n^+$ Coordination States are Molecules with Distinct Chemical Identity

The idea that the weakly-interacting solvent molecules have become part of the chemical identity of the solute is more than just a semantic definition; it has real implications for the behavior of the Na_2^+ molecule in liquid THF. To illustrate this, Fig. 3.5a compares the potential energy surface (PES) along the Na–Na bond distance of the gas-phase Na_2^+ molecule (black curve) to the PMF along this coordinate for Na_2^+ in liquid Ar (orange curve) and in liquid THF; the purple dashed curve shows the average behavior in THF, the green and blue curves show the individual PMFs for the two stable coordination states, and the red curve shows the PMF in THF for the all-classical simulation. The average PES of the quantum-treated molecule in THF shows what appears to be unphysical behavior – an imaginary vibrational frequency – in the region near the bottom of the potential well. This behavior can be explained, however, by the fact that quantum Na_2^+ in THF is not a single molecule but instead is made of two distinct chemical species that are in equilibrium with each other: the average PES is simply the Boltzmann-weighted average of the surfaces of the individual species. Each of these species differs only in the number of coordinating solvent molecules, and it's clear from Fig. 3.5a that each of the unique coordination states has its own distinct bond length and vibrational frequency. Clearly, the coordination states must be thought of as separate molecules for the average behavior to be properly understood.

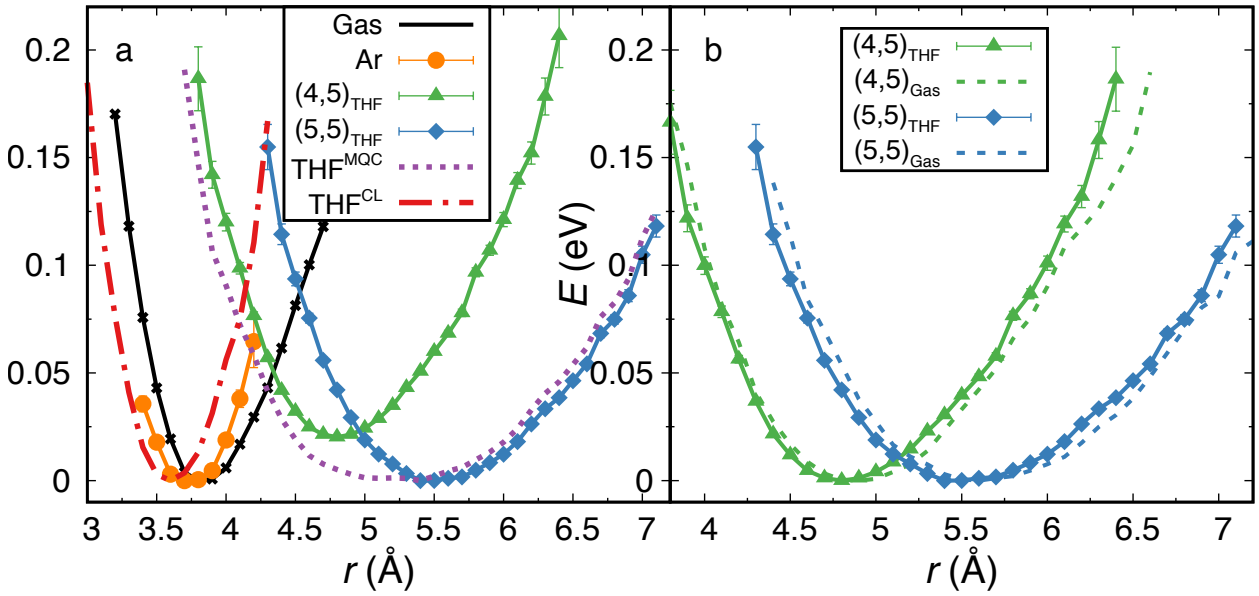

Figure 3.5: Different local solvent environments lead to different potentials of mean force for the Na_2^+ molecule. In panel (a), the gas phase potential energy surface, as calculated with our MQC model, is plotted in black with the minimum set to zero. The different colored curves show the PMFs in different environments: orange for Na_2^+ in liquid argon, dashed purple for the overall dynamics of Na_2^+ in THF, green for the $Na(THF)_4{-}Na(THF)_5^+$ coordination state, blue for the $Na(THF)_5{-}Na(THF)_5^+$ coordination state, and dashed red for the all-classical simulation. Notably, the overall PMF in liquid THF is not smooth but shows a small bump near the bottom of the energetic well where the statistics are highest. This is because the Na_2^+ molecule exists in multiple interconverting coordination states in THF; therefore, the full PMF is a Boltzmann-weighted average of the PMFs of the individual coordination states. Panel (b) plots a comparison between the $Na_2(THF)_n^+$ states in the gas and condensed phases, with the gas phase plotted as solid lines and liquid phase as dashed lines. Clearly, the complexed molecules show only modest changes in their properties upon solvation, similar to dissolving uncomplexed Na_2^+ in liquid Ar. The error bars represent 95% confidence intervals.

Unlike the case in Ar, where the shorter bond length and higher vibrational frequency of Na_2^+ are readily explained by the solvent confinement of the bonding electron density due to Pauli repulsion, the bond length of the molecule in THF is longer and the vibrational frequency is lower than in the gas phase. This clearly is related to the dative bonding by the complexed solvent molecules, but the changes in Na_2^+ bond structure in THF also pose an important question: since the molecule has changed chemical identity in THF solution, what is the best gas phase/condensed phase comparison? We believe that it makes more sense to compare the condensed-phase behavior to a gas-phase species that includes the THF molecules forming dative bonds to the sodium cores. Indeed, we find that $Na_2(THF)_n^+$ species are stable in the gas phase. This allows us to make a direct comparison between the gas-phase and condensed-phase coordinated species, which is shown in Fig. 3.5b.

We find that for the complexed species, solvation in the condensed phase produces only a small decrease in the average bond length and small increase in vibrational frequency; this means that the effects of solvating the datively-bonded complex in THF are similar to those that take place when solvating the uncomplexed Na_2^+ in liquid Ar. However, the differences observed between the gas- and condensed-phase $Na_2(THF)_n^+$ complexes are on average less than those of Na_2^+ in the gas phase versus Na_2^+ solvated in liquid Ar. For instance, the Na_2^+ bond length is compressed on average by 0.1 Å when the molecule is solvated in argon but the bond of the $Na_2(THF)_n^+$ complexes are only compressed by half as much when solvated in THF. This is because the datively-bonded THF molecules actually shield the bonding electron from some of the bulk solvent effects, lessening the overall degree of quantum solvation effects on the complexed molecule.

In addition to having distinct bond lengths and vibrational frequencies, the individual coordinated species in THF also have their own spectroscopic signatures that would allow them to be differentiated by experiment. Figure 3.6a shows the power spectra (Fourier transform of the Na–Na bond velocity autocorrelation function) of Na_2^+ in different environments. In liquid argon (orange curve), a single peak is evident, corresponding to a molecular

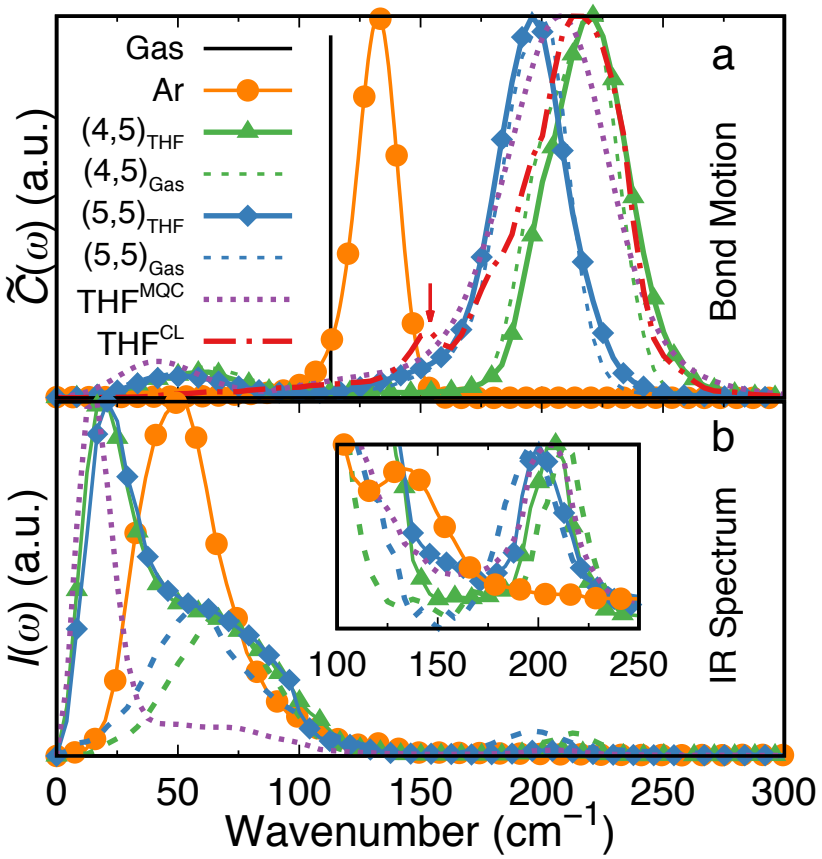

Figure 3.6: Vibrational spectra of Na_2^+. (a) Power spectrum of Na_2^+ calculated from the Fourier transform of the bond velocity autocorrelation function in different environments. The gas-phase vibrational frequency is shown as the black line at 113 cm^{-1}. The orange curve shows the vibrational spectrum of Na_2^+ in liquid Ar. The spectrum is blue-shifted relative to that in the gas phase due to the compression of the bonding electron from Pauli repulsion interactions with the first-shell Ar solvent atoms. However, the spectra in liquid THF (shown as a purple dotted curve for the overall dynamics, green solid curve for $Na(THF)_4$–$Na(THF)_5^+$, blue solid curve for $Na(THF)_5$–$Na(THF)_5^+$, and dashed curves for the $Na_2(THF)_n^+$ complexes in the gas phase) show that the main Na–Na vibration is red-shifted. The second, sharper peak near 200 cm^{-1} corresponds to the vibration of the Na^+–THF oxygen site dative bonds. The all-classical spectrum, shown as the dashed red curve, displays a broad dative bonding peak as well as a small feature at ∼150 cm^{-1} (indicated by the red arrow) corresponding to the Na_2^+ classical vibrational frequency. (b) Infrared spectrum of Na_2^+ calculated as the Fourier transform of the dipole moment autocorrelation function. Although Na_2^+ has no IR spectrum in the gas phase, all of the condensed-phase environments show strong IR absorption. The largest peaks (at ∼50 cm^{-1} in liquid Ar and ∼20 cm^{-1} in liquid THF) are due to intermolecular rattling motions in the solvent cage, but specific features from the Na_2^+ vibrational motion are also apparent (∼130 cm^{-1} for the Na_2^+ vibration in Ar, ∼55 cm^{-1} for Na_2^+ in THF) as well as the ∼200 cm^{-1} dative-bond stretches in THF).

vibration that is blue shifted from that in the gas phase. However, for the power spectrum of Na_2^+ in THF (plotted as the purple dashed curve, with the green curve for the $Na(THF)_4{-}Na(THF)_5^+$ state and the blue curve for the $Na(THF)_5{-}Na(THF)_5^+$ state), there are two significant peaks for each coordination state: a large, sharp peak at about 200 cm^{-1} and a shallower, broader peak at about 55 cm^{-1}. The shallower, lower frequency peak corresponds to the Na–Na vibrational frequency: this frequency is much lower than that in the gas phase both because of the weaker bond and increased bond length, and because the movement of the Na atoms also requires carrying along the heavy datively-bonded THF molecules. The location of this peak only marginally shifts when the $Na_2(THF)_n^+$ complexes are taken out of solution (plotted as the dashed green and blue curves), indicating that it is the datively-bonded THF molecules that most strongly modulate this motion, with only minor effects from the non-datively-bonded solvent molecules.

The second, sharper and higher-frequency peak observed in the power spectrum for the coordinated species in THF corresponds to the dative-bond stretch between the Na cation cores and the complexed THF oxygen atoms. The complexes with different numbers of coordinating THFs have different vibrational frequencies for this dative-bond stretching motion: less-coordinated sodium cation cores hold onto their dative-bonding solvent molecules more tightly, leading to a higher frequency vibration while more-coordinated cores hold their dative-bonded THFs more loosely, leading to a lower frequency vibration. These dative-bond vibrational peaks appear at the same $\sim$200 cm^{-1} location as previously observed for Na_2 in liquid THF,[109] indicating that this interaction is not strongly influenced by the number of bonding electrons present in the molecule. It is therefore not surprising that the all-classical simulation of Na_2 in THF correctly predicts the location of this peak, albeit broader than the MQC predictions due to the greater variety of coordination states accessed in the all-classical simulation, which leads to more dative-bonding environments averaged into the dative bond vibrations. However, the all-classical simulation completely misses the correct the Na–Na vibrational frequency, instead predicting it to be even further blue-shifted relative to the gas

phase than Na_2^+ in liquid Ar, as indicated by the red arrow in Fig. 3.6a.

The different power spectra strongly suggest that the infrared (IR) spectrum could be used to experimentally investigate the bonding of the Na_2^+ species in different solvent environments. Thus, in Fig. 3.6b we show the IR spectra of Na_2^+ in each of the various environments, calculated as the Fourier transform of the dipole autocorrelation function. Although the Na_2^+ molecule is not IR active in the gas phase, the fact that Pauli repulsion from the surrounding solvent atoms/molecules pushes bonding electron off center means that an instantaneous dipole moment is induced. In all solvent environments, this fluctuating dipole gives rise to a large IR absorption peak appears at low wavenumbers, which corresponds to the dynamics of the solvent cage surrounding the molecule: essentially, this is the frequency of collisions in liquid Ar or the frequency of non-complexed THF molecular rotations that push on the Na_2^+ bonding electron to induce a net dipole. The calculated IR spectra also show a peak corresponding to the vibrational frequency of the Na_2^+ molecule. This peak is weak in liquid Ar, as the Na–Na stretching motion affects the molecular dipole only indirectly because this motion helps modulate interactions with the surrounding solvent cage that breaks the molecular symmetry. The peak is stronger in liquid THF, as the complexed molecule has a permanent dipole induced by the datively-bonded solvents. The IR spectra for the gas-phase $Na_2(THF)_n^+$ complexes lack the large peaks from intermolecular rattling but still show the broad peak for the Na–Na stretching motion. For the THF–complexed molecules, both in and out of solution, the dative bonding vibrational frequency is also observed in the IR as the Na–THF-oxygen stretch also modulates the dipole of the complex. These observed IR features showing that IR spectroscopy would provide a direct handle on the solvent-induced changes in chemical identity.

Finally, we can also simulate the UV-visible absorption spectra for Na_2^+ in different environments, as shown in Figure 3.7. For Na_2^+ in liquid Ar, the absorption spectrum strongly resembles that in the gas phase, but with the electronic transitions blue-shifted and broadened. The blue-shift results directly from the compression of the bonding electron by the

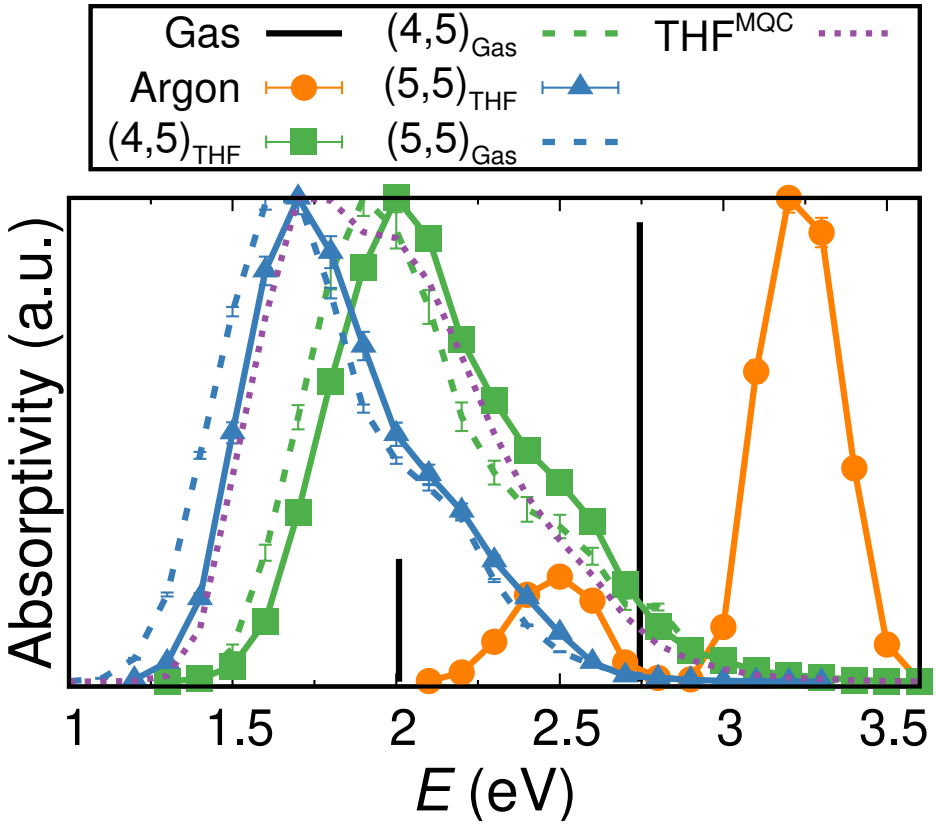

Figure 3.7: The electronic absorption spectrum of Na_2^+ in various environments reveals the dramatic change in electronic structure in THF as well as distinct spectral signatures of the different coordination states. The gas-phase absorbance is plotted as vertical black lines whose height represents their relative oscillator strengths. In liquid Ar (orange curve), the Na_2^+ absorption spectrum is blue-shifted and broadened relative to that in the gas phase, reflecting confinement of the bonding electron and the fluctuations of the surrounding solvent. In liquid THF (purple dashed curve), however, the shape of the spectrum is red-shifted and clearly different from that in the gas phase or in liquid Ar. This shows that the electronic structure of THF-complexed Na_2^+ is entirely altered from that in the gas phase, and the spectrum of the individual underlying coordination states are shown as the blue and green solid curves (the corresponding spectra of the complexes in the gas phase are shown as the blue and green dashed curves). The error bars shown represent 95% confidence intervals.

caging solvent: the spectrum is now that of a particle in a box rather than just in a molecule, and the confinement in the 'box' of the solvent cage raises the energy of the larger excited state (see below) more than the ground state, blue-shifting the electronic transitions. In liquid THF, on the other hand, the absorption spectra of the different coordination states of the molecule have an entirely different, red-shifted structure. This is not surprising, as the molecular identity is entirely different. The red shift observed here for Na_2^+ in THF relative to gas-phase Na_2^+ is even larger than the one previously observed for Na_2, indicating that the electronic changes to the single electron are even greater than for the two electrons of Na_2. Since the change in electronic structure depends on the datively-bonded THFs, the spectrum of the two different underlying complexes are also different, with the $Na(THF)_4{-}Na(THF)_5^+$ species absorbing to the blue of the $Na(THF)_5{-}Na(THF)_5^+$ species. Each $Na_2(THF)_n^+$ complex displays the expected blue shift relative to its own unique complexed gas-phase counterparts (plotted as the dashed curves in Fig. 3.7) due to solvent confinement of the bonding electron. Clearly, the two different complexed molecules have distinct absorption spectra as well as distinct IR spectra.

The fact that the different complexed species in liquid THF have different electronic absorption spectra means that the average absorption spectrum for Na_2^+ in THF is inhomogeneously broadened. This means that it should be possible to experimentally distinguish the two species by transient spectroscopy. This is because one could selectively excite only one of two predominate coordination species and then watch the effect on the absorption spectrum as the two re-equilibrate, a classic transient hole-burning experiment.

We have simulated this transient hole-burning experiment, shown in Fig. 3.8, to demonstrate precisely how these discrete coordination states could be probed experimentally. To do this, we took our equilibrium trajectory for the Na_2^+ molecule in THF and calculated the spectrum the molecule would have had following times when the energy gap was resonant on the red edge of the absorption band: in other words, following selective excitation of the $Na(THF)_5{-}Na(THF)_5^+$ species with a pump of approximately 1.7 eV. The results show that

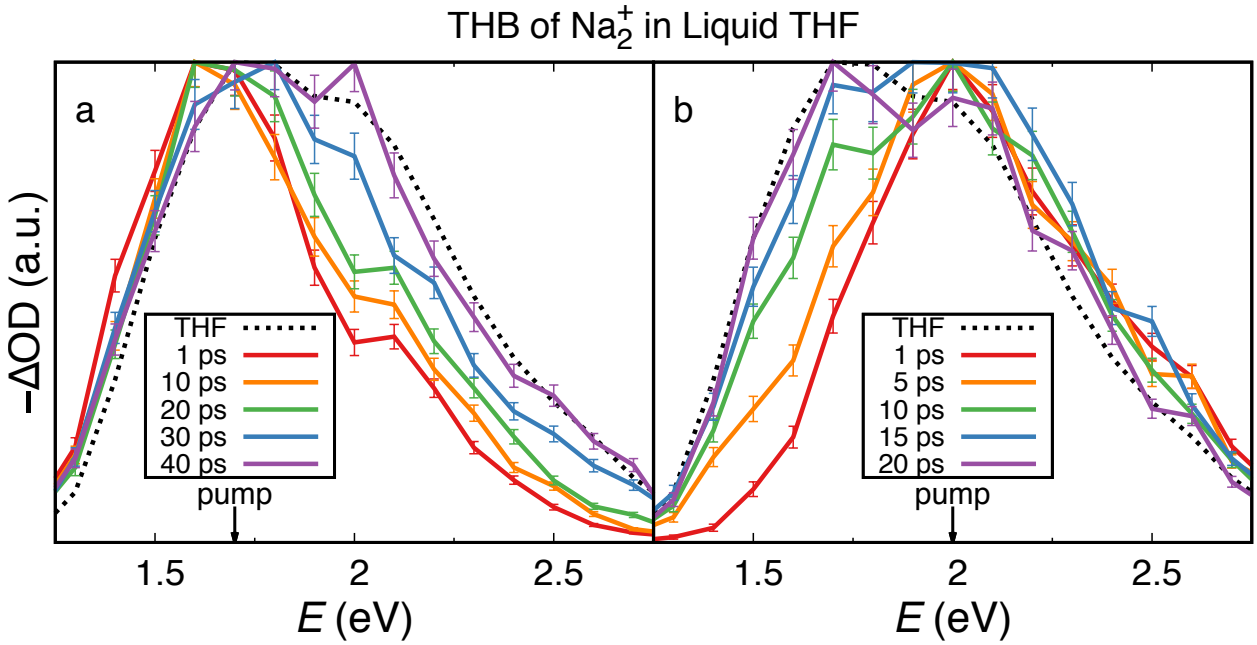

Figure 3.8: Simulated transient hole-burning show that the underlying coordination states could be readily distinguished experimentally because the underlying spectrum is inhomogeneously broadened. Panel (a) shows that following excitation at approximately 1.7 eV, a spectral position where $Na(THF)_5{-}Na(THF)_5^+$ absorbs strongly but $Na(THF)_4{-}Na(THF)_5^+$ does not, there is a selective bleach of the $Na(THF)_5{-}Na(THF)_5^+$ contribution to the total spectrum. The interconversion between the complexed species that takes place on a tens-of-ps time scale leads to spectral diffusion, so that eventually the entire band is bleached. Panel (b) shows that excitation at approximately 2.0 eV similarly selectively bleaches only the $Na(THF)_4{-}Na(THF)_5^+$ species at early times; spectral diffusion to the full spectrum takes place more quickly as this species is less stable and has a lower Boltzmann weight in the equilibrium. These results show that transient hole-burning could probe the discrete coordination states present in a bulk solution of Na_2^+ in THF. The error bars shown represent 95% confidence intervals.

the bleached spectrum at early times resembles that of the solvated $Na(THF)_5{-}Na(THF)_5^+$ species. However, over the approximately 30-ps coordination-state interconversion time, the bleached spectrum undergoes spectral diffusion and broadens until it lies within error of the calculated average spectrum of Na_2^+ in THF. Similarly, when a pump wavelength of approximately 2.0 eV is used, we see that $Na(THF)_4{-}Na(THF)_5^+$ is selectively bleached. With a faster interconversion time of $\sim$15 ps, reflecting the fact that this coordination state is less stable than the $Na(THF)_5{-}Na(THF)_5^+$ state, the spectrum broadens until it again is within error of the average spectrum. This suggest that transient hole-burning experiments could be used to distinguish the discrete coordinated states of $Na_2(THF)_n^+$ and measure their interconverstion time, either in mass-selected clusters in a supersonic expansion or in the bulk room-temperature liquid.

3.4.4 Distortion of the Na_2^+ First Excited State in THF

In the gas phase, the first excited state of the Na_2^+ molecule is dissociative. This means that this solute offers a unique chance to study condensed-phase photodissociation dynamics and how those dynamics change when the chemical identity of the molecule is altered by interactions with the solvent. Indeed, as shown in Fig. 3.9a, in the gas-phase first excited state, the bonding electron density is equally distributed between the two sodium cores, exactly as expected for an anti-bonding σ^* orbital in molecular orbital theory:[95, 96] the excited electron has a node that sits perpendicular to the bond axis. In liquid Ar, the same basic electronic structure is observed, with some perturbations due to the surrounding cage of Ar atoms; one can see that the reason the electronic absorption spectrum in liquid Ar is blue-shifted relative to the gas phase is that the excited-state wavefunction is more strongly confined in the liquid than the ground state wavefunction.

In stark contrast, when there are local specific interactions between THF molecules and Na_2^+, the electronic structure of the excited state is completely altered: the bonding density is confined between the two nuclei rather than being pushed outside the nuclei, and there

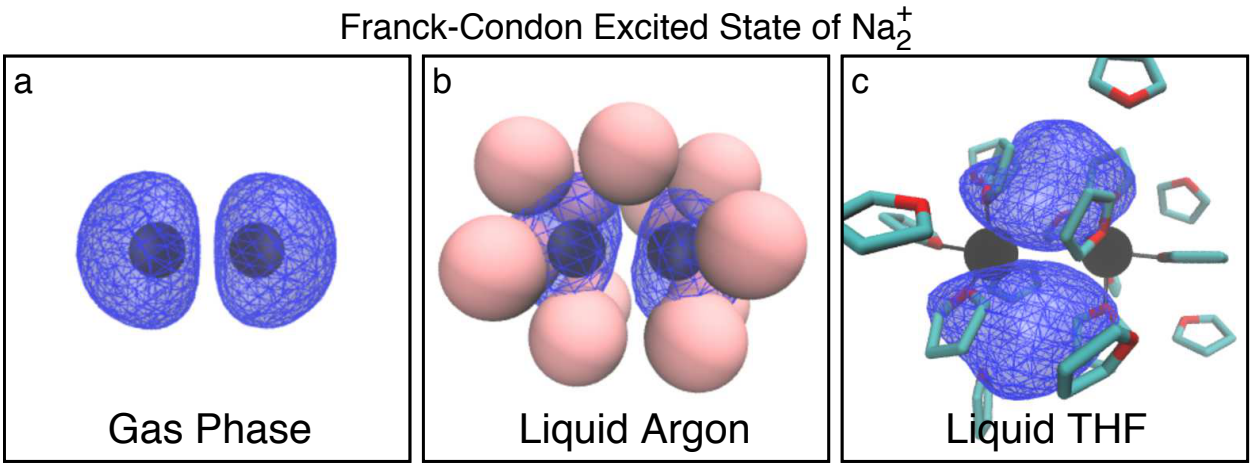

Figure 3.9: Snapshots of the lowest electronic excited state of Na_2^+ in different environments reveal an entirely different electronic structure in THF than in the gas phase or liquid Ar. In the gas phase (a), the electron density of the first excited state distributes equally between each Na^+ core with a node perpendicular to the bond axis located at the center of the molecule, much like the σ^* antibonding orbital expected from molecular orbital theory. In liquid Ar, the electron density distributes in a similar manner, with some perturbations and additional confinement due to the surrounding cage of Ar atoms. However, in THF the molecule's first excited state has an entirely different structure: electron density is confined to reside between the nuclei rather than outside them, with a node along the internuclear axis, similar to a molecular π bond. This suggests that although the Na_2^+ molecule photodissociates in the first excited state in the gas phase and liquid Ar, the dynamics following photoexcitation of Na_2^+ in THF will follow an entirely different pathway.

is a node that is parallel to the bond axis rather than normal to it. Thus, the Na_2^+ THF-coordinated species have a lowest-energy excited state that better resembles a molecular π orbital than a σ^* orbital. This behavior holds true for the Na_2^+ coordinated states both in and out of the condensed phase. This means that photoexcitation of a THF-complexed Na_2^+ molecule would not lead to immediate photodissociation: the bond may weaken upon Franck-Condon excitation, but there is no reason to expect a strong dissociative force along the Na–Na bond distance coordinate as would take place in the gas phase or liquid Ar. Moreover, the excited-state wavefunction also appears to interact with the datively-bonded THFs in a different way than the ground state, so that photoexcitation may be coupled with a possible change in the chemical identity of the molecule. We will explore the excited-state molecular dynamics of Na_2^+ in all of these different environments in a future investigation.

The dramatically different excited-state electronic structure for what is nominally the same Na_2^+ molecule is what give rise to the differences in the UV-Vis spectra shown above in Fig. 3.7. The change in electronic structure with solution environment not only changes the excited-state wavefunction in the Franck-Condon region, but also the entire equilibrium potential energy surface of the molecule. Figure 3.10 shows the potential energy curves (PEC) of the ground and first excited states of the gas-phase Na_2^+ molecule and for the gas-phase coordinated $Na(THF)_4{-}Na(THF)_5^+$ and $Na(THF)_5{-}Na(THF)_5^+$ molecules; the latter curves are calculated as room-temperature equilibrium averages along the ground state (PMFs). The figure makes clear that when Na_2^+ is complexed by THF, the excited-state dynamics will follow an entirely different pathway than the bare molecule in the gas phase because of the large changes in the excited-state wavefunction induced by the presence of the datively-bonded solvents. It is important to note that is clearly a quantum mechanical effect. This also opens the interesting question as whether or not the actual dynamics will follow the PECs shown in Fig. 3.10, which are linear response predictions, as the solvent motions (including the datively-bonded THFs) might be entirely different on the ground and first excited states. Clearly, the ways in which solvent molecules interact with the electronic structure of solutes

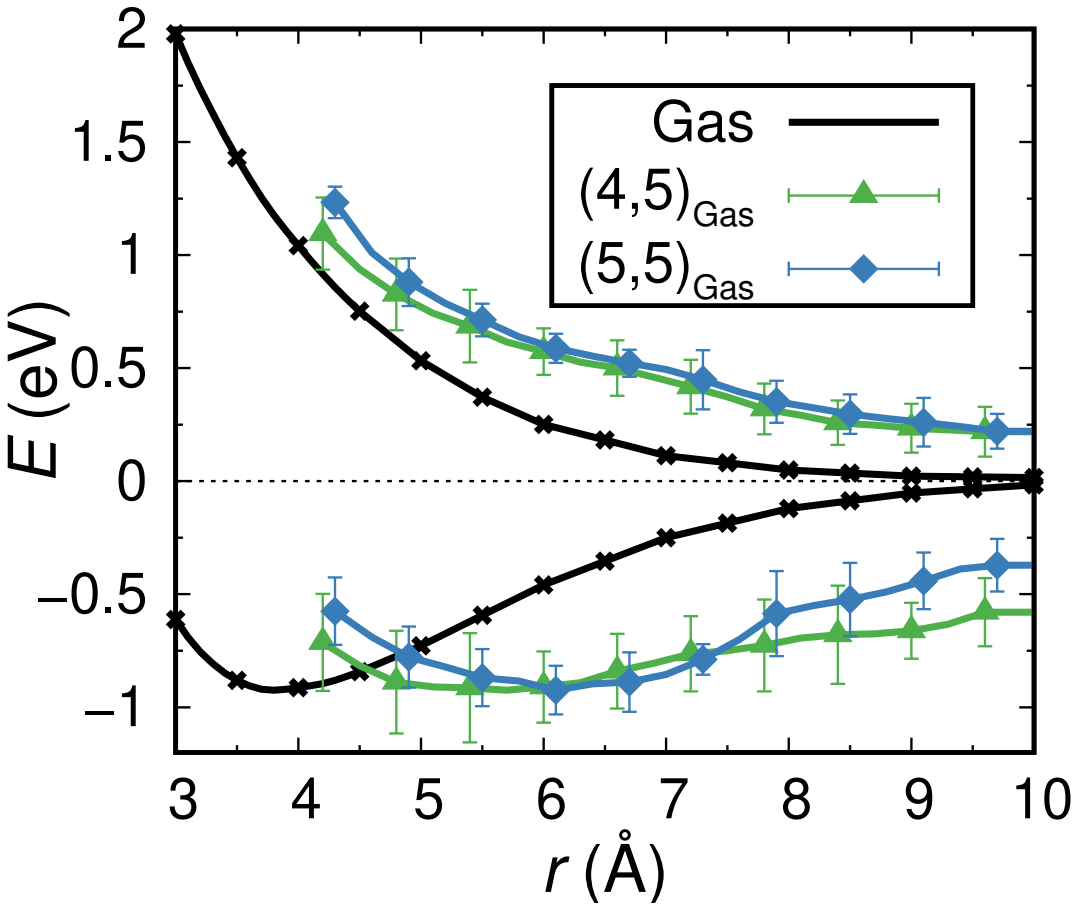

Figure 3.10: Potential energy curves (PECs) of the ground and first excited state of gas-phase Na_2^+ and the $Na_2(THF)_n^+$ coordinated structures in the gas phase. Clearly, the dynamics upon photoexcitation would be very different for the Na_2^+ in the gas phase and when solvated in liquid THF.

are not negligible, and we must go beyond a 'gas-phase potential surfaces transfer directly to the liquid' picture if we are to understand chemical bond dynamics in condensed phases.

3.5 Conclusions

In summary, comparative all-classical and MQC simulations of Na_2^+ in liquid Ar and liquid THF reveal that treating the solute's bonding electron explicitly quantum mechanically is necessary to understand the condensed-phase dynamics of this or indeed any solute. Even for simulations in apolar Ar, neglect of quantum effects of the solvent on the bonding electron density misses important features, such as the fluctuating dipole moment and thus IR activity of Na_2^+ induced by Pauli repulsion forces in the condensed phase. For Na_2^+ in THF, all-classical simulations not only miss these features but also predict changes in the bond length and vibrational frequency of the molecule that are completely opposite to the correct behavior, which can be properly described only quantum mechanically.

As we saw previously in studies of Na_2 in THF,[109] Na_2^+ in THF exists in several stable, interconverting coordination states that behave as discrete molecules with their own bond dynamics and spectral signatures. All the changes in chemical identity we noted in our previous work[109] are magnified when one of the bonding electrons of the molecule is removed: the solvent has an easier time altering the electronic structure of the sodium dimer cation than the neutral sodium dimer simply because it's easier to create dative bonds with the sodium cation cores when there's only one electron to push out of the way. For the sodium dimer cation, we also have shown that these coordinated states are stable in the gas phase and thus should be the 'true' gas-phase reference molecules for understanding the $Na_2(THF)_n^+$ coordinated species in the condensed phase, even though the strength of an individual dative bond is only $\sim$4 kcal/mol. Perhaps more importantly, we have predicted that these unique chemical species not only have distinct bond lengths and IR spectra, but also that they can be distinguished experimentally through transient hole-burning experiments by bleaching

one of the primary species and watching the spectral diffusion that interconverts the stable coordination states.

Finally, our MQC studies of Na_2^+ in THF also suggest that the electronic structure of the solute is dramatically altered by the local solvent environment, as shown by the completely different shape of the excited-state wavefunction and the correspondingly altered UV-Vis spectra of the $Na_2(THF)_n^+$ complexes compared to the gas phase. The coordination states also have potential energy surfaces that are qualitatively different from those of the gas-phase molecule, which suggests that the basic chemical identity of the solute, including its reactivity such as the breaking of the bond by photodissociation, will be entirely different for the $Na_2(THF)_n^+$ coordinated structures than for Na_2^+ in other environments.

3.6 Supplemental Information

To avoid repetition, only the sections of the supplemental information for "The Role of the Solvent in the Condensed-Phase Dynamics and Identity of Chemical Bonds: The Case of the Sodium Dimer Cation in THF" that differ from those given in Chapter 2 Section 6 are included here. If not otherwise specified, the simulation and analysis methods used for the work presented in this paper are the same as those used in "Solvents Can Control Solute Molecular Identity."

3.6.1 Mixed Quantum/Classical and All-Classical Models

Our mixed quantum/classical (MQC) molecular dynamics (MD) simulations consisted of two classical Na^+ cations, one fully quantum mechanical electron, and hundreds of classical solvent molecules (254 solvent molecules for simulations in liquid THF and 1600 for simulations in Ar). The simulation cell wide length was 32.5 Å for simulations in THF and 43.8 Å for simulations in Ar, sizes chosen to reproduce appropriate solvent densities at the simulation temperatures (0.89 g/mL at 298 ± 6 K for THF simulations and 1.26

g/mL at 120 ± 2 K for Ar simulations, which is well within the liquid region of simulated Ar's phase diagram[106]). The THF molecules were treated as rigid, planar five-membered rings following the work of Chandrasekar and Jorgensen.[103] This rigid planarity was enforced using the RATTLE algorithm, as in our previous MQC MD work.[86, 109] Periodic boundary conditions were implemented with minimum image convention[87] and all interactions were tapered smoothly to zero at 16 Å over a 2 Å range with a center of mass-based switching function according to Steinhauser.[105] The all-classical simulations in THF were constructed in the same manner as the MQC simulations in THF with the notable exception of the quantum mechanical electron, which is instead accounted for by allocating -0.5 e to each Na^+ core, making the simulation consist of two classical $Na^{+0.5}$ cores and 254 classical solvent molecules. All simulations were performed in the microcanonical ensemble.

For the MQC studies, the classical interaction between the two Na^+ cations was modeled through a point-charge Coulomb potential, $U^{Na^+-Na^+}(R) = 1/R$, since the short-range repulsion between the cores is negligible around the internuclear separation of Na_2^+. For the all-classical studies, this was replaced with a Morse Potential fit to the gas phase potential energy curve of Na_2^+:

$$V(r) = D_e(1 - e^{-a(r-r_e)})^2 \tag{3.1}$$

where D_e is the well depth, r is the distance between the two sodium cores, r_e is the equilibrium bond distance, and the factor a influences the width of the potential. The parameters for the Morse Potential used to model the $Na^{+0.5}$-$Na^{+0.5}$ surface are : D_e = 0.998889 eV, r_e = 3.86209 Å, and α = 0.537616 Å$^-$1.

All other classical interactions were modeled with Lennard-Jones potentials:[87]

$$u_{ij}(r_{ij}) = \frac{1}{4\pi\epsilon_0}\frac{q_i q_j}{r_{ij}} + 4\epsilon_{ij}\left[\left(\frac{\sigma_{ij}}{r_{ij}}\right)^{12} - \left(\frac{\sigma_{ij}}{r_{ij}}\right)^{6}\right] \tag{3.2}$$

where r_{ij} is the distance between the i^{th} and j^{th} solvent/Na^+ site, q_i is the charge on the i^{th} site, ϵ_{ij} is the potential well depth, and σ_{ij} is the finite distance at which the inter-particle

potential is zero. The Lennard-Jones parameters used in this study are listed in Table 3.2. The Lennard Jones parameters for the half-charged sodium cation cores used in the all-classical simulations were calculated by combining the Lennard Jones parameters for Na^+ and Na^0 used in our previous studies[86, 109] as per Chandrasekhar and Jorgensen,[103] using the Lorentz rule for σ and the Berthelot rule for ϵ. The standard Lorentz-Berthelot combining rules were also used to calculate the solute-solvent site and solvent site-solvent site interactions in THF.[87]

	σ (Å)	ϵ (kJ/mol)	q (e)
Argon	3.405	0.996	0.0
THF-oxygen	3.0	0.71	–0.5
THF-α-methyl	3.8	0.49	+0.25
THF-β-methyl	3.905	0.49	0.0
Na^+	1.67	22.07	+1.0
$Na^{+0.5}$	2.45	13.53	+0.5

Table 3.2: Lennard-Jones and coulomb potential parameters for Na_2^+, Ar, and THF.

Phillips Kleinman (PK) pseudopotentials were used to account for the interactions between the classical particles and the quantum mechanical electrons.[88] These PK potentials were modified with polarization potentials to correct for the frozen core approximation implicit in PK formalism.[27, 33, 89] For the electron-Ar interaction, $V^{e^- - \mathrm{Ar}}$, we used a modified version of the pseudopotential developed by Gervais *et al*,[92] described in detail in our previous work.[46] For $V^{e^- - \mathrm{Na}^+}$ and $V^{e^- - \mathrm{THF}}$, we used rigorously-derived psedopotentials previously developed by our group, the details of which can be found in Refs. 89 and 27, respectively. The final pseudopotential fits are presented here in Tables 3.3 and 3.4.

3.6.2 Simulation Setup

For the quantum mechanical valence electron in MQC simulations in THF, we used a basis of 64×64×64 grid points distributed over the entire 32.5 Å simulation cell. For simulations in liquid Ar, we used a basis of 32×32×32 grid points distributed over a cubic box with

i	c_i (a.u.)	α_i (a.u.)
1	-16.3145	0.124293
2	0.0455219	0.0322129
3	16.3213 81	0.124181

Table 3.3: Parameters used in the construction of the sodium-electron pseudopotential for use in Na_2^+ simulations, $\phi(r) = \sum_{i=1}^{3} c_i e^{-\alpha_i r^2}$. Further details of the sodium-electron pseudopotential can be found in Ref 89.

25-Å. The grid size and number of grid points were increased from our previous studies to accommodate future dissociation studies of Na_2^+ which will necessitate a larger grid. Still, the dimensions were chosen to keep the basis set as small as possible for each system while still capturing the spatial extent of electronic wave function, which was larger in THF than Ar. We centered the grid in the middle of the simulation cell and shifted all classical particles relative to the grid every 500 fs to avoid leakage of the wave function off the edges of the grid basis, so that the wave function was always located roughly in the center of the simulation cell. The classical particles were shifted an integer number of grid spaces to avoid discontinuities in the quantum energy that would prevent total energy of simulation from being conserved.[39] We used the velocity Verlet algorithm[87] to propagate the classical degrees of freedom ($\boldsymbol{v}_{\mathrm{Na}^+{}_i}$, $\boldsymbol{v}_{\mathrm{solv}_i}$, $\boldsymbol{R}_{\mathrm{Na}^+{}_i}$, and $\boldsymbol{R}_{\mathrm{solv}_i}$) of the Hamiltonian in Eqs. 1 and 2 in the microcanonical (N, V, E) ensemble. We determined the forces from the sum of the classical-classical and classical-quantum interactions described above. We used the implicit restart Lanczos method to iteratively solve the TISE for the ground state wavefunction at every time step (5 fs in Ar and 4 fs in THF).[108] The quantum forces on the classical particles were then found using the Hellman-Feynman theorem:

$$\boldsymbol{F}_i^Q = -\langle\Psi|\,\boldsymbol{\nabla}_{\boldsymbol{R}_i}\hat{H}\,|\Psi\rangle \tag{3.3}$$

where, $\boldsymbol{F}_i^Q$ is the quantum force on classical particle i at position $\boldsymbol{R}_i$. Because the wave function is expanded in a basis that does not functionally depend on the position of the

classical particles, Eq. 6 is exact (in other words, there are no issues with Pulay forces from the basis functions changing with time).[85]

Initial coordinates for these studies were taken from our previous MQC studies of Na_2 in Ar and THF and then propogated for an equilibriation period of several hundred ps to allow the system to adjust to the presence of only a single valence electron rather than the two valence electrons of Na_2. During equilibration, the classical particle velocities were occasionally rescaled to adjust the average temperature to the desired temperature (120 K for Ar and 298 K for THF) before a 1-ns production runs without velocity rescaling.

3.6.3 Coordination Number Interconversion

We extracted interconversion times between coordination states from our THF simulation trajectory by binning up the times the Na_2^+ molecule spent in each coordination state before converting to another. From this analysis, we determined conversion times of 15 $\pm$ 10 ps and 32 $\pm$ 11 ps for the $Na(THF)_4{-}Na(THF)_5^+ \rightarrow Na(THF)_5{-}Na(THF)_5^+$ and $Na(THF)_5{-}Na(THF)_5^+ \rightarrow Na(THF)_4{-}Na(THF)_5^+$ chemical reactions respectively.

To further support the concept that these conversions occur as chemical reactions, we performed an analysis of our data using transition state theory, similar to the method described in our previous work,[101, 109] briefly outlined here. According to transition state theory, inverse rates, τ, can be predicted according to $\tau = \tau_0 \exp\left(\frac{\Delta A^\ddagger}{k_B T}\right)$, where $\Delta A^\ddagger$ is the free energy barrier height for the interconversion and τ_0 is an inverse attempt frequency. We took $\Delta A^\ddagger$ to be the barrier height between coordination states, extracted from Fig. 3.2. With τ_0 set to 0.05 ps, conversion times of 16 ps and 35 ps for the $Na(THF)_4{-}Na(THF)_5^+ \rightarrow Na(THF)_5{-}Na(THF)_5^+$ and $Na(THF)_5{-}Na(THF)_5^+ \rightarrow Na(THF)_4{-}Na(THF)_5^+$ transitions. Presumably the free energy barriers to other coordination states are too high to enable access during equilibrium dynamics but could be explored using umbrella sampling.

3.6.4 Potential of Mean Force Calculations

All potential of mean force plots along the coordination number coordinate were calculated as the negative natural logarithm of the occurance probability of each state. First, we binned up the number of production run configurations in each state, assuming Poisson statistics such that the error was simply its square root of the number of counts in each bin. Next, we normalized the histogram results by dividing by the maximum bin count. Finally, we generated the PMF free energy values, A, in $k_{\mathrm{B}}T$ by taking the negative natural logarithm of the normalized bin counts. The normalization ensured that the most probable state is plotted at 0 $k_{\mathrm{B}}T$. The free energy error was propagated according to $\sigma = \pm\frac{\sqrt{\mathrm{bincount}}/\mathrm{maxbincount}}{\mathrm{bincount}/\mathrm{maxbincount}}$. Because the number of configurations in each Na_2^+ coordination state accessed at equilibrium in THF were similar, we did not need to use umbrella sampling to improve statistics (the relative population values for the $Na(THF)_4$−$Na(THF)_5^+$, and $Na(THF)_5$−$Na(THF)_5^+$ were 1:2 respectively). We also performed a similar analysis with bins along a coordinate consisting of the Na^+–Na^+ for each solvated configuration state.

The results of this analysis for the Na_2^+ coordination state and bond length are shown in the Figs. 3.2-3.3 (coordination state) and 3.5 (bond length). The free energy values for Fig 3.5 were converted to eV for better comparison between the results in liquid Ar and THF with the gas-phase potential energy surface.

3.7 Going Beyond The Frozen Core Approximation: Analysis of Na_2^+ in THF Utilizing a Coordinate-Dependent Na_2^{2+} Pseudopotential

In MQC simulations, the majority of the system is treated classically with quantum mechanics reserved for only a select few degrees of freedom. One way to determine this is by distinguishing between the system's valence electrons, which actively participate in the chem-

ical processes of interest, and the core electrons, which remain relatively unaffected. The interactions between the quantum mechanical valence electron(s) and the classical components of the system can be implicitly accounted for by using effective potentials that replace the explicit interactions between the core and valence electrons. These effective potentials are call pseudopotentials.[93] For our MQC MD simulations, we utilize Phillips-Kleinman (PK) based electron—Na^+ and electron—solvent pseudopotentials derived using methods that have been developed by our group.[27, 33, 89]

However, our pseudopotentials, like all pseudopotentials, are subject to the frozen core approximation (FCA)[114, 115] because such potentials are developed from a single configuration of the core electrons. Thus, for any situations where the wave function(s) of the core electron(s) change dynamically, the FCA pseudopotential will fail to capture the nuances of the interactions. For instance, in our MQC studies, only the bonding electron(s) of the simple diatomic molecule (Na_2 or Na_2^+) are treated quantum mechanically. Thus, the molecule's pseudopotential must be equal to the sum of the individual Na^+ pseudopotentials at the dissociation limit since the atoms have no interaction at that point. However, at shorter bond distances, simply summing the atomic pseudopotentials no longer correctly describes the bonding because at short distances the core orbitals of each Na^+ distort as the core electrons on one atom are polarized by those of the other. Because the FCA pseudopotential does not account for these changes to the core electrons, error is introduced into the simulations. Of course, due to their straightforward structure, we would not expect the Na_2 or Na_2^+ molecule to be strongly affected by the FCA. Likewise, for closed-shell solvents like Ar and THF, the FCA ought to do a reasonable job, especially for the Ar pseudopotential as we have added polarization terms to crudely account for the breakdown of the FCA at least in a pairwise additive way. Nevertheless, it is worth exploring how strongly the FCA influences the results of MQC MD simulations of Na_2^+, particularly given the complexity of this molecule's condensed phase dynamics.

In previous work,[116] our group outlined a way to avoid this issue by keeping track of

these core orbital changes and then calculating the pseudopotential as a function of the internuclear spacing, thus resulting in a pseupotential that is accurate at any given bond length. The coordinate-dependent pseudopotential thus constructed for Na_2^+ was found to be as accurate as a full Hartree-Fock calculation at all internuclear distances for gas phase Na_2^+.[116] However, it remained unclear how much difference this coordinate-dependent pseudopotential would make in condensed phase studies of Na_2^+. Here are briefly outlined results of MQC-MD simulations of Na_2^+ in THF utilizing the coordinate-dependent pseudopotential developed in [116] for comparison with the PK based pseudopotential used in the main studies outlined in this chapter.

3.7.1 Methods

The methods used for this study were identical to those used in the previous sections of this chapter with the exception of the use of the coordinate-dependent pseudopotential (as outlined in [116]) instead of the fixed-coordinate FCA pseudopotential. After equilibration, the MD trajectory (which contained 254 classical THF molecules, two classical Na^+ cores, and one quantum mechanical valence electron) was propagated adiabatically on the electronic ground state with a 4-fs time step for a 500-ps production trajectory.

3.7.2 Results

Because the classical interaction between the THF solvent molecules and the Na+ cores is unchanged in this simulation, we expect to see that same dative bonding peak in the Na–O pair distribution function here as observed in the above studies of Na_2^+ in THF. Indeed, as shown in Fig. 3.11, the $g(r)$ for the simulation utilizing the coordinate-dependent pseudopotential (dashed red curve, labeled as CD) is nearly identical to that of the $g(r)$ for the simulation using the pseudopotential subject to the FCA (black curve labeled FC), which is the same curve shown in Fig. 3.1 above. For both simulations, the dative bonding peak appears at 2.35 Å, just as it did for MQC simulations of THF-solvated Na^+–e^- tight-contact

pairs[85] and THF-solvated Na_2.[109] Although integration of the FCA dative-bonding peak reveals an average of 4.88 dative bonds per Na^+ core, the coordinate-dependent peak integrates to slightly less at 4.62 dative bonds per Na^+ core. This indicates that although the peak's position and sharpness is nearly identical, the subtle influence of a coordinate-dependent pseudopotential for the Na_2^{2+}–valence electron interaction does lead to differences in the observed behavior of Na_2^+ in THF.

Just as done previously for the simulations utilizing the FCA Na_2^{2+} pseudopotential, we used the counting function $S(r)$ (plotted in Fig 3.1 and 3.11) to define a continuous coordination number by counting the number of THF oxygen sites that reside within a given distance of the center of each sodium core and then calculated the free energy, or potential of mean force (PMF) of the system as a function of n, the number of coordinating solvent molecules on each sodium core, labelled Na_a^+ and Na_b^+, which is shown in Fig. 3.2a for the simulation utilizing the FCA Na_2^{2+} pseudopotential and Fig. 3.11 for the simulation using the coordinate-dependent pseudopotential.

Fig. 3.12a shows the plot of this potential of mean force (PMF) as a function of the number of Na^+ core–THF oxygen dative bonds on each Na^+ core, revealing energetic minima at the same $Na(THF)_5$−$Na(THF)_5^+$ and $Na(THF)_4$−$Na(THF)_5^+$ states that are accessed in the simulation utilizing the FCA Na_2^{2+} pseudopotential as well as at the $Na(THF)_4$−$Na(THF)_4^+$ state, as compared to Fig. 3.2a. As seen before, these states are connected via interconversion pathways. However, unlike in Fig. 3.2a, in this case, interconversation pathways also reach toward a few more coordination states (most notably the $Na(THF)_3$−$Na(THF)_5^+$ state) that are not energetically favored enough to retain the molecule. Slices along the coordination PMF for restricted values of either four ($n_{Na_a^+} = 4$) or five ($n_{Na_a^+} = 5$) THFs coordinated to one of the two sodium cores for the MQC simulation are plotted in Figs. 3.12b and c, respectively. Like the studies utilizing the FCA Na_2^{2+} pseudopotential, the stable coordination states are separated by energetic barriers of many k_BT, indicating that these states will likewise behave as discrete molecules with solvent integrated as part of the chemical identity of the solute.

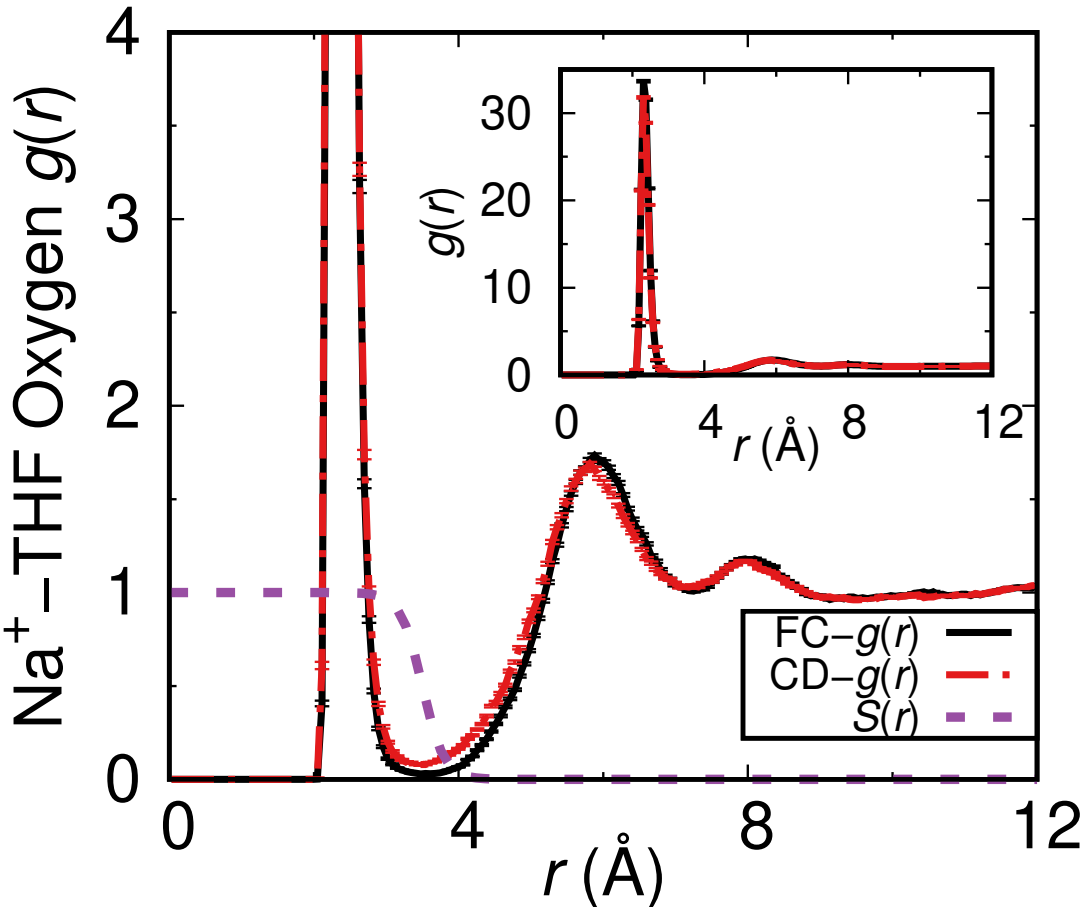

Figure 3.11: The pair distribution function, $g(r)$, shows near-identical Na^+–THF oxygen site chelation peaks for both the coordinate-dependent and FCA Na_2^{2+} pseudopotentials. The $g(r)$ for the simulations using the FCA Na_2^{2+} pseudopotential is plotted as a solid black curve while the $g(r)$ for the simulations using the coordinate-dependent Na_2^{2+} pseudopotential is plotted as red dashed line. In both sets of simulations, $g(r)$ is averaged over the Na+–THF oxygen site distances for both Na+ cores. The smooth weighting function, $S(r)$ (dashed purple curve) was used to define the solvent coordination number around each Na+core, as plotted in Figs. 3.2 and 3.12. The inset shows $g(r)$ on an expanded scale to reveal the full peak at the 2.35 Ådative-bonding distance. The error bars shown represent 95% confidence intervals.

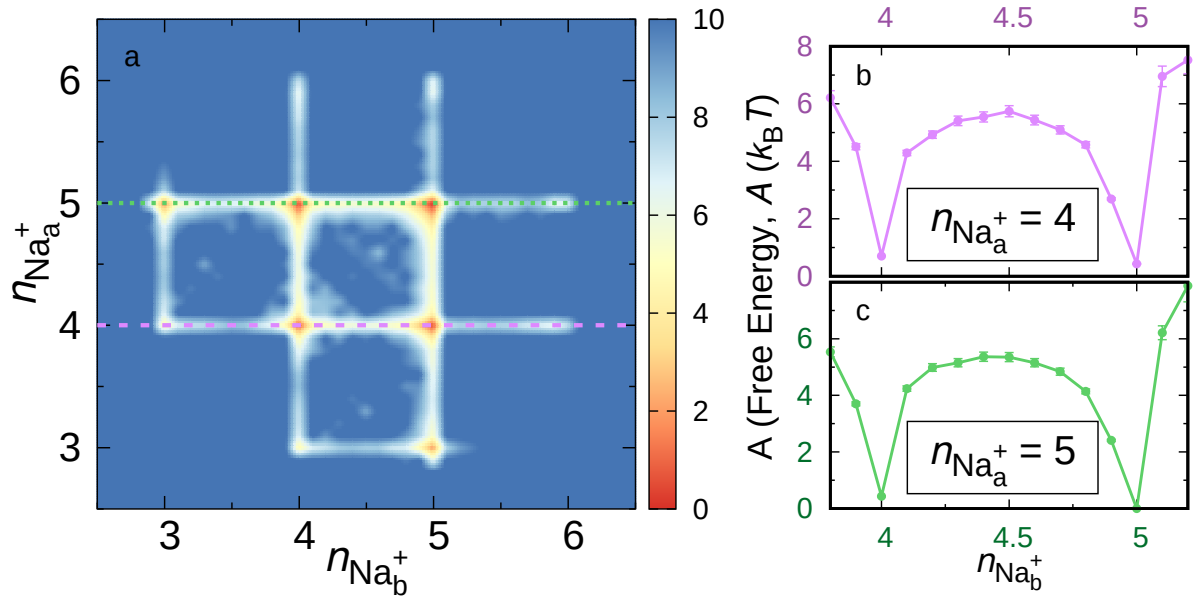

Figure 3.12: Potential of mean force as a function of the number of Na^+ core–THF oxygen dative bonds on each Na^+ core for the simulation utilizing a coordinate-dependent Na_2^{2+} pseudopotential calculated in the same manner as with Fig. 3.2. The energetic minima (shown as red/orange colors in panel (a)) occur at integer values. As seen previously for the simulation using the FCA Na_2^{2+} pseudopotential, the most prominent minima are those with four to five datively bond THF molecules per sodium core. However, here the $Na(THF)_4$-$Na(THF)_4^+$ state is fully accessed, along with pathways reaching toward but never quite settling into other coordination states. Slices along then $n_{Na_b^+}$ coordinate with $n_{Na_a^+}$, panel (b), and $n_{Na_a^+}$, panel(c), show more detail on the heights of the different minima and the barriers between them, indicating that as with previous studies, the accessed coordination states behave as discrete molecules. The only difference presented here is the accessing of new coordination states.

The energetic barriers depicted in Fig. 3.12b and c are shallower by about half a $k_{\mathrm{B}}T$ than those found when utilizing the fixed-coordinate FCA Na_2^{2+} pseudopotential, which assists the molecule in better accessing the $Na(THF)_4{-}Na(THF)_4^+$ state.

Figure 3.13 shows the potential energy surfaces (PES) along the Na–Na bond distance for the gas-phase Na_2^+ molecule both utilizing the FCA Na_2^{2+} pseudopotential (black curve) and the coordinate-dependent pseudopotential (grey curve). The most notable difference between these two curves is the decreased average bond distance of Na_2^+ when using the coordinate-dependent Na_2^{2+} pseudopotential ∼3.5 Å compared with ∼3.8 Å), which is more in line with the Hartree-Fock average Na_2^+ bond distance. For Na_2^+ in THF, the curves are plotted as follows: blue for the $Na(THF)_5{-}Na(THF)_5^+$ state (light blue for coordinate-dependent and dark blue for FCA), green for the $Na(THF)_4{-}Na(THF)_5^+$ state (light green for coordinate-dependent and dark green for FCA), and pink for the $Na(THF)_4{-}Na(THF)_4^+$ state (only accessed for simulations utilizing the coordinate-dependent Na_2^{2+} pseudopotential). The overall curves for THF are plotted as dashed purple (light purple for coordinate-dependent and dark purple for FCA). The apparent unphysical behavior of the overall surface in THF is even more pronounced for the simulation using the coordinate-dependent Na_2^{2+} pseudopotential. This is because the Na_2^+ molecule exists in multiple interconverting coordination states in THF; therefore, the full PMF is a Boltzmann-weighted average of the PMFs of the individual coordination states. Since the simulation using the coordinate-dependent Na_2^{2+} pseudopotential accesses the additional $Na(THF)_4{-}Na(THF)_4^+$, which has a lower average bond length (4.0 Å) than the other two stable states, thus causing even more distortion to the overall dynamics. This shows that in simulation using the coordinate-dependent Na_2^{2+} pseudopotential, treating Na_2^+ as multiple chemical species in equilibrium, rather than a single molecule in solution, is just as necessary, if not more so, than with the the simulation using the FCA Na_2^{2+} pseudopotential.

Overall, simulations of Na_2^+ in THF utilizing the coordinate-dependent Na_2^{2+} pseudopotential reveal similar results to those using the FCA Na_2^{2+} pseudopotential. Because the

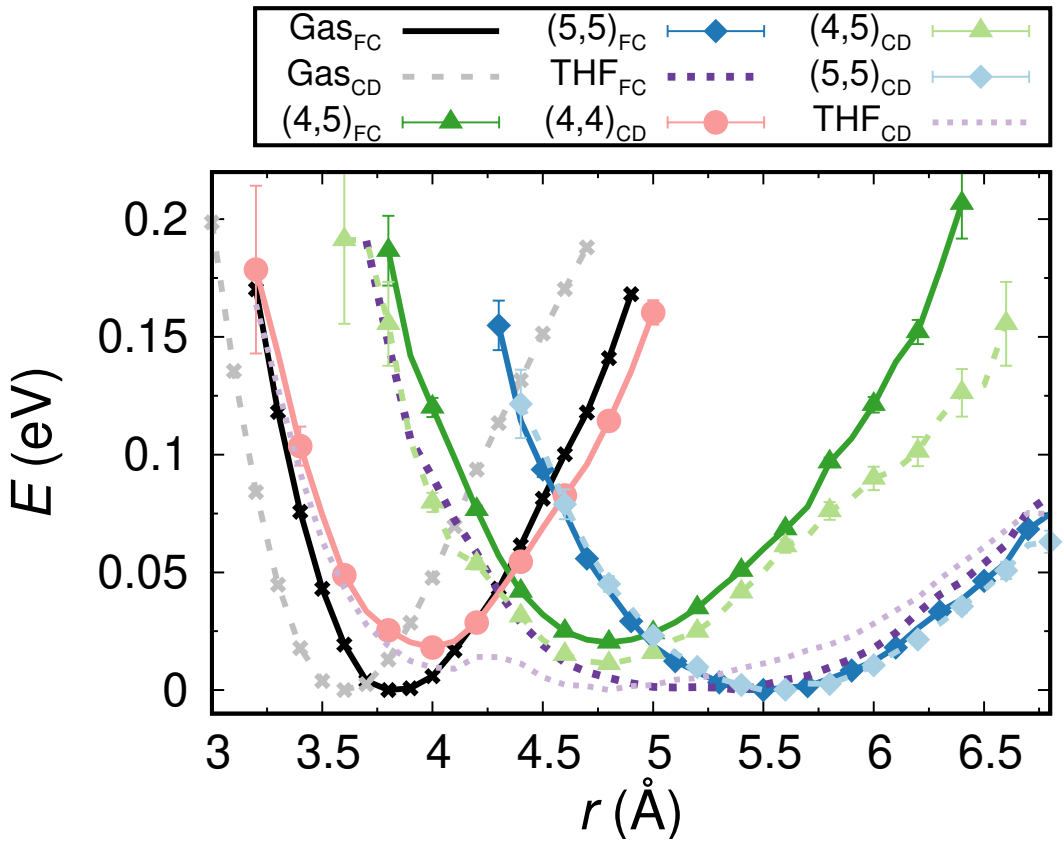

Figure 3.13: Potential of mean force for the simulations using the coordinate-dependent Na_2^{2+} pseudopotential reveal similarities to PMFs for simulations utilizing the FCA Na_2^{2+} pseudopotential with the notable exception of the contribution from the $Na(THF)_4$–$Na(THF)_4^+$ state (pink curve). The presence of this additional state in the overall dynamics causes an even greater broadening and distortion of the all-encompassing THF PMF. The gas phase curves are plotted as black (FCA) and grey (coordinate-dependent) curves while the curves in THF are plotted as blue for the $Na(THF)_5$–$Na(THF)_5^+$ coordination state, green for the $Na(THF)_4$–$Na(THF)_5^+$ state and pink for the $Na(THF)_4$–$Na(THF)_4^+$ states. The PMFs for the overall dynamics in THF are plotted as dashed purple curves. The error bars represent 95% confidence intervals

coordinate-dependent Na_2^{2+} pseudopotential captures the details of changes to the valence electron's wavefunction when the two Na^+ cores are close, the results should match more closely with those that would be obtained by full Hartree-Fock analysis, if full quantum simulations of such a complicated system were computationally feasible . However, several downsides prevent the use of the coordinate-dependent Na_2^{2+} pseudopotential for our current studies of Na_2^+ in the THF. First, because the coordinate-dependent Na_2^{2+} pseudopotential must be calculated on the fly at each timestep of the simulation, it is computationally much more expensive and time consuming than the fixed-coordinate FCA pseudopotential. Second, the coordinate-dependent Na_2^{2+} pseudopotential as described in [116] is tapered starting at 5.0 Å to the correct asymptotic r^{-1} behavior. Although such tapering is appropriate for the gas phase Na_2^+ molecule, it is not optimal for the $Na_2(THF)_n^+$ coordinated states because the average bond distance of these states fall right around the tapering distance. Therefore, if any minor irregularities are present in the pseudopotential at the onslaught of the tapering, they will be magnified in the $Na_2(THF)_n^+$ dynamics. It is important to note that the reason the $Na(THF)_4{-}Na(THF)_4^+$ state becomes allowed when using the coordinate-dependent pseudopotential is because the the Na–Na bond length for the $Na(THF)_4{-}Na(THF)_4^+$ falls within the the tapering region for the pseudopotential while the $Na(THF)_4{-}Na(THF)_5^+$ lies just at the edge of the tapering region and the $Na(THF)_5{-}Na(THF)_5^+$ beyond it. This means that it is expected for the $Na(THF)_4{-}Na(THF)_5^+$ and $Na(THF)_5{-}Na(THF)_5^+$ to behave quite similarly to their fixed-coordinate counterparts while the $Na(THF)_4{-}Na(THF)_4^+$ state, which is within the region influenced by the coordinate dependence, behaves differently.

To rectify any inaccuracies caused by the early tapering of the coordinate-dependent pseudopotential, a new coordinate-dependent pseudopotential would have to be developed using the methods in [116]. However, because for this system the differences between the simulation utilizing the coordinate-dependent Na_2^{2+} pseudopotential and the FCA pseudopotential are not qualitative–the behavior of the $Na_2(THF)_n^+$ species is the same in both simulations

with the only difference the relative stabilities of the various coordination states–and the computational cost of using the FCA pseudopotential is considerably less, we have chosen to use the FCA Na_2^{2+} pseudopotential for our further studies of Na_2^+ in THF.

Chapter 4

Linear Response Breakdown in Liquid Photodissociation: Caging and Chemical Identity

4.1 Abstract

Although most chemical reactions take place in solution, there is not a unifying set of principles for describing solution-phase chemistry. Typically, one assumes that solutes have the same electronic structure and bonding properties as in the gas phase, and it is often assumed that the equilibrium solvent fluctuations are enough to understand nonequilibrium chemical reaction kinetics, the so-called linear response (LR) approximation. In this paper, we use quantum simulation methods to show that neither of these assumptions holds during the photodissociation of simple diatomic solutes in solution. By studying the photoexcitation of Na_2^+ in both liquid Ar and liquid tetrahydrofuran, we show that LR not only breaks down, but that the reason for the breakdown is different in the two solvents. In liquid Ar, caging of the solute by the surrounding solvent molecules causes LR to fail because the solvent fluctuations are slower than the time scale of the photodissociation reaction. In liquid THF,

the breakdown of LR is more complicated, as the way both the electronic structure of the Na–Na bond and the chemical identity of the molecule changes as the bond lengthens is different at and away from equilibrium. Clearly, even simple reactions such as the breaking of chemical bonds need to be treated at a realistic level when they take place in solution.

4.2 Introduction

Most chemical reactions, including photodissociation reactions that use light to break chemical bonds, take place in solution. Since solution-phase reactions are inherently more complex than those in the gas phase, most studies of photodissociation and recombination dynamics have focused on simple diatomic molecules to elucidate solvent effects on chemical reaction dynamics,[1, 49–52, 64] with a particular emphasis on molecular iodine (I_2).[59, 61, 63, 70, 71, 117] Photoexcitation of I_2 and other solution-phase molecules results in fast dissociation followed by collision with the surrounding cage of solvent molecules that in turn results in direct (geminate) recombination, delayed (geminate) recombination, or dissociation and eventual non-geminate recombination.[1, 118]

How can one think about the solute and solvent motions involved in solution-phase photodissociation? For the solute, the standard approach when considering solution-phase reactions is to simply assume that the solute moves on the same potential energy surfaces as in the gas phase.[1] We have shown in recent work, however, that the Pauli repulsion interactions between the solvent and the solute's bonding electrons can change the electronic structure of a diatomic solute, inducing large instantaneous dipole moments and causing changes in the vibrational frequency and dissociation energy.[46] Moreover, we also have found that when there are local specific interactions between the solvent molecules and the solute that only need to have a strength comparable to a hydrogen bond, the electronic structure and even the chemical identity of the solute can be dramatically altered.[109, 119] Thus, the way in which solutes and solvents interact needs to be described in detail to understand

solution-phase chemical reactions.

For the solvent, the standard assumption made to understand solution dynamics is that of linear response (LR): the idea of LR is that for small perturbations, a nonequilibrium system should relax along a pathway identical to the regression of the spontaneous fluctuations of the system at equilibrium.[120] This means that one only needs to study the solvent fluctuations at equilibrium to understand nonequilibrium reaction dynamics, and the assumption is often invoked even when the strength of the reactive perturbation is many $k_{\mathrm{B}}T$. In other words, LR suggests that understanding equilibrium fluctuations is sufficient to be able to predict the kinetics a system follows away from equilibrium. Indeed, LR is commonly assumed in theories of electron transfer reactions.[4, 121, 122] However, LR has been shown experimentally to fail for a simple electron transfer reaction[121, 122] and for the rotational motions of photofragments produced following photodissociation;[123, 124] there is also evidence that the breakdown of LR can sometimes be hidden.[122] Many workers also have explored the failure of LR in solvation dynamics[121, 122, 125–127] and this breakdown has been associated with the presence of non-Gaussian solvent fluctuations.[128, 129]

This leads to the key questions explored in this paper: how does one think about the solute and solvent dynamics during a condensed-phase photodissociation reaction? Given that the solvent can influence a solute's dissociation pathway through effects like caging,[1, 52, 64] can we expect solution-phase photodissociation reactions to obey the LR approximation? If LR fails for such reactions, why? And what generalities about solution-phase photodissociation reactions can be learned by studying model systems, especially when local specific solute-solvent interactions can potentially alter the chemical identity of the solute?[109, 119] We directly address all of these questions through mixed quantum/classical (MQC) molecular dynamics (MD) simulations of the photodissociation of the Na_2^+ molecule in both liquid Ar and liquid tetrahydrofuran (THF). We choose this system because it is straightforward to model the appropriate quantum mechanical excited-state dynamics based on our previous studies of Na_2 in these solvents,[46, 109] and because unlike Na_2, Na_2^+ dissociates in its lowest

electronic excited state.[116] We find that not only does LR fail for the photodissociation of this diatomic solute in the condensed phase, but that the reasons for the breakdown can be entirely different depending on the specific solvent environment. In particular, by introducing a 'dynamical' potential of mean force (PMF), we show that solvent caging is a process that cannot be properly described with LR, and that changes in chemical identity during photodissociation also can cause LR to fail by completely altering the course of the excited-state dynamics.

4.3 Results and Discussion

To investigate how the linear response approximation breaks down in condensed-phase photodissociation reactions, we must first understand the LR predictions of the system of interest. We do this through a series of MQC MD simulations, the computational specifics of which are summarized in the methods section below and detailed in the Supporting Information (SI). Briefly, we treat the Na_2^+ molecule as two classical Na^+ cores that are held together by a single quantum mechanical valence bonding electron. We utilize previously-developed pseudopotentials[93] to describe the interaction between the bonding electron and the Na^+ cores[39] and 254 THF molecuels [27, 41, 86] or 1600 Ar[92] atoms, and solve the Schrodinger equation for the electron in a basis of 32^3 grid points in Ar and 64^3 grid points in THF. This methodology reproduces gas-phase quantum chemistry calculations quite well,[39, 116] and also has successfully reproduced the experimental properties of sodium cation:solvated electron tight-contact pair.[86, 101] Here, we calculate the behavior of the Na_2^+ molecule in 120 K liquid Ar at a density of 1.26 g/mL, well in the liquid region of the phase diagram, and at 298 K in liquid THF at the experimental density of 0.89 g/mL.

The LR approximation can be invoked in different ways. The simplest version says that the solvent fluctuations are independent of the electronic state of the solute, so that the solvent fluctuations at equilibrium with the solute's ground state can be used to predict what will

happen away from equilibrium even when the solute is placed on its electronic excited state. A more strict definition says that one should use LR only with the fluctuations associated with the solute electronic state of interest; that is, we need to examine the excited-state equilibrium fluctuations to predict nonequilibrium behavior on the excited state.[123, 124, 126, 128]

To begin our investigation of LR, we examined the equilibrium solvent fluctuations on both the electronic ground and first excited state of Na_2^+ in different liquid environments. This was accomplished by holding the Na–Na bond length at fixed distances through the application of an umbrella potential[87] centered at the distance of interest; we let the condensed-phase system equilibrate at each distance, and then calculated the average energy of both the ground and first electronic excited states. Stitching together these energies results in potentials of mean force (PMFs),[130] which are shown in Fig. 4.1. The black curves in Fig. 4.1 show the ground- and first excited-state potential energy surfaces of the Na_2^+ molecule in the gas phase calculated with our MQC methodology; the curves do an excellent job reproducing the known surfaces of this molecule, including the ground state vibrational frequency, bond dissociation energy, and lowest-energy electronic absorption.[116]

The solid, colored curves in Fig. 4.1 show the ground- (blue solid triangles) and first excited-state (red solid diamonds) PMFs for Na_2^+ in Ar (panel a) and in THF (panel b) calculated with the solvent at equilibrium with the solute occupying the state under investigation. The data in Fig. 4.1a show that on the Na_2^+ electronic ground state, compared to the gas phase, interactions with liquid Ar lead to a shorter equilibrium bond length (3.74 Å in Ar vs. 3.84 Å in the gas phase) and a higher Na–Na vibrational frequency (134 cm^{-1} in Ar vs. 113 cm^{-1} in the gas phase), much like we observed previously for the Na_2 molecule.[46, 109, 119] The red solid diamonds show that when the molecule is placed on the electronic excited state, the LR-predicted PMF is nearly identical to the potential energy surface in the gas phase, indicating that the equilibrium excited-state solvent interactions are small compared to the intrinsic gas-phase energy.

The dashed, colored curves in Fig. 4.1a test whether LR holds in the simplest sense: can PMFs for one solute state be predicted from equilibrium data when the solute resides in a different electronic state? In other words, are the solvent fluctuations associated with the two solute electronic states similar enough that the PMFs are independent of which surface we choose? The blue open triangles show the LR prediction for the Na_2^+ first excited state while the solvent is equilibrated with the electronic ground state; this prediction yields a dissociative surface that is raised in energy relative to the gas phase because when the solvent is equilibrated around the ground-state solute, it is in an unfavorable geometry for solvating the solute excited state. The red open diamonds show that when the solvent is equilibrated for the solute's excited state, there is a significant de-solvation and thus increase in energy and decreased vibrational frequency of the ground electronic state. Clearly, the simple application of LR fails: we cannot accurately predict the excited-state PMF while the solute resides in its electronic ground state because the way the solvent equilibrates around one solute electronic state destabilizes the other electronic state. Therefore, for this system, it makes more sense to use the stricter definition of LR: one should use the solvent fluctuations associated with the solute electronic state of interest to predict nonequilibrium dynamics.

Although the LR predictions for Na_2^+ in Ar are qualitatively similar to the gas-phase potentials, the situation turns out to be completely different for Na_2^+ in liquid THF. In previous work, we found that the oxygen atoms on THF make weak dative bonds with the Na^+ cores inside the Na_2^+ molecule.[109, 119] These dative bond interactions are only about the same strength as a hydrogen bond ($\sim$4 kcal/mol), but they cause the bonding electron density to be pushed out of the internuclear region, leading to a significant increase in bond length (increase from 3.84 Å in the gas phase to 5.24 Å in liquid THF) and a decrease in both vibrational frequency (from 113 cm^{-1} to 42 cm^{-1}) and bond dissociation energy (from 0.92 eV in the gas phase to 0.23 eV in THF).[119] We also found that the dative bonding interactions stabilize the Na_2^+ solute in two primary coordination states:

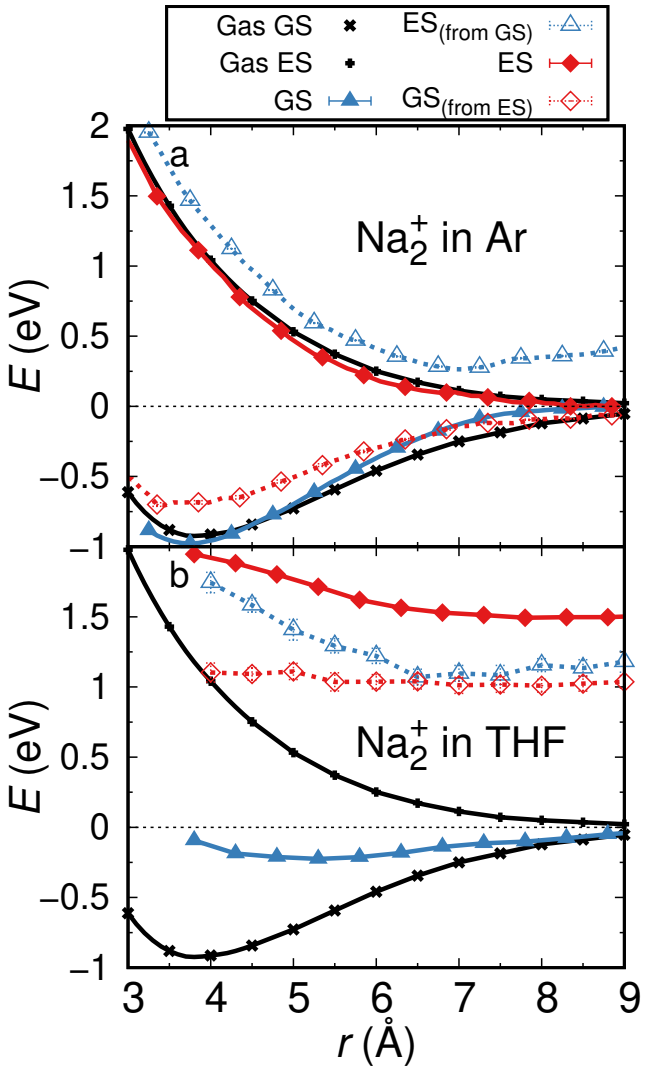

Figure 4.1: Equilibrium, linear response potentials of mean force for the Na_2^+ molecule in Ar and $Na_2(THF)_n^+$ in THF. The Na_2^+ gas-phase potential energy surfaces are plotted as the black curves. The condensed-phase PMFs are plotted as follows: solid blue triangles for the ground state, solid red diamonds for the excited state, dashed blue for the excited state calculated while propagating the solvent dynamics on the ground state, and dashed red for the ground state as calculated while propagating the solvent dynamics on the excited state. Panel (a) shows the PMFs for Na_2^+ in Ar while panel (b) shows the results in THF. A comparison of the solid and dashed curves shows that the solvent fluctuations are different on the ground and excited electronic states. Thus, for the best comparison of the equilibrium, LR prediction for the excited state to the nonequilibrium photodissociation dynamics, we will focus on the excited-state PMF calculated with the solvent dynamics also run on the excited state (solid red diamonds).

$Na(THF)_4$−$Na(THF)_5^+$ and $Na(THF)_5$−$Na(THF)_5^+$. These coordination states behave as distinct molecules whose chemical identity is different both from gas-phase Na_2^+ and from each other; the two coordination states are in equilibrium with each other and have to surmount a barrier of $\sim 8\ k_B T$ to interconvert.[119] Each coordination state has its own bond length, vibrational frequency and dissociation energy. In other words, in THF, the solvent has integrated itself as part of the chemical identity of two different Na_2^+-based solutes.[109]

Figure 4.1b shows that because of the change in chemical identity, the LR predictions for the Na_2^+ molecule in THF are entirely different than those in the gas phase or in liquid Ar. First, the PMFs shown in Fig. 4.1b must be understood as the combined result of the behavior of multiple coordination states that interconvert; we will argue below that one of the issues concerning breakdown of LR in this solvent is that the chemical identity actually changes as a function of the Na–Na bond distance. The most prominent feature of Fig. 4.1b is that the excited-state PMF for solvation on the ground state (open blue triangles) is hardly dissociative in the Frank-Condon region relative to the gas phase, and has almost no driving force for dissociation past a Na–Na distance of ∼7 Å. This trend is exacerbated for the stricter LR definition with the PMF calculated with the solvent equilibrated with the solute excited state (solid red diamonds), indicating that the local specific interactions with the solvent completely change the electronic structure of the molecule. Moreover, the LR prediction for the ground-state surface while propagating on the excited state (open red diamonds) is completely destabilized and is not bound at all along the Na–Na coordinate. Clearly, one cannot assume the solvent fluctuations are anywhere remotely similar on the ground and electronic excited states of Na_2^+ in liquid THF, constituting a breakdown of the simpler application of LR[126, 128, 129] from the outset. This again leads us to the question of whether the stricter version of LR, using PMFs calculated with the solvent equilibrated for each state, are at all meaningful in predicting the nonequilibrium dynamics of the Na_2^+ molecule following photoexcitation.

To test the stricter version of LR, we need a method to compare the LR predictions to the

actual excited-state dissociation dynamics. We ran a series of 15 nonequilibrium trajectories in Ar and 20 nonequlibrium trajectories in THF, starting from equilibrated configurations near the PMF minimum in the Na_2^+ electronic ground state (∼3.7 Å in Ar; ∼5.4 Å in THF), and then placing the molecule on the electronic excited state to simulate photoexcitation. We then calculated the effective potential surface on which the excited Na_2^+ moved during nonequilibrium dissociation by:

$$U(t) = -\int_{t_0}^{t} F(t)v(t)dt, \tag{4.1}$$

where $F(t)$ is the total force (from the solute and solvent) on the Na nuclei along the bond axis, $v(t)$ is the bond velocity, and t_0 is the time at which photoexcitation takes place. Since we also know the trajectory that the dissociating molecule takes, $r(t)$, we can parametrically combine $U(t)$ and $r(t)$ to produce an effective potential surface followed during the dynamics, $U(r)$, as described in the SI. The time t in Eq. 4.4 is chosen to range up to ∼300 fs in liquid Ar and to ∼1000 fs in liquid THF, which is long enough to have sampled all the appropriate photodissociation dynamics but short enough to avoid diffusive recrossings that occur at longer distances. We refer to the nonequilibrium $U(r)$ curves as 'dynamical PMFs'; they show the effective potential the system moves on when away from equilibrium. The dynamical PMFs and our analysis of it serve as parallels to the work presented by Zanuttini et al where they connect solvent collisions to dissociation pathways.[52] The nonequilibrium ensemble-averaged dynamical PMFs following photoexcitation of Na_2^+ in solution are shown as the green curves in Fig. 4.2. The raw trajectory data used for the dynamical PMF calculations are shown in the SI for reference.

Figure 4.2a shows that following the initial excitation, the nonequilibrium dynamical PMF for Na_2^+ in liquid Ar has a slope that is quite similar to that in the gas phase, which is also very similar to the strict LR prediction. This is in agreement with prior work studying diatomic photodissociation in rare-gas solids,[52, 81, 117] and with the idea of early time

'inertial' solvent motions in solvation dynamics following LR.[121, 122] But after the first ∼1 Å (∼60 fs) of separation, the dynamical PMF in liquid Ar shows a positive slope; this occurs at exactly the internuclear distance at which the expanding Na_2^+ molecule collides with the first-shell solvent; there is essentially always a collision with the first-shell solvent that exerts a force on the expanding molecule back towards shorter bond distances. By ∼7 Å (∼200 fs), the slope of the dynamic PMF has decreased to roughly zero, indicating that the dissociated solute has on average escaped the solvent cage and that the dynamics are now governed more by diffusion than the electronic structure of Na_2^+. Clearly, LR breaks down for the photodissociation of Na_2^+ in Ar because even the strict LR definition does not include solvent caging, which is clearly a nonequilibrium effect: there are no strong directional collisions like this at equilibrium.

The green curve in Fig. 4.2b shows the dynamical PMF following photoexcitation of Na_2^+ in liquid THF. The dynamical PMF displays two main features: a small initial 'dip,' at an internuclear separation of ∼5.6 Å, followed by a general increase in energy at longer distances. What this dynamical PMF shows is that following photoexcitation, the Na_2^+ species elongates but does not dissociate due to a kinetic trap stemming from the dative bonds formed between Na^+ and THF. These effects are discussed later in Fig. 4.5. The dynamical PMF provides a strong contrast to the gas-phase (black curve) potential surface and the solution-phase LR predictions (red diamonds), both of which predict that the molecule would dissociate. Thus, the breakdown of LR for photodissociation of Na_2^+ in liquid THF is strikingly different than that in liquid Ar. It is perhaps not surprising that LR fails in both solvents, as photodissociation represents an input of energy that is 20–40 times k_BT, but Figure 4.2 shows clearly that the reasons for LR breakdown are highly dependent on the specifics of the solvent environment for what is nominally the same molecule.

To understand why LR fails so differently for photodissociation of Na_2^+ in liquid Ar and liquid THF, we next turn to exploring the nonequilbrium behavior in each solvent in more detail. In liquid Ar, the failure of LR involves a strong interaction of the photofragments

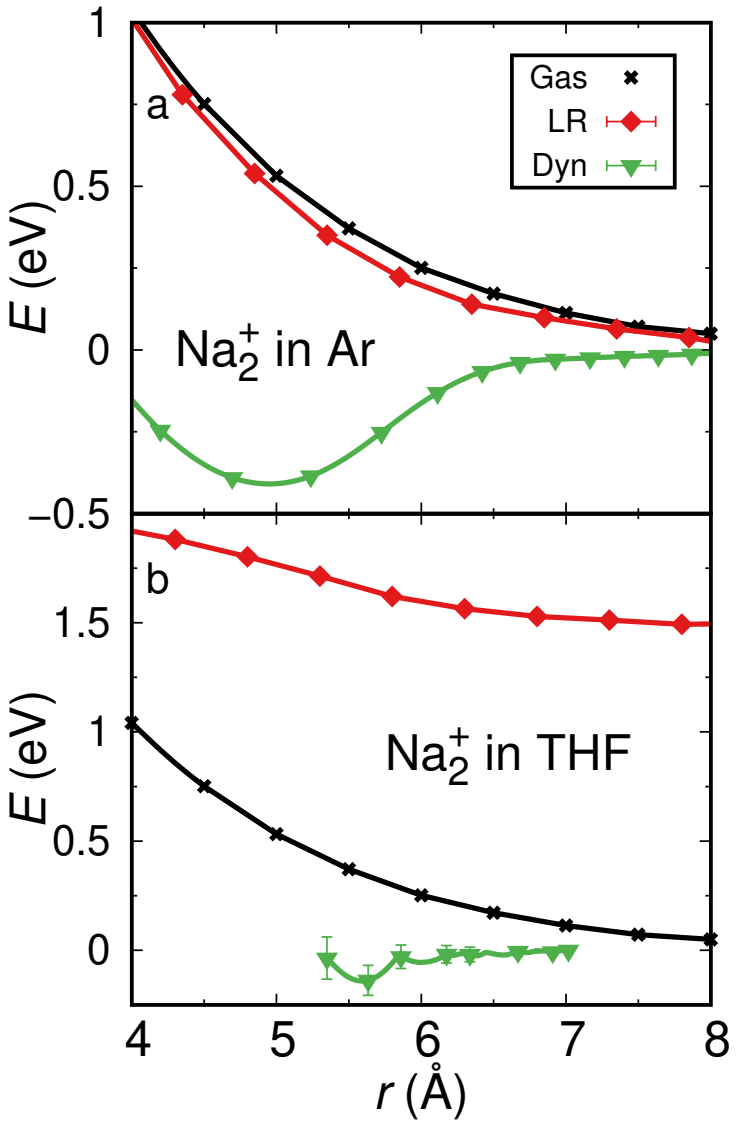

Figure 4.2: Dynamic potentials of mean force reveal the breakdown of linear response for the photodissociation of Na_2^+ in solution. The potential energy surface for the first excited state of gas-phase Na_2^+ (black crosses) and the PMF for the electronic excited state as predicted from LR (red diamonds) are the same curves as in Fig. 4.1; the dynamic PMF calculated from nonequilbrium trajectories using Eq. 1 (green triangles) is shown for Na_2^+ in Ar (panel a) and in THF (panel b). The dynamic PMFs show clear nonequilibrium features of the Na_2^+ dissociation reaction that are not predicted by LR at equilibrium. In Ar, the well at $\sim$ 5 Å in the dynamic PMF is the result of nonequilibrium caging by the surrounding solvent, as explored further in Fig. 4.3, below, while the gradual upward slope of the dynamic PMF in THF comes from changes in the electronic structure and chemical identity of Na_2^+ in this solvent, as detailed in Figs. 4.4 and 4.5, below.

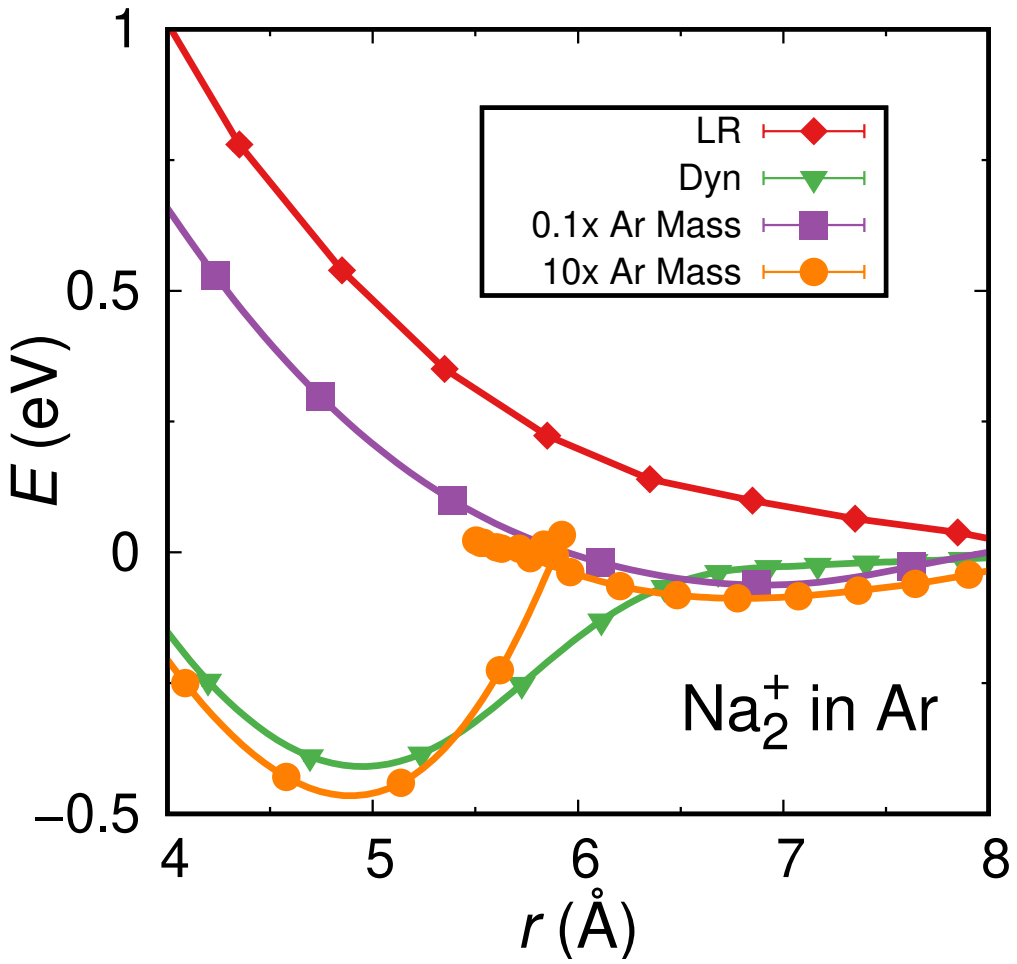

Figure 4.3: Dynamic potentials of mean force from nonequilibrium simulations of the photodissociation of Na_2^+ in liquid Ar as a function of the Ar mass reveal that the magnitude of the breakdown of linear response due to solvent caging is dependent on the time scale of the solvent fluctuations. Panel (a) shows the results when the Ar mass is divided by 20 (purple squares) and increased by a factor of 5 (orange circles) but the intermolecular potentials are left unchanged from the original simulations (green triangles, same curve as in Fig. 4.2a) and the LR approximation (red diamonds, same curve as in Fig. 4.1a). When the solvent mass is reduced to the point where fluctuations occur on a time scale comparable to the Na_2^+ photodissociation dynamics, the dynamical PMF begins to resemble the LR prediction. When the solvent mass is increased, however, the initial collision with the solvent cage knocks the photofragments back with much greater force, dynamics that are not seen at equilibrium. This leads to a temporary shortening of the Na–Na bond length before the fragments ultimately escape the solvent, creating the loop in the dynamical PMF.

with the Ar solvent cage that does not occur at equilibrium. This leads to the question of whether equilibrium dynamics could ever capture this type of caging event. To explore this, we tuned the time scale of the Ar solvent fluctuations by artificially changing the Ar mass while leaving all the intermolecular potentials unchanged; this means that the equilibrium solvation structures do not change, but the time scale for equilibration does. We then ran nonequilibrium trajectories with the altered solvent mass. Figure 4.3 shows that when the mass of the Ar atoms is reduced by a factor of 20 (purple squares), the dynamical PMF now strongly resembles the LR prediction (red diamonds). The solvent is now so light that the dissociating Na_2^+ molecule can easily push the nearby atoms aside, removing the 'caging' event that dominated the dynamics when the Ar had its full mass. In other words, the artificially lighter Ar solvent can equilibrate on a time scale comparable to the time it takes photoexcited Na_2^+ to dissociate, so that LR becomes a better predictor of the nonequilibrium dynamics.

Figure 4.3 also explores the other extreme, where the mass of the Ar solvent atoms is increased by a factor of 5 (orange curve). Now the 'cage effect' is exaggerated, as the dynamical PMF shows not only a stronger reflection, but actually a small loop at internuclear separations near 6 Å, the result of the fact that the dissociating Na_2^+ solute has to undergo multiple bounces before being able to escape the surrounding solvent cage, as seen for I_2 in solid rare gas matrices.[70] Thus, even in a simple, non-interacting solvent like liquid Ar, LR will fail to describe photodissociation reactions when the time scale of dissociation is faster than the intrinsic time scale of the solvent fluctuations.

To better visualize solvent caging, Fig. 4.4 shows plots of the average solvent positions around Na_2^+ in liquid Ar as a function of distance both at equilibrium, panel (a), and during the nonequilibrium photodissociation dynamics, panel (b). The plots show an isosurface at a distance about the van der Waals size of the solute molecule, ∼3.3 Å from each Na^+ nucleus, and the color represents the cylindrically-averaged probability of finding a solvent atom at that point on the surface relative to the bulk solvent density. The red color indicates

that more Ar is present than the average density, white shows about an average amount of solvent, while blue color shows a deficit of solvent at that position. The points are evenly spaced so that the color density provides an accurate representation of the spatial density of solvents.

The left-most plots compare the solvent distribution around Na_2^+ in Ar at equilibrium in the excited state (panel a) and at equilibrium in the ground state (panel b, which has a ground-state solvent configuration because it shows the Franck-Condon excited solute before the solvent has had time to move). Clearly, the equilibrium ground and excited-state solvation structures are different. When the Na–Na bond is separated by 3.5 Å and 5.5 Å at equilibrium on the excited state (left and center plot in panel (a)), there is a clear preference for the solvent to reside near the 'neck' of the molecule, as the excited-state electron density has a node between the two atoms, causing the solvent to move into this region to maximize ion-induced dipole interactions. During the nonequilibrium dynamics, however, the center plot of panel (b) shows that there is a deficit of solvent in the neck region, and excess solvent at the ends of the molecule as it encounters the solvent cage. The solvent has not had time during the 180 fs since excitation to move into the neck region or away from the ends of the dissociating molecule, showing the caging that explains the breakdown of LR. This breakdown persists even as the molecule separates to 8 Å which is 260 fs after excitation, as evidenced by the deficit of solvent on the inside of the bond in the right plot of panel (b) compared to the excited-state equilibrium prediction in panel (a).

Unlike in liquid Ar, where LR can be largely recovered if the solvent can fluctuate on fast time scales compared to the molecular dissociation, the LR breakdown for photodissociation of Na_2^+ in liquid THF occurs because the chemical identity of the Na_2^+ molecule is intricately linked with its local solvent environment, such that it is better thought of as $Na_2(THF)_n^+$.[109, 119] To understand how the complexation by the solvent affects LR, we turn to Fig. 4.4 c and d (left), which shows that when $Na_2(THF)_n^+$ is initially photoexcited to its lowest energy excited state, the node in the electron density lies oriented along the bond axis: the electronic

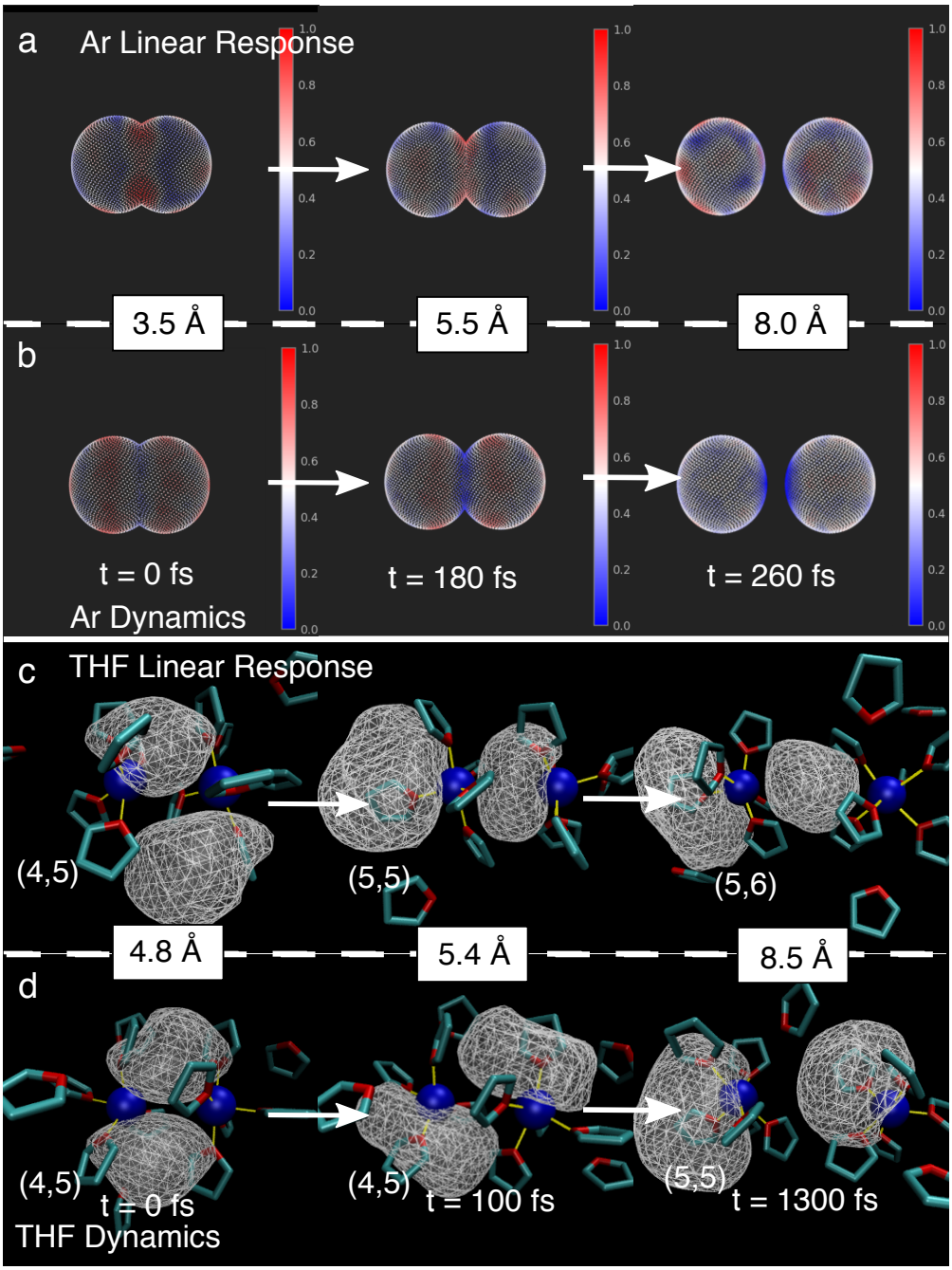

Figure 4.4: Representative solvent distributions around excited-state Na_2^+ at equilibrium, panel (a), and during non-equilibrium dynamics, panel (b), in liquid Ar. Surfaces are drawn ~3.3 Å from the Na^+ core and colored to show either bulk solvent density (white), excess solvent density (red), or solvent deficit (blue). Corresponding representative snapshots of excited-state $Na(THF)_4$−$Na(THF)_5^+$ in liquid THF are shown at equilibrium, panel (c), and during the non-equilibrium dynamics, panel (d). Na^+ cores are plotted as blue spheres and THF as turquoise sticks with red O atoms. The bonding electron is drawn as a wire mesh containing 75% of the charge density.

structure resembles that of a molecular π bonding orbital rather than the σ^* antibonding orbital seen with gas-phase Na_2^+ or Na_2^+ in liquid Ar (see SI).[119] This is a reflection of the fact that the coordination complex in liquid THF is truly a different molecule with a different chemical identity from the gas-phase Na_2^+ species.

If we start from a $Na(THF)_4{-}Na(THF)_5^+$ configuration, the molecule begins its dissociation process from its equilibrium ground state distance of ∼4.8 Å.[119] Following photoexcitation, the molecule's Na–Na bond distance increases to ∼5.4 Å after approximately 100 fs, but the electronic structure at this time (Fig. 4.4d, center) is clearly very different than the LR prediction at the same distance (Fig. 4.4c, center). The LR prediction when the molecule reaches this distance has the node of the electronic wavefunction perpendicular to the bond, creating a dissociative force. But the wavefunction during the nonequilibrium dynamics is clearly unable to have its node fully rotate from parallel to perpendicular to the Na–Na bond. This rotation of the excited-state node requires significant rearrangement of the datively-bonded THF molecules; there is simply insufficient time for these THFs to reach their equilibrium stable orientation. Finally, even 1.3 ps after photoexcitation, the molecule is not able to dynamically reach distances past 8.5 Å; this is because there is significant electron density still between the nuclei, holding the molecule together. This is what is responsible for the positive slope in the dynamical PMF at long distances seen in Fig. 4.2b: even though the molecule would prefer to dissociate at equilibrium, there is no easy kinetic pathway to achieve dissociation following the actual photoexcitation.

In addition to the inability of the excited-state wavefunction to achieve the correct configuration for dissociation, there is a second reason LR breaks down for photoexcitation of Na_2^+ in liquid THF: the chemical identity of the molecule changes differently during photodissociation than when the bond is stretched at equilibrium. At the Franck-Condon ground-state equilibrium distance, the molecule prefers to reside in the $Na(THF)_4{-}Na(THF)_5^+$ coordination state. As the Na–Na distance is increased at equilibrium on the excited state, Fig. 4.4c shows that the coordination state changes to predominantly $Na(THF)_5{-}Na(THF)_5^+$ by 5.4

Å and to the $Na(THF)_5{-}Na(THF)_6^+$ state by 8.5 Å, the result of the extra space available to form additional dative bonds shown as yellow lines. During the photodissociation process, however, Fig. 4.4d shows that there has been insufficient rearrangement of the coordination complex to allow an additional dative bond to form when the Na–Na distance reaches 5.4 Å, and only a single additional dative bond can form by 8.5 Å instead of the two extra dative bonds seen at equilibrium. The insertion of the last dative bond is what is critical to allowing the molecule to fully dissociate, as this is what weakens the bonding electron's association with the more coordinated sodium.

To better visualize how the electronic structure and chemical identity explain the breakdown of LR for the photodissociation of Na_2^+ in THF, Fig. 4.5a plots the number of solvent molecules forming dative bonds with each Na^+ core as a function of the Na–Na bond distance both at equilibrium on the excited state (red curves) and during the nonequilibrium dynamics (green curves). The dashed curves in this figure show the average number of THF dative bonds to the lesser-coordinated sodium core (referred to as Na_a) while the solid curves show the number of dative bonds around the more-coordinated sodium core (referred to as Na_b). At equilibrium on the excited state, the LR prediction is that there are two transitions to new coordination states, a $Na(THF)_4{-}Na(THF)_5^+ \rightarrow Na(THF)_5{-}Na(THF)_5^+$ transition around 5.5 Å and a $Na(THF)_5{-}Na(THF)_5^+ \rightarrow Na(THF)_5{-}Na(THF)_6^+$ transition around 8.5 Å, as visualized in the snapshots in Fig. 4.4c. However, the photodissociation dynamics shows only the first of these transitions (which is not complete until a distance of nearly 7 Å, in concordance with the snapshots shown in Fig. 4.4d.

Figure 4.5b provides a way to understand the changes in electronic structure that contribute to the breakdown of LR. The plot shows the angle of the node in the excited electronic wavefunction with respect to the Na–Na bond axis, calculated as an ensemble-averaged dot product of the Franck-Condon excited state at the equilibrium distance with the LR (red diamonds, equilibrated on the excited state) or dynamic (green triangles) excited state at other Na–Na distances. As such, a 'node orientation' of zero indicates that the node is

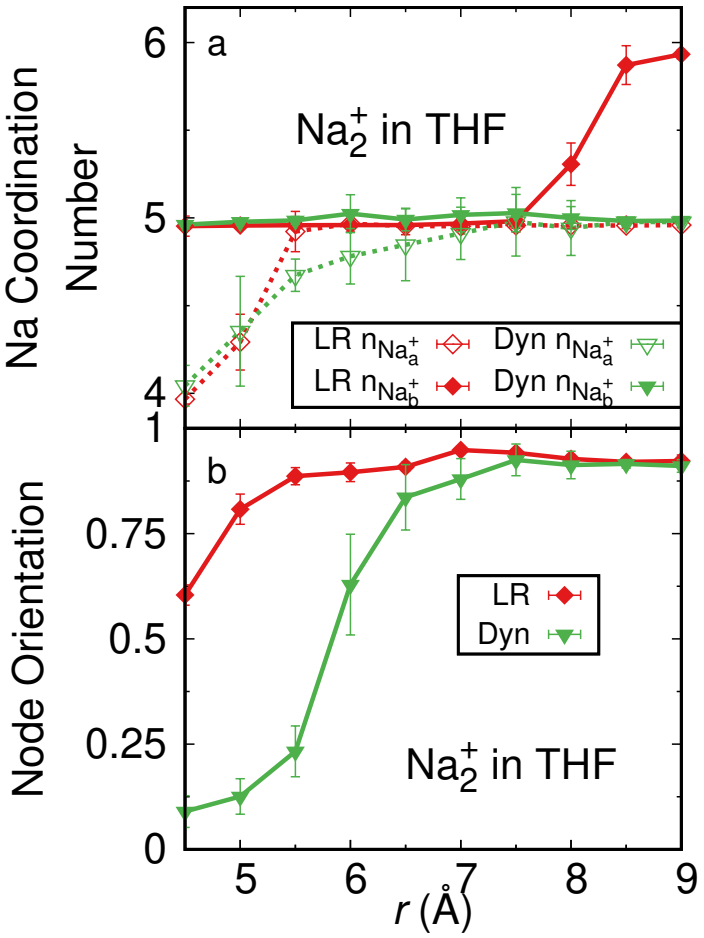

Figure 4.5: Changes in the $Na_2(THF)_n^+$ chemical identity (i.e., THF coordination number) and the orientation of the bonding electron density explain the breakdown of linear response for the photodissociation of Na_2^+ in THF. Panel (a) plots the THF dative bond coordination number around each sodium core (more coordinated Na^+, solid curves; less coordinated Na^+, dashed curves) as a function of Na–Na bond length for the LR equilibrium approximation (red) and during the dynamic, nonequilibrium dissociation (green); there is insufficient time for the coordination number to change during the nonequilibrium dynamics to match the LR prediction. Panel (b) shows the orientation of the excited-state bonding electron's node for the LR equilibrium approximation (red) and the dynamic, nonequilibrium dissociation (green) as a function of Na–Na bond length. Clearly, the node rotation is hindered during the nonequilibrium dynamics. Together, the inability for the node to rotate and the coordination number to change during the dynamics explains the breakdown of LR.

perfectly parallel with the Na–Na bond axis while a value of one means that the node is perfectly perpendicular to the Na–Na bond axis. Figure 4.5b shows that at equilibrium, the node is able to rotate fully at a much lower Na–Na bond distances (∼5.5 Å) than following dynamic photoexcitation (where the node doesn't fully rotate until ∼7 Å), the result of the fact that following photoexcitation the datively-bonded THFs don't have time to move to an appropriate position to allow the node to rotate.

The changes in the Na_2^+ chemical identity coupled with the changes in the electronic structure of the bonding electron during the nonequilibrium dissociation of Na_2^+ in THF explain the dramatic deviation of the dynamical PMF from the LR prediction shown in Fig. 4.2b. The preliminary 'dip' in the dynamic PMF arises because upon photoexcitation, the bonding electron's wavefunction must orient on the fly from a π-like to a σ^*-like electronic structure; in addition, the molecule must potentially change chemical identity through the formation of new Na–THF oxygen-site dative bonds. However, these processes consume the energy the molecule needs to form the final dative bond that at equilibrium takes the loosely-bound $Na(THF)_5{-}Na(THF)_5^+$ state to the $Na(THF)_5{-}Na(THF)_6^+$ state allowing the bond to break. This leaves the nonequilibrium molecule without an easy kinetic pathway to dissociate until sufficient time has passed for equilibration to occur.

4.4 Conclusions

In summary, through MQC MD simulations of Na_2^+ in the condensed phase, we have shown that LR breaks down for the photodissociation of Na_2^+ in both liquid Ar and in liquid THF for very different reasons. In liquid Ar, the initial collision of the dissociating molecule with the surrounding cage of Ar atoms is a nonequilibrium event that is not captured by the LR approximation. This singular event, which is reminiscent of the single-collision that causes breakdown of LR in photofragment rotational dynamics,[123, 124] is captured by the dynamical PMF, which shows the strong restoring force provided by the surrounding solvent

cage. The cage effect is clearly dynamical, as we showed that it depends on the magnitude of the solvent's mass: heavier masses amplify the bounce back of the photofragments upon collision with the solvent cage, while sufficiently light masses lead to better agreement with LR because the lighter solvent can equilibrate on the time scale of the dissociation dynamics. We also showed that the LR approximation fails for the photodissociation of Na_2^+ in THF; however, the reason for this LR breakdown arises not from solvent caging but from solvent-induced changes in the Na_2^+ molecule's chemical identity and electronic structure. During dynamic, nonequilibrium dissociation, the solute is unable to re-orient its bonding electron density from the π-bonding-like state created initially upon photoexcitation to the more σ^*-like state that is needed for dissociation. In addition, photoexcitation does not provide sufficient time for the molecule to undergo the change in chemical identity, via the creation of new dative bonds with the solvent, that is also needed for the bond to fully break. This leaves the molecule without a kinetically favorable path to dissociation, leading to a failure of LR, which is unable to capture these important solvent-induced features. All of this work shows that in solution environments, a detailed understanding of the coupling of solute and solvent motions is needed even to understand the simplest of chemical reactions, such as the breaking of a chemical bond.

4.5 Methods

4.5.1 Overview of Simulation Details

The work in this paper consists of mixed quantum classical (MQC) molecular dynamics (MD) simulations of Na_2^+ in the condensed phase. In these simulations, which were performed in the microcanonical ensemble, we treated the Na_2^+ molecule as two classical Na^+ cores held together by a single quantum-mechanically-treated valence bonding electron plus hundreds of classical solvent molecules. The interactions between the classical particles and the quantum mechanical electron were accounted for using Phillips-Kleinman (PK) pseudopotentials,[88]

modified with polarization potentials to correct for the frozen-core approximation implicit in the PK formalism. These pseudopotentials, which are identical to those used in our previous studies,[27, 39, 46, 89, 109, 119] are described in more detail in the SI. The classical interactions between the Na^+ cations and the Ar and rigid OPLS THF solvent molecules were modeled with the same potentials used in our earlier studies in these solvents[46, 119] and are detailed in the SI.

The cubic simulation cells had a side length of 43.8 Å for simulations in Ar and 32.5 Å for those in THF, which given the number of solvent molecules yielded densities of 1.26 g/mL at 120 K for Ar 0.89 g/mL at ∼298 K for THF. In Ar, we expanded the electronic eigenstates of the quantum mechanical electron in a basis of 32 × 32 × 32 plane waves over a 25 $Å^3$ box. Due to the diffuse nature of the valence electron's excited state in THF, particularly at larger Na–Na distances, we used 64 × 64 × 64 plane waves that spanned the entire cubic simulation cell. For all simulations, we utilized periodic boundary conditions with the minimum image convention.[87] All interactions in the cell were tapered smoothly to zero at 16 Å over a 2-Å range using a center-of-mass-based switching function.[105] The single-electron Hamiltonian, which is shown explicitely in the SI, was diagonalized at every MD time step using the implicitly-restarted Lanczos method as implemented in ARPACK.[108] For simulations in THF, the solvent molecules were treated as rigid, planar five-membered rings following the work of Chandrasekar and Jorgensen.[103] All simulations were propagated using the velocity Verlet algorithm[87] with a 4-fs time step, except for simulations with light Ar in which case a 2-fs time step was used.

We performed both equilibrium umbrella sampling, where the Na_2^+ bond length was restrained and nonequilibrium dissociation trajectories where the molecule was placed into the excited state from its equilibrium ground state configuration and allowed to propagate adiabatically on its electronic excited state. For umbrella sampling in Ar, bins were set at every 0.1 Å from 3.0 Å out to a dissociative distance of 9.0 Å. For umbrella sampling in THF, bins were set every 0.1 Å from 4.0 Å out to a dissociative distance of 10.0 Å. Within

each bin after appropriate equilibration, umbrella trajectories were run for 10 ps to ensure ample statistics across the potential of mean force. Details of the umbrella sampling and the process used to stitch the individual umbrella sampled windows together to create the LR PMFs shown in Fig. 4.1 are given in the SI. For the nonequilibrium trajectories, the Na_2^+ molecule was placed in the first excited state starting from ground-state configurations taken from an equilibrated ground-state trajectory; 15 nonequilibrium trajectories were run in Ar and 20 nonequilibrium trajectories were run in THF to provide statistics for nonequlibrium ensemble averages. Details of the initial configurations chosen for these studies as well as the process used to construct the LR and dynamic PMFs shown in Fig. 4.1 and 2 are provided in the SI.

4.6 Supplemental Information

To avoid repetition, only the sections of the supplemental information for "Linear Response Breakdown in Liquid Photodissociation: Caging and Chemical Identity" that differ from those given in Chapter 2 Section 6 and Chapter 3 Section 6 are included here. If not otherwise specified, the simulation and analysis methods used for the work presented in this paper are the same as those used in "The Role of the Solvent in the Condensed-Phase Dynamics and Identity of Chemical Bonds: The Case of the Sodium Dimer Cation in THF."

Mixed Quantum/Classical Model

Our mixed quantum/classical (MQC) molecular dynamics (MD) simulations consisted of two classical Na^+ cations, one fully quantum mechanical electron, and hundreds of classical solvent molecules. Simulations in liquid argon (Ar) contained 1600 Ar atoms in a simulation cell with a side length of 43.8 Å, and simulations in liquid tetrahydrofuran (THF) contained 254 THF molecules in a 32.5 Å simulation cell. The sizes of the simulation cells were chosen to reproduce the appropriate solvent densities at the simulation temperatures (1.26 g/mL

at 120 ± 2 K for Ar simulations, which is well within the liquid region of simulated Ar's phase diagram[106] and 0.89 g/mL at 298 ± 6 K for THF simulations). For simulations in THF, the solvent molecules were treated as rigid, planar five-membered rings following the work of Chandrasekar and Jorgensen.[103] This rigid planarity was enforced using the RATTLE algorithm, as in our previous MQC MD work.[86, 109, 119] In all simulations, periodic boundary conditions were implemented with minimum image convention[87] and all interactions were tapered smoothly to zero at 16 Å over a 2 Å range with a center of mass-based switching function according to Steinhauser.[105] All simulations were performed in the microcanonical ensemble.

4.6.1 Simulation Setup

The eigenstates of the quantum mechanical valence bonding electron were expanded on a three dimensional grid. For simulations in Ar, we used a basis of 32 × 32 × 32 grid points distributed over a 25 Å^3 box. Because the valence electron is more diffuse in THF, for simulations in THF, we used a larger grid that spanned the entire simulation cell and contained 64 × 64 × 64 grid points. These dimensions were chosen to keep the basis set as small as possible for each system while still capturing the spatial extent of the electronic wave function. We centered the grid in the middle of the simulation cell and shifted all classical particles relative to the grid every 500 fs to avoid leakage of the wave function off the edges of the grid. In this way, the wave function was always located roughly in the center of the simulation cell. The classical particles were shifted an integer number of grid spaces to avoid discontinuities in the quantum energy that would prevent total energy of the simulation from being conserved.[39] We used the velocity Verlet algorithm[87] to propagate the classical degrees of freedom ($\boldsymbol{v}_{\mathrm{Na^+}_i}$, $\boldsymbol{v}_{\mathrm{solv}_i}$, $\boldsymbol{R}_{\mathrm{Na^+}_i}$, and $\boldsymbol{R}_{\mathrm{solv}_i}$) of the Hamiltonian in Eqs. 1 and 2 in the microcanonical (N, V, E) ensemble. We determined the forces from the sum of the classical-classical and classical-quantum interactions described above. We used the implicit restart Lanczos method to iteratively solve the TISE for the ground state wavefunction at every 4

fs time step.[108] The quantum forces on the classical particles were then found using the Hellman-Feynman theorem:

$$\boldsymbol{F}_i^Q = -\langle\Psi|\,\boldsymbol{\nabla}_{\boldsymbol{R}_i}\hat{H}\,|\Psi\rangle \tag{4.2}$$

where, $\boldsymbol{F}_i^Q$ is the quantum force on classical particle i at position $\boldsymbol{R}_i$. Because the wave function is expanded in a basis that does not functionally depend on the position of the classical particles, Eq. 5 is exact (in other words, there are no issues with Pulay forces from the basis functions changing with time).[85]

For this paper, we collected data in two ways: 1) by holding the Na–Na bond length at a fixed distance to collect equilibrium statistics on either the ground or first excited state (umbrella sampling) and 2) by placing the Na_2^+ molecule into the first excited state from an equilibrium ground state configuration and then allowing the molecule to propagate adiabatically on its electronic excited state (dynamic dissociation). To conduct umbrella sampling, we set bins at every 0.1 Å and spanned enough distance to adequately capture the shape of both the ground and excited state electronic surfaces. Within each bin, 10 ps of data was collected to ensure ample statistics at each point on the potential energy surface.

For dynamic dissociation, we selected starting configurations from simulations of Na_2^+ in the ground state. We picked uncorrelated configurations where the Na_2^+ molecule was at its ground state equilibrium bond length. For Na_2^+ in Ar, this meant a starting Na–Na bond length of ∼3.7 Å. Because ground state Na_2^+ is stabilized in two primary coordination states in THF, we selected starting configurations for each. For the $Na(THF)_4$−$Na(THF)_5^+$ species, the equilibrium bond length is ∼4.8 Å and for the $Na(THF)_5$−$Na(THF)_5^+$ species the equilibrium bond length is ∼5.6 Å. Fifteen dissociation trajectories were run for Na_2^+ in Ar and twenty for dissociation from each of the two $Na_2(THF)_n^+$ coordination states in THF.

In the next few sections, we will outline the details of various analysis methods used to produce the results described in the paper, including how the umbrella sampling data was used to calculated the equilibrium, linear response (LR) potentials of mean force (PMFs) and the dissociation data was used to calculate the nonequilibrium, dynamic PMFs.

4.6.2 Construction of Linear Response Potentials of Mean Force

As mentioned above, we utilized umbrella sampling to collect equilibrium statistics from the condensed phase Na_2^+ molecule at a wide range of Na–Na bond lengths. Umbrella sampling is a technique used to explore potential energy surface of a system, especially ones in which large energetic barriers prevent adequate sampling of higher energy configurations during normal equilibrium dynamics. Therefore, to force the system to remain in a specific configuration in order to gather statistics, even if that configuration is energetically unfavorable, we define a collective variable and then use a potential well at a target value. Because we want to apply our biasing potential to the Na–Na bond coordinate, the umbrella potential took the form:

$$U(\boldsymbol{r}) = \frac{1}{2}k(\boldsymbol{r} - \zeta)^2 \tag{4.3}$$

where, $U(\boldsymbol{r})$ is the umbrella potential applied to the Na–Na bond coordinate, k is the force constant, $\boldsymbol{r}$ is the Na–Na bond length, and ζ is the target bond length. Because we know the form of the biasing potential, the statistics of the unbiased system can be recovered from the biased statistics.

We then performed multiple simulations, differing only in the target bond length, such that the statistics of neighboring umbrella sampled bins overlapped. These series of umbrella sampled simulations were then stitched together via the multistate Bennet acceptance ratio (MBAR) method[130] to produce the LR PMFs displayed in main text Fig. 4.1.

4.6.3 Construction of Dynamic Potentials of Mean Force

To compare the LR PMFs to our nonequilibrium, dissociation trajectories, we needed a way to construct a dynamic PMF. To do this, we first calculated $U(t)$ by taking advantage of the relation:

$$U(t) = -\int_{t_0}^{t} F(t)v(t)dt, \tag{4.4}$$

where $F(t)$ is the total force (from the solute and solvent) on the Na nuclei along the bond axis, $v(t)$ is the bond velocity, and t_0 is the time at which photoexcitation takes place. Thus knowing the potential in terms of time, $U(t)$, as well as the bond distance during dissociation, $r(t)$, we can parametrically combine the two to produce the effective potential surface followed during the dynamics, $U(r)$. The integration is calculated in reverse time so that U following dissociation is set to zero.

Because the Na_2^+ molecule dissociates at different time scales in different solvents, the value of t in Eq. 4.4 was chosen such that they were long enough to have sampled all the appropriate photodissociation dynamics but short enough to avoid diffusive recrossings that occur at longer distances. For simulations in liquid Ar, this time was ∼300 fs, while in THF it was much longer at ∼1000 fs.

As mentioned previously, we ran 15 nonequilibrium, dissociation trajectories for Na_2^+ in Ar and 20 from each of the two coordination states in THF. Uncorrelated starting configurations were chosen from equilibrated ground state dynamics. These starting configurations were selected to be at the equilibrium Na–Na bond length of the Na_2^+ electronic ground state. In Ar, this meant selecting 15 initial configurations with a 3.7 Å Na–Na bond length. In THF, this meant selecting 20 initial configurations in the $Na(THF)_4{-}Na(THF)_5^+$ state with a 4.8 Å Na–Na bond length and 20 in the $Na(THF)_5{-}Na(THF)_5^+$ state with a 5.6 Å Na–Na bond length. The individual dynamic PMFs for the $Na(THF)_4{-}Na(THF)_5^+$ and $Na(THF)_5{-}Na(THF)_5^+$ species are plotted below. The data shown in main text Fig. 4.2b for the overall dynamic PMF in THF was produced by combining the individual PMFs according to the Gaussian weighted ratio of the two coordination states from our previous ground state studies of Na_2^+ in THF,[119] which means that the $Na(THF)_4{-}Na(THF)_5^+$ trajectories counted for about 30% and the $Na(THF)_5{-}Na(THF)_5^+$ for 70%.

4.6.4 Construction of Ar Heat Maps

To compare the Ar cage during dissociation to that at equilibrium, we needed to create an ensemble average of the Ar positions relative to the Na^+ cores. To do so, we created a Fibonnaci sphere of radius 3.3 Å, which is the average Na^0–Ar distance, around each Na^+ core. The advantage of using a Fibonnaci sphere is that it creates any number of evenly spaced points on a sphere. For each point, we then calculate the distance between it and each Ar atom. If an Ar atom is within 1.7 Å, which is the Lennard-Jones radius of Ar, of that point, then it is assigned a value of 1. If not, then it is assigned a value of 0. We then average the spheres over 100+ configurations to get an ensemble picture of the Ar cage at equilibrium.

To generate an ensemble picture of the Ar cage during dissociation, we duplicated each trajectory six times with 60 degree rotations between each duplicate to enhance our statistics. The rotations allow us to force cylindrical symmetry about the Na–Na bond axis. The configurations were also rotated before created the spheres so that the initial Na–Ar collision occurs on the same Na each time.

4.6.5 Additional Data

In the main text, we described how the LR approximation breaks down for the photodissociation of Na_2^+ in Ar due to a single nonequilibrium event−the solute's collision with the surrounding cage of Ar atoms. Furthermore, we showed that this LR breakdown is dependant on the mass of the solvent. With sufficiently light Ar atoms, the solvent fluctuations occur on a similar time scale to the Na_2^+ photodissociation dynamics; thus, the LR behavior can be recovered. On the other hand, with heavier solvent, the collision of the solute with the solvent cage actually knocks the photofragments back toward each other, leading to a temporary shortening of the Na–Na bond length before the fragments are able to eventually escape the solvent cage. This manifests as a loop in the dynamical PMF, shown in main text Fig. 4.3.

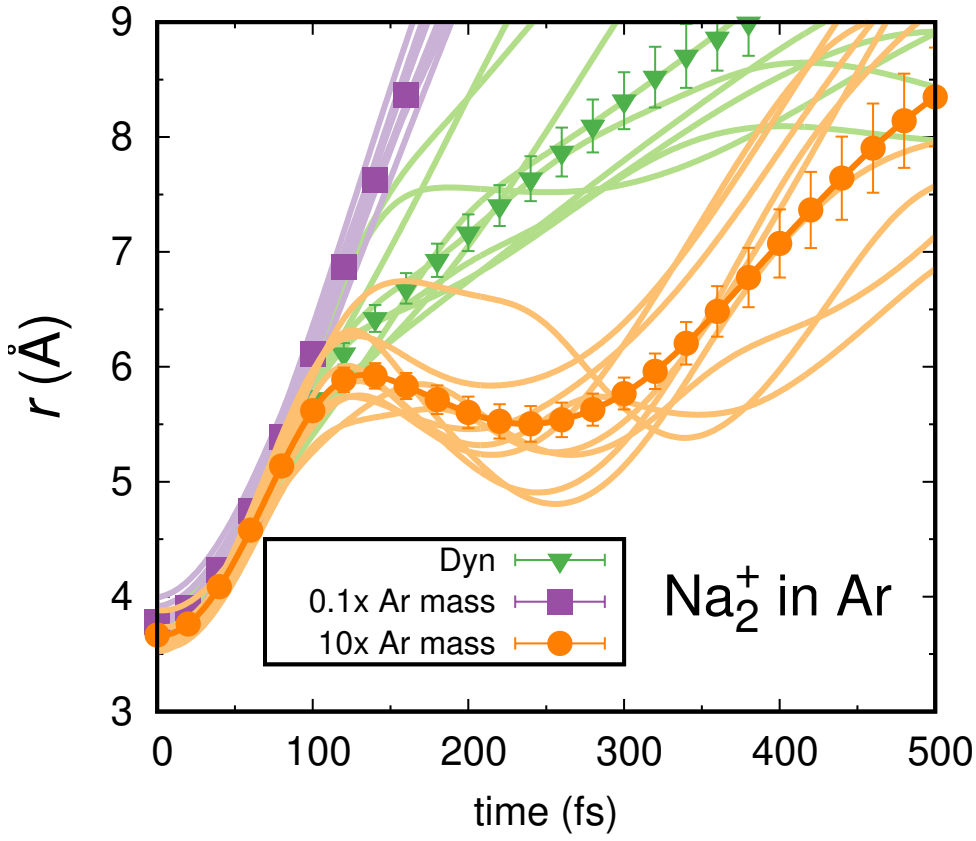

Figure 4.6: Trajectories of the photodissociation of Na_2^+ in Ar of various mass show that the magnitude of the breakdown of linear response due to solvent caging is dependent on the time scale of the solvent fluctuations. The trajectories where Ar is at its normal mass are plotted in green while those with five times heavier Ar are plotted in orange and those with twenty times lighter Ar are plotted in purple. The average of each type of dissociation trajectory is also included with green triangles form normal mass Ar, orange circles for 5x mass Ar, and purple squares for 0.05x mass Ar.

Here, in Figure 4.6, we plot the actual dissociation trajectories for these three scenarios: Ar of normal mass (green), Ar 20 times lighter than normal (purple), and Ar 5 times heavier than normal (orange). The average of each group of trajectory is also included with green triangles for normal mass Ar, purple squares for the lighter Ar, and orange circles for the heavier Ar. The influence of the solute's nonequilibrium collision with the solvent cage are evident in the average curves. For normal mass Ar, a change in slope is observed at the same Na–Na bond distance that the photofragments first encounter the solvent cage. This change in slope is not present for dynamic dissociation with lighter Ar atoms. Instead, the photofragments simply blow through the solvent cage. Finally, with heavier Ar atoms, the photofragments are actually knocked back, such that the Na–Na bond length temporarily decreases, before escaping the solvent cage to continue dissociation.

These and other interesting solvent-induced effects are visible in snapshots from the Na_2^+ trajectories in Ar, as shown in Fig. 4.7, which includes snapshots from the equilibrium, LR pathway (a) and from dynamic dissociation (b). In the LR approximation, the molecule is able to smoothly pull apart from an initial Na–Na bond distance of 3.5 Å out to 5.5 Å, where the electron collides with the solvent cage. During nonequilibrium dissociation, however, the photofragments must work their way dynamically through the solvent cage. This is evident when comparing the two snapshots at 5.5 Å. In dynamic dissociation, this is the point where the solute encounters the cage of surrounding Ar atoms. This collision squishes the bonding electron density and knocks the photofragments temporarily back. A direct collision between the right-hand sodium and an Ar atom is even evident, shown with the red arrow. In the LR prediction, however, we see a completely different scenario. Whereas there are no Ar atoms in-between the two photofragments at this point during dynamic dissociation, in the LR prediction, several Ar atoms are working to insert themselves between the sodiums. This actually shoves electron density outward, facilitating dissociation.

Now we move on to a brief discussion of the dynamic Na_2^+ PMFs in liquid THF. Main text Fig. 4.2b plots the dynamic PMF for the nonequilibrium photodissociation of Na_2^+

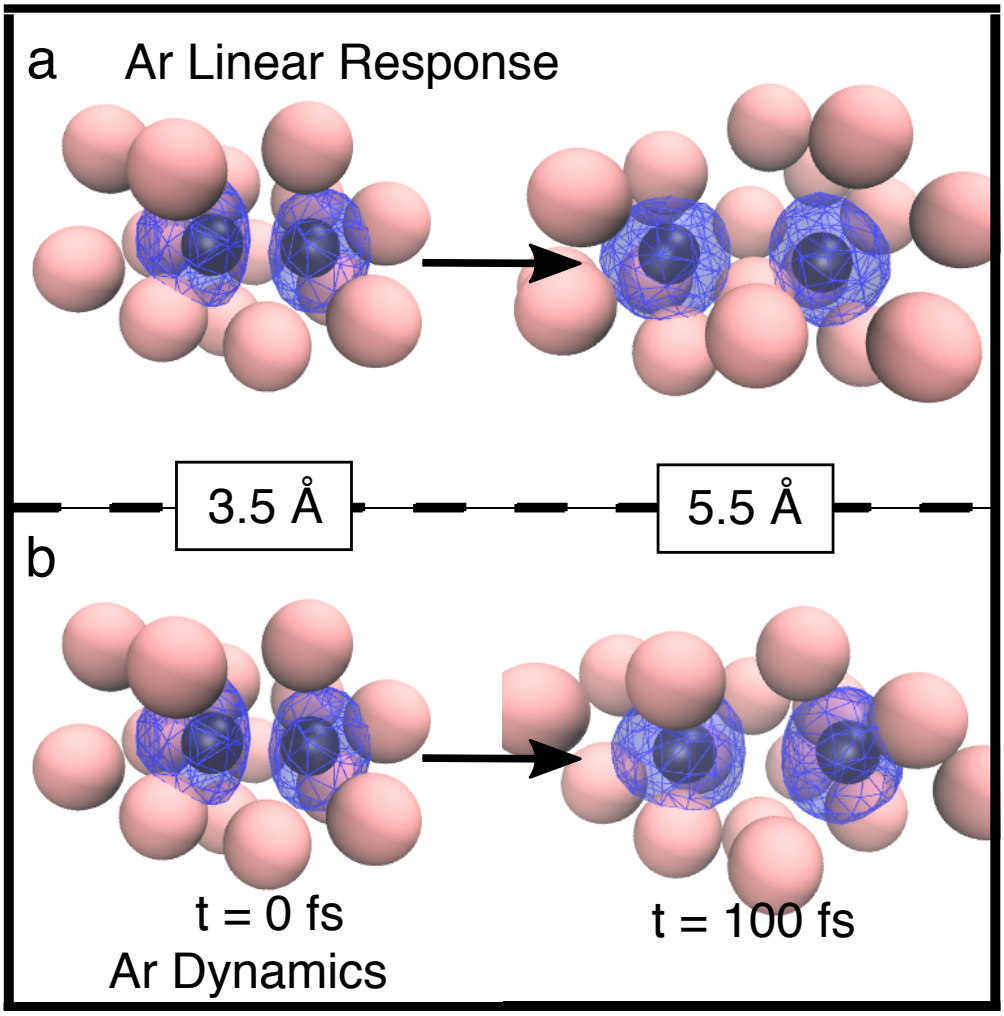

Figure 4.7: Representative snapshots of excited-state Na_2^+ in Ar at equilibrium (panel (a)) and during the nonequilibrium photodissociation dynamics (panel (b)). The Na^+ cores are plotted black spheres at the size of the Na^+ ionic radius, the Ar atoms as pink spheres, and the THF molecules as turquoise sticks with red oxygen atoms. The electron is drawn as a blue wire mesh containing 75% of the density.

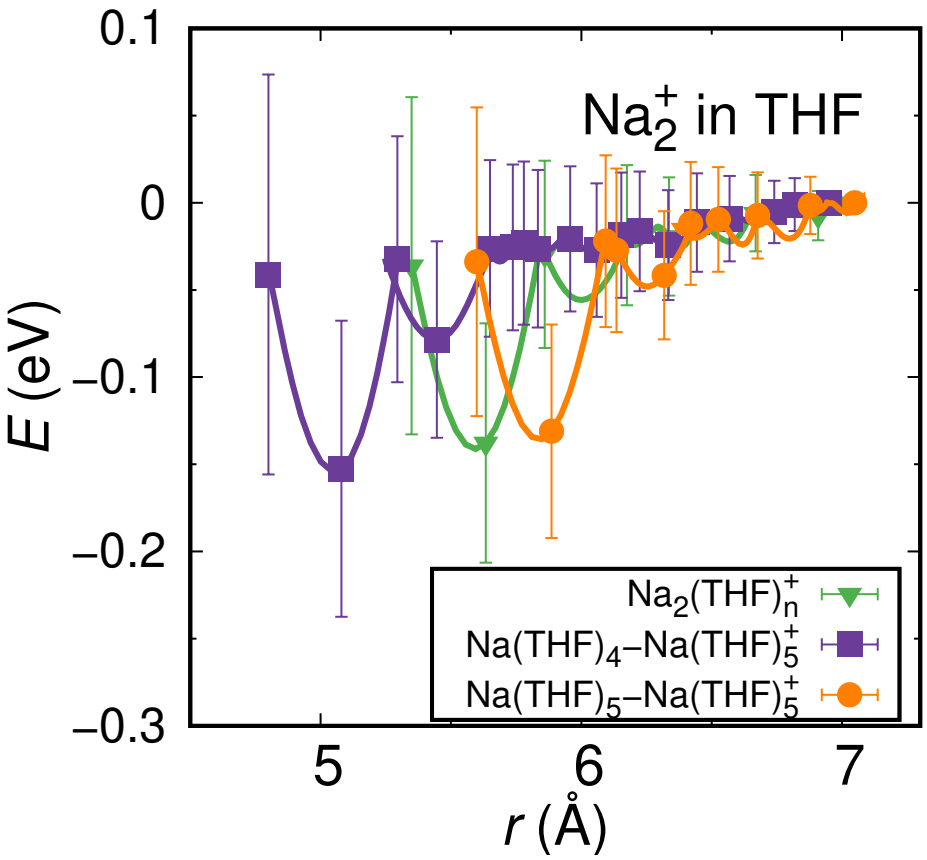

Figure 4.8: Dynamic potentials of mean force for Na_2^+ in THF. The PMFs are plotted for $Na(THF)_4{-}Na(THF)_5^+$ (purple squares), $Na(THF)_5{-}Na(THF)_5^+$ (orange circles), and $Na_2(THF)_n^+$ (green triangles).

in THF. However, we know from previous studies[119] that the Na_2^+ molecule exists in THF not as a single species but as an equilibrium mixture of $Na(THF)_4{-}Na(THF)_5^+$ and $Na(THF)_5{-}Na(THF)_5^+$, each of which behaves as its own discrete molecule. Therefore, to construct the overall dynamic PMF, we conducted twenty dissociation trajectories from each of these stable coordination states. From those trajectories, we prepared dynamic PMFs as outline above and in the main text. These dynamic PMFs for the $Na(THF)_4{-}Na(THF)_5^+$ (purple squares) and $Na(THF)_5{-}Na(THF)_5^+$ (orange circles) states are plotted here in Fig. 4.8 along with the overall Na_2^+ dynamic PMF in THF (green triangles). The overall dynamic PMF was prepared by combining the dynamic PMFs of the individual coordination states using their Gaussian weighted averages.

As can be seen in Fig. 4.8, all three curves have the same main features: an initial 'dip' in energy followed by a gradual increase in energy at longer distances. The initial dip arises for three primary reasons. First, as we explored in the main text, in liquid THF, when the Na2+ is placed in the first excited state, the bonding electron density initially orients in a π-like state. This is a weakly bound electronic structure which drives the Na–Na bond to lengthen. Second, the bonding electron density then rotates into a σ*-like position as the molecule dissociates. Finally, the $Na_2(THF)_n^+$ species is capable of forming new Na–THF oxygen-site dative bonds during dissociation. All of these factors combine to initially drive the molecule longer bond lengths. However, after expending the energy needed to perform these processes, the molecule has no more energy to escape the solvent cage. Thus, there is not a kinetically favorable pathway to Na_2^+ to fully dissociate during dynamic photodissociation in THF. Other wiggles are present in the dynamic PMfs on the gradually rising energetic tail. These come from small shifts in the position of the electronic density as the molecule pulls apart as well as the vibrations of the Na–THF oxygen-site dative bonds.

Chapter 5

How Local Solvent Environment Can Alter Solute Electronic Structure During Photodissociation Dynamics

5.1 Abstract

If a molecule readily photodissociates in the gas phase, can we assume that it will follow a similar dissociation pathway in the condensed phase? Through mixed quantum classical (MQC) molecular dynamics (MD) simulations of sodium dimer cation (Na_2^+) in THF, we show that when the solute–solvent interactions are energetically on the order of a hydrogen bond, the solute's electronic structure and thus dynamics and reactivity are controlled nearly entirely by the local solvent environment. Thus, the molecule in solution can behave very differently than its gas-phase counterpart. In the previous chapter, we saw that linear response (LR), the assumption that a nonequilibrium system can be understood through study of the fluctuations of its equilibrium dynamics, breaks down for the photodissociation of this system, and in this chapter we are going to take apart precisely why. In particular, we delve into the details of how changes in the local solvent environment facilitate changes

in the electronic structure of the Na_2^+ bonding electron and how this process eventually leads the Na_2^+ molecule, which dissociates in the gas phase and as gas phase $Na_2(THF)_n^+$ clusters, to become trapped in full-condensed phase THF.

5.2 Introduction

The linear response (LR) approximation, a staple of models exploring how solvation influences chemical reactivity, predicts that, for a small perturbation, a nonequilibrium system will relax along a pathway identical to the regression of the spontaneous fluctuations of the system at equilibrium.[120] According to this approximation, study of solvent fluctuations at equilibrium should be sufficient to understand nonequilibrium reaction dynamics.

In previous studies, we showed that LR breaks down for the photodissociation of Na_2^+ in liquid Argon (Ar) as well as in liquid THF−but for very different reasons in each system.[131] In Ar, the initial collision of the dissociating molecule with the surrounding cage of Ar atoms knocks the photoexcited fragments back toward each other before they are able to make their way through the solvent cage. We showed that this event was dependent on the relative time scales of the solvent fluctuations and the dissociation event, such that changing the fluctuation rate by changing the solvent mass could exacerbate or mitigate the breakdown of LR. LR likewise fails for the photodissociation of Na_2^+ in THF; however, the reason for this LR breakdown arises not from the solvent cage but from solvent-induced changes in the Na_2^+ molecule's electronic structure and chemical identity.[131]

We have shown previously that when solute-solvent interactions are energetically on the order of a hydrogen bond, the solute molecule can undergo a change in chemical identity.[109, 119] Such is the case for Na_2^+ in THF, which, due to the dative-bonding interactions between THF oxygen-sites and the sodium atoms, is better thought of as the coordinated structure $Na_2(THF)_n^+$. These Na–THF oxygen-site dative-bonding interactions result in two stable, chemically-distinct ground state coordination structures ($Na(THF)_4$-$Na(THF)_5^+$

and $Na(THF)_5$-$Na(THF)_5^+$), which interconvert by surmounting an energy barrier of several k_BT.[119] These coordination states behave as discrete molecules with their own chemical identities that are distinct from that of gas phase Na_2^+.[109, 119] Furthermore, each $Na_2(THF)_n^+$ species is stable as its own gas-phase molecule with an electronic structures that is completely different than that of gas-phase uncoordinated Na_2^+.

In our previous studies of the excited-state dissociation dynamics of Na_2^+ in the gas and condensed phase,[119, 131] we saw that when gas-phase Na_2^+ is placed in its first electronic excited state, the molecule readily falls apart, the result of an electronic structure which places the node of the excited state electron perpendicular to the Na–Na bond axis, much like the σ^* orbital one would expect based on molecular orbital theory.[95, 96] In liquid Ar, the same basic excited state electronic structure is observed, with some minor perturbations to the energies and wavefunction of the Na_2^+ bonding electron due to the surrounding cage of Ar atoms.[119, 131] The first excited state of the $Na_2(THF)_n^+$ structures, on the other hand, is initially completely different. It is simply not energetically favorable for the molecule to place the bonding electron in the σ^* position due to crowding from the coordinating THF molecules, which take up all of the space on the backside of each Na^+ core. Instead, for these structures, the electron's density initially resides above and below the molecule with a node parallel to the Na–Na bond axis, similar to a π bonding orbital.[119, 131]

In this paper, we utilize nonadiabatic mixed quantum/classical (MQC) molecular dynamics (MD) simulations to delve into the intricate link between the modest solute–solvent interactions present between the Na^+ cores and their dative-bonded THF molecules and the rotation of the excited state bonding electron's density from the π bonding to σ^* position after photoexcitation of the $Na_2(THF)_n^+$ species. Through studies of gas-phase $Na(THF)_4-Na(THF)_5^+$ and $Na(THF)_5-Na(THF)_5^+$, we find that this π bonding to σ^* antibonding electronic transition can only occur when the dative-bonded solvent molecules shift out of their preferred ground state configurations in response to the new excited state bonding electron structure. LR breaks down because the process of rotating the electron's

density into the dissociative position occurs at much shorter Na–Na bond lengths for the LR, equilibrium prediction, where the solvent has plenty of time to move into the optimal positions, than during dynamic dissociation, where the solvent must move concurrently with the dissociation of the molecule. This effect is compounded by the changing chemical identity of the solute during dissociation in the full condensed phase, which is caused by the formation of new Na–THF oxygen-site dative bonds as the molecule pulls apart: this dynamic change in identity is a process that differs between equilibrium and dynamic dissociation, further contributing to the breakdown of the LR approximation for the dissociation of $Na_2(THF)_n^+$. Overall, our work shows that even relatively modest interactions between a solute and solvent can completely alter simple chemical dynamics between the gas phase and solution.

5.3 Computational Details

For the work in this paper, we conducted MQC MD simulations of the $Na_2(THF)_n^+$ coordination states both in the full condensed phase and as gas-phase molecules. In these simulations, which were performed in the microcanonical ensemble, we treated the Na_2^+ molecule as two classical Na^+ cores held together by a single quantum-mechanically-treated valence bonding electron. Our simulations also contained classical solvent molecules: 254 THF molecules for full condensed phase simulations and the dative-bonded THF molecules (nine in total for the $Na(THF)_4{-}Na(THF)_5^+$ state and ten for the $Na(THF)_5{-}Na(THF)_5^+$ state) for gas-phase $Na_2(THF)_n^+$ simulations. Our THF molecules were treated as rigid, planar five-membered rings following the work of Chandrasekar and Jorgensen.[103] The rigid planarity of the THF molecules was enforced using the RATTLE algorithm.[85]

The interactions between the classical particles and the quantum mechanical electron were accounted for using Phillips-Kleinman (PK) pseudopotentials,[88] modified with polarization potentials to correct for the frozen-core approximation implicit in PK formalism. These are the same pseudopotentials used in our previous studies.[27, 39, 46, 89, 109, 119, 131] The

classical interactions between the Na^+ cations and the THF solvent molecules were modeled with the same Lennard-Jones potentials used in our earlier studies of Na_2^+ in THF.[119, 131]

Our cubic simulation cell had a side length of 32.5 Å, a length chosen to give the correct density for the full condensed phase simulations (0.89 g/mL density at ∼298 K). We utilized periodic boundary conditions with the minimum image convention.[87] All interactions in the cell were tapered smoothly to zero at 16 Å over a 2 Å range using a Steinhauser center-of-mass-based switching function.[105] We expanded the electronic eigenstates of the quantum mechanical electron in a basis of $64 \times 64 \times 64$ plane waves that spanned the cubic simulation cell, and the single-electron Hamiltonian was diagonalized at every MD time step using the implicitly-restarted Lanczos method as implemented in ARPACK.[108] All simulations were propagated using the velocity Verlet algorithm[87] with a 4-fs time step.

We performed both umbrella sampling, where the Na_2^+ bond length was held at a fixed distance to collect equilibrium statistics on the particular energetic state and local solvent environment of Na_2^+ at various bond lengths, and nonequilibrium dissociation trajectories where the molecule was placed into the excited state from its equilibrium ground state configuration and allowed to propagate adiabatically on its electronic excited state. Data was collected both for gas phase $Na(THF)_4{-}Na(THF)_5^+$ and $Na(THF)_5{-}Na(THF)_5^+$ as well as $Na_2(THF)_n^+$ in liquid THF.

For umbrella sampling, bins were set at every 0.1 Å and ran from the lowest Na–Na bond length achievable without disrupting the $Na_2(THF)_n^+$ structure, generally around 4.0 Å, out to a dissociative distance of 10.0 Å. While the simulation box could accommodate larger dissociation distances, due to the diffuseness of the Na_2^+ excited state, we chose the 10.0 Å cut off as a safe distance to avoid self-interaction of the valence electron via electron density spilling over the edge of the grid. Within each bin, 10 ps of data was collected to ensure ample statistics across the potential energy surface.

For nonequilibrium trajectories, initial configurations were chosen where the molecule was at it's most stable bond distance (3.84 Å for gas phase Na_2^+, 4.95 Å for gas phase

$Na(THF)_4{-}Na(THF)_5^+$, and 5.70 Å for gas phase $Na(THF)_5{-}Na(THF)_5^+$. Twenty dissociation trajectories were collected for the dissociation of each of the $Na_2(THF)_n^+$ structures in both the gas and condensed phase.

5.4 Results and discussion

Our previous studies of ground state Na_2^+ in THF have shown that the dative-bonding interactions between the Na^+ cores and THF oxygen-sites stabilize the molecule in discrete coordination states which each behave as unique molecules distinct both from gas phase Na_2^+ and from each other.[109, 119, 131] Indeed, these $Na_2(THF)_n^+$ states are even stable as gas-phase molecules. We will thus begin our investigation into the shift of the $Na_2(THF)_n^+$ electronic structure from the π bonding position to the σ^* anti-bonding position through simulations of the photodissociation of gas-phase $Na(THF)_4{-}Na(THF)_5^+$ and $Na(THF)_5{-}Na(THF)_5^+$ (i. e., the coordination complexes isolated in a vacuum as opposed to being immersed in liquid THF). We do so because in the gas phase, these molecules are unable to form new Na–THF oxygen-site dative bonds. Thus, they retain their structural chemical identity by remaining in the same coordination state throughout dissociation. This presents the opportunity to explore the exact motions of the dative-bonded solvent that allow for the rotation of the bonding electron's density.

5.4.1 Potential Energy Curves of the Gas-Phase $Na_2(THF)_n^+$ Lowest Excited State Reveal a Shift in the Bonding Electron's Structure During Dissociation

We begin by establishing the LR approximations for the photodissociation pathways of the gas-phase $Na_2(THF)_n^+$ species. Figure 5.1 shows the potential energy curves (PECs) of the lowest energy excited state of gas-phase Na_2^+ (black curves) and the two stable gas-phase $Na_2(THF)_n^+$ states: $Na(THF)_4{-}Na(THF)_5^+$ (red triangles) and $Na(THF)_5{-}Na(THF)_5^+$

(purple circles). Note that the $Na(THF)_4{-}Na(THF)_5^+$ state is labeled as (4,5) and the $Na(THF)_5{-}Na(THF)_5^+$ as (5,5) in all figures. As expected, the dissociative pathway of gas phase Na_2^+ is smooth. LR predicts that, following excitation from the ground state to the lowest energy excited state, the Na_2^+ molecule simply falls apart.

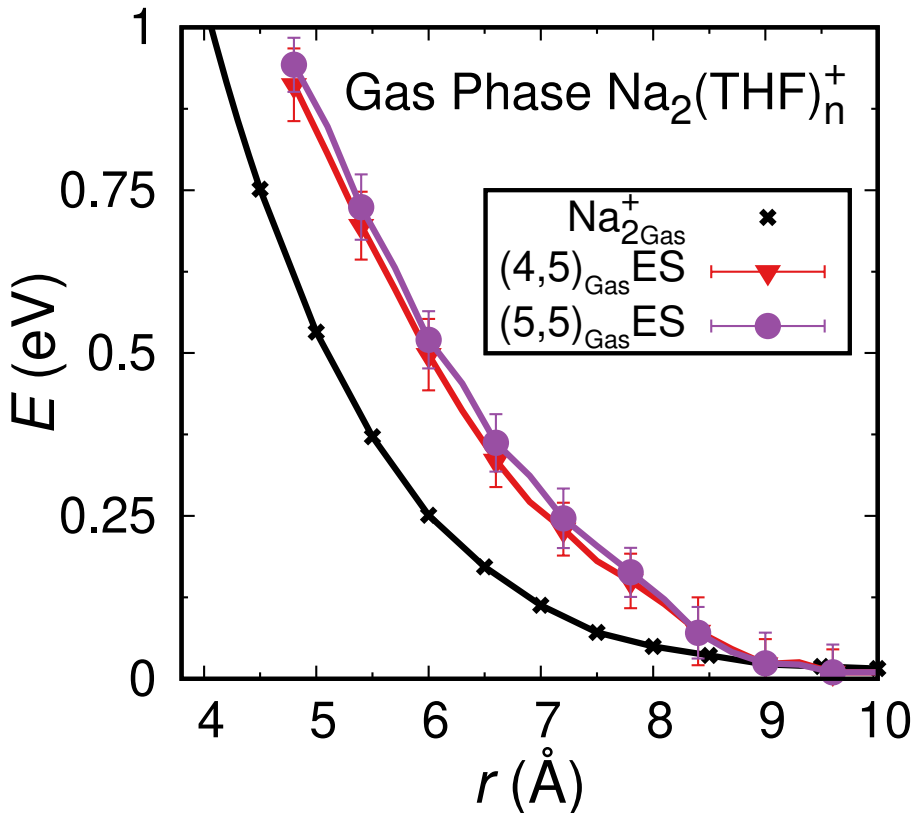

Figure 5.1: Equilibrium, linear response potential energy curves of the first excited state of the gas-phase $Na_2(THF)_n^+$ coordinated structures predict dissociation. Upon excitation from the ground state to the lowest energy excited state, the Na_2^+ molecule falls apart following a smooth dissociative surface (black curve). The LR prediction for the $Na(THF)_4{-}Na(THF)_5^+$ (red triangles) and $Na(THF)_5{-}Na(THF)_5^+$ (purple circles) also appears consistently dissociative and relatively smooth, suggesting that the molecule will dissociate.

The LR predicted dissociation pathways for the gas-phase $Na_2(THF)_n^+$ species are actually nearly identical to each other: when either of the $Na_2(THF)_n^+$ species is photoexcited to the first excited state from its equilibrium ground state, LR predicts that the molecule dissociates via a relatively smooth surface, similar to that of gas-phase Na_2^+ but shifted toward higher Na–Na distances. However, we know from our previous studies of Na_2^+ that

when propagating in ground state dynamics, the coordinated $Na_2(THF)_n^+$ species, whether in the gas or condensed phase, orient the electron density of their first excited state like a π bonding orbital by placing electron density above and below the bond axis such that the electron's node resides along the bond axis.[119] This is entirely different than the electronic structure of the first excited state of gas phase Na_2^+, which distributes electron density equally between both Na^+ core with the node perpendicular to the bond axis in the ideal dissociation structure of a σ^* orbital.[119] However, if the valence electron of the $Na_2(THF)_n^+$ excited state were to remain in this π bonding position, the molecule would never fully dissociate; yet the LR PECs shown in Fig 5.1 do indeed predict dissociation.

To investigate how the electronic structure of the $Na_2(THF)_n^+$ first excited state evolves during LR dissociation, Fig 5.2 shows simulation snapshots of gas-phase Na_2^+ (a), gas-phase $Na(THF)_4{-}Na(THF)_5^+$ (b), and gas-phase $Na(THF)_5{-}Na(THF)_5^+$ (c) in the ground state, after initial excitation to the first excited state, and after the molecule has dissociated to a bond distance of 8 Å. For bare Na_2^+ in the ground state, the electronic density forms a symmetric ovoid around the two Na^+ cores, much like a σ bonding orbital from molecular orbital theory.[95, 96] Upon excitation at the equilibrium ground state Na–Na bond distance (3.84 Å) to the first excited state, the electronic density distributes evenly between the two Na^+ cores with a node perpendicular to the bond axis just like a σ^* orbital. Finally, by the time the molecule has dissociated to a distance of 8 Å, the two lobes of electron density can form symmetric spheres around each Na^+ core.

The dissociation of the $Na_2(THF)_n^+$ coordination structures, however, follows a very different pathway, as shown in Fig. 2b and c. In the ground state, the electronic density is distorted by the presence of the dative-bonded THF molecules which shove the electron aside to expose the Na^+ cores for chelation. This causes electronic density to spill out above and below the bond axis, which in turn creates the π-like structure of the first excited state, as we observed in our preliminary studies of Na_2^+ in THF.[119] Because the coordinating THF molecules block the backside of each Na^+ core, the excited state electronic density

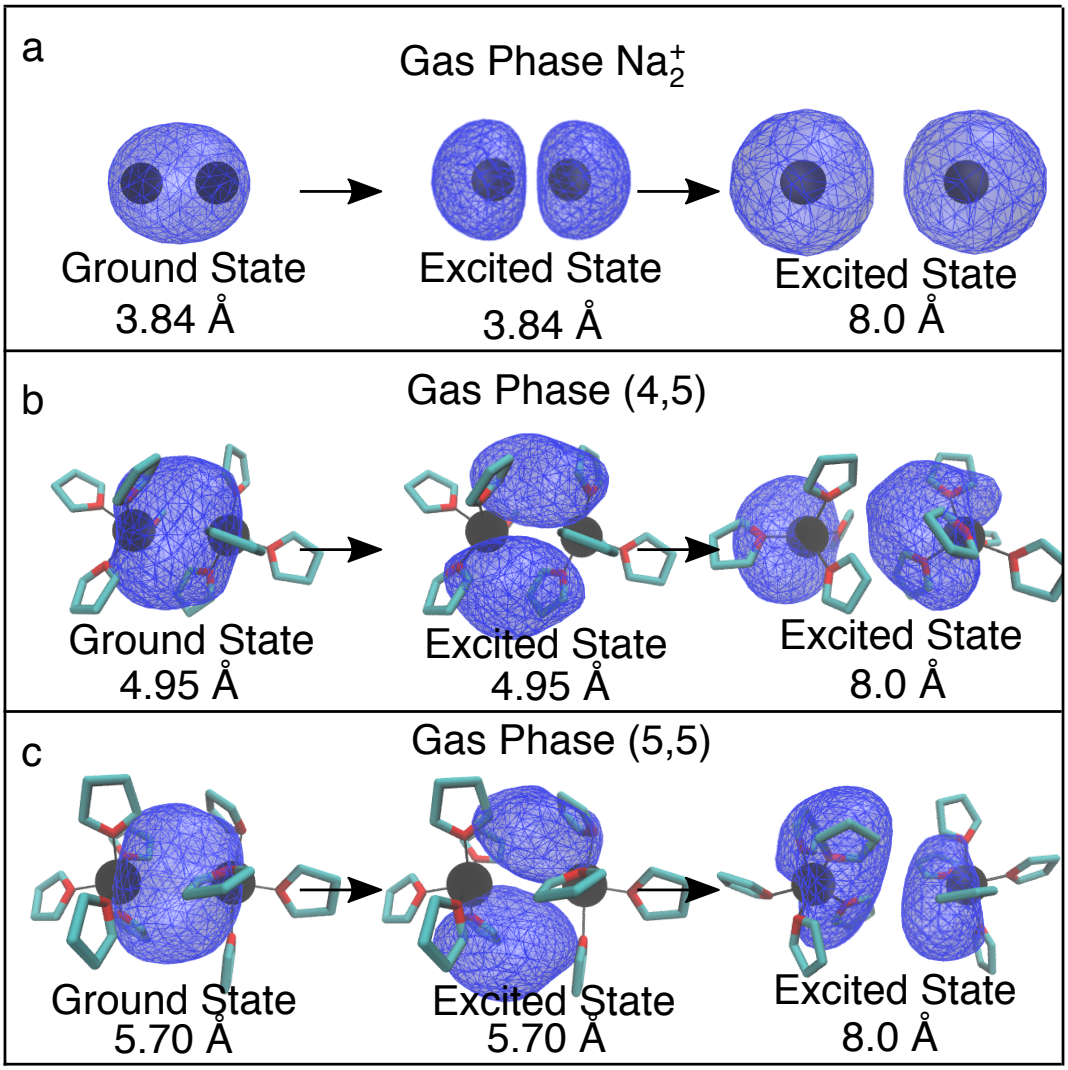

Figure 5.2: Simulation snapshots of gas-phase Na_2^+ and $Na_2(THF)_n^+$ reveal how the excited state electron density of the $Na_2(THF)_n^+$ states rotates from a π bonding to a σ^* orientation during dissociation. Panel (a) shows the process of dissociation for Na_2^+, starting with the ground state structure at the equilibrium bonding distance of 3.84 Å, followed by the first excited structure upon initial excitation, and ending with the electronic structure of the molecule after it has dissociated to a bond distance of 8 Å. Panels (b-c) show the same for the $Na(THF)_4$–$Na(THF)_5^+$ (b) and $Na(THF)_5$–$Na(THF)_5^+$ (c) coordinated structures, which have equilibrium bonding distances of 4.95 Å and 5.70 Å respectively. In all snapshots, the Na^+ cores are plotted as black spheres scaled to the Na^+ ionic radius. The valence electron is displayed as a blue wire mesh which contains 90% of the electron density. The dative-bonded THF molecules in panels (b-c) are plotted as turquoise sticks with red oxygen atoms. The dative bonds themselves are shown with black lines connecting the THF oxygen site to the Na^+ core.

cannot initially be accommodated in the σ^* position while also retaining the necessary node between the two lobes of electronic density. Therefore, when $Na_2(THF)_n^+$ is photoexcited to its first excited state from the equilibrium ground state Na–Na distance (4.95 Å for $Na(THF)_4{-}Na(THF)_5^+$ and 5.70 Å for $Na(THF)_5{-}Na(THF)_5^+$), the electron's density goes into the next most stable position: placing electron density above and below the bond while the node lies parallel to the bond axis, essential a π bond. This position is favored by both the $Na(THF)_4{-}Na(THF)_5^+$ and $Na(THF)_5{-}Na(THF)_5^+$ state. However, as the bond length increases and the coordinating THF molecules have time to react to the forces from the newly excited electron, the structure shifts. By the time the molecule has dissociated to a distance of 8 Å, the two lobes of the electron density have migrated to a σ^* position with the node aligned perpendicular to the bond axis. The $Na_2(THF)_n^+$ states are now in a fully dissociative position.

To track the movement of the $Na_2(THF)_n^+$ electronic density from the π bonding orientation to the σ^* orientation, we take a dot product of the overlap of the Franck-Condon ground and excited states with the Na_2^+ bond axis. We refer to this as the 'node angle' as it tracks the orientation of the node between the two lobes of electronic density in the excited state. Figure 5.3 plots the node angle of gas-phase Na_2^+ (black crosses) as well as the gas-phase $Na_2(THF)_n^+$ states (red triangles for $Na(THF)_4{-}Na(THF)_5^+$ and purple circles for $Na(THF)_5{-}Na(THF)_5^+$) at various bond lengths. Note that a node angle of zero indicates that the node is aligned perfectly parallel to the bond axis while a node angle of one indicates that the node is aligned perfectly perpendicular to the bond axis. For Na_2^+, the node angle remains in the 'one' position (perpendicular to the bond axis) regardless of bond length. However, at low bond lengths, the $Na_2(THF)_n^+$ bonding electron prefers to remain in the π bonding structure. Then, as the Na–Na bond distance increases, the node can rotate to put the electron in a σ^* structure. As shown in Fig. 5.3, the $Na_2(THF)_n^+$ node achieves $\sim$75% rotation around 5.5 Å for both the $Na(THF)_4{-}Na(THF)_5^+$ and the $Na(THF)_5{-}Na(THF)_5^+$ state.

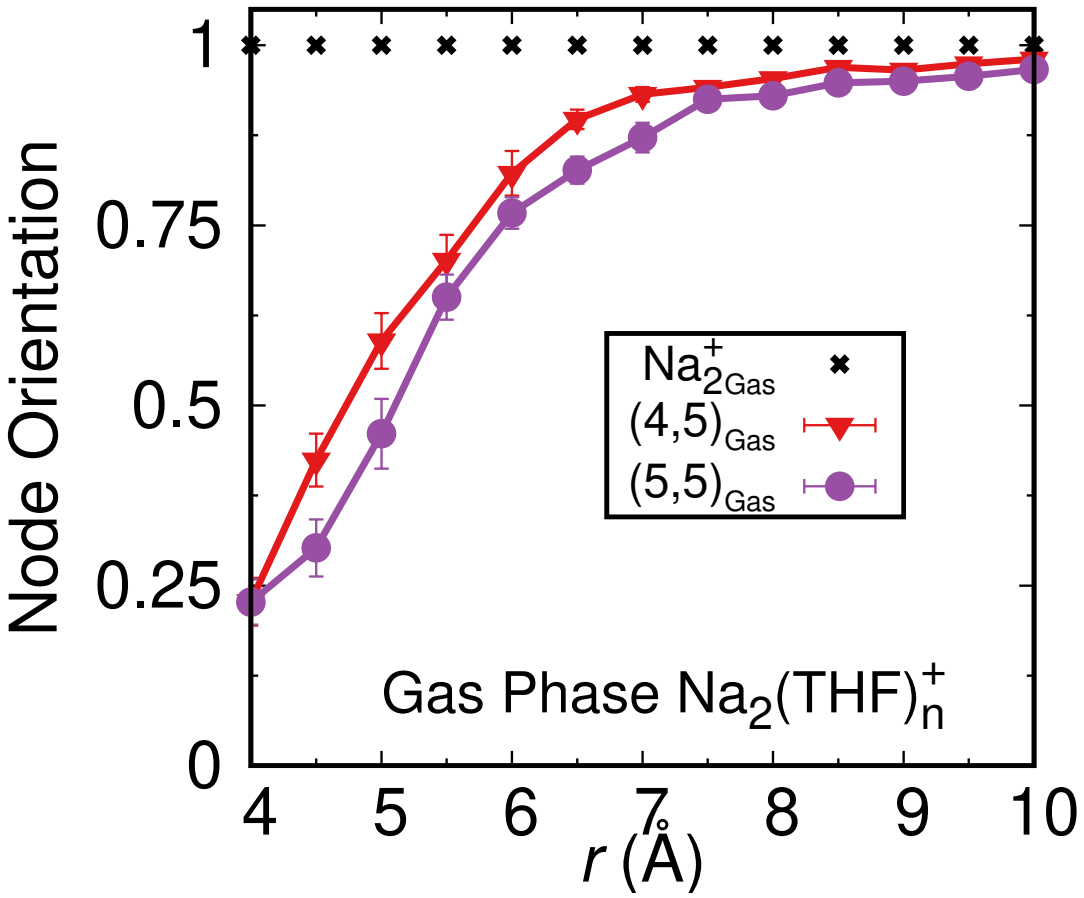

Figure 5.3: Orientation of the node of the Na_2^+ excited state rotates from along the bond axis to perpendicular to the bond axis with increasing bond length. The dot product of the Na_2^+ bond axis with the Frank-Condon ground/excited state overlap tracks the orientation of the node between the two lobes of electron density in the Na_2^+ or $Na_2(THF)_n^+$ excited state. We call this the node angle, which is here plotted on a scale from zero (node parallel to the bond axis) to one (node perpendicular to the bond axis). For Na_2^+, (black crosses) the node angle remains perpendicular to the bond axis regardless of bond length. However, for the $Na_2(THF)_n^+$ species, the node angle must rotate from a parallel π bonding structure to a perpendicular σ^* structure. The error bars shown represent 95% confidence intervals.

5.4.2 Rotation of the $Na_2(THF)_n^+$ Valence Electron's Density is Controlled by the Dative-Bonded THF Molecules

The reason the bonding electron is able to rotate from the π-like to σ*-like position can only lie with how the coordinated THF molecules respond to the excited state electron differently than the ground state electron. For the ground state $Na_2(THF)_n^+$ species, most of the electron's density sits between the two Na^+ cores, like a σ bonding orbital. This means that in order for the coordinating THFs to form dative bonds with the Na^+ cores, they shove even more electron density to the center of the molecule. This causes the Na_2^+ bond length to increase to accommodate the extra electron density, and any further excess spills out above and below the bond. This results in coordination structures around each Na^+ core that resemble the square pyramidal (for the penta-coordinated Na^+ of $Na(THF)_4{-}Na(THF)_5^+$ and $Na(THF)_5{-}Na(THF)_5^+$) and seesaw (for the tetra-coordinated Na^+ of $Na(THF)_4{-}Na(THF)_5^+$) molecular geometries from simple VSEPR theory.[132] Table 5.1 shows the average O–O bond angles between the datively-bound THF molecules when there are five THFs coordinating a Na^+ core (penta-coordinated), regardless of whether that core is part of the $Na(THF)_4{-}Na(THF)_5^+$ or $Na(THF)_5{-}Na(THF)_5^+$ molecular species, both during ground state dynamics and when the molecule is held at a dissociative distance of 10.0 Å.

According to Table 5.1, during ground state dynamics, the THFs around a penta-coordinated Na^+ core take on angles similar to those of a square pyramidal molecular geometry, which would predict two ∼180 degree angles while everything else is ∼90 degrees apart. This makes sense because in the ground state, the electronic density lies primarily in-between the two Na^+ cores. Thus, each Na^+ core sees approximately the full valence electron much like a 'lone pair' from VSEPR theory.[132] However, after the molecule has dissociated, each Na^+ core sees only about half an electron. Thus, the coordinating THFs have more room to spread out and begin to take on a hybrid square pyramidal/trigonal bipyramidal structure. The main effects on the bond angles is a ∼25 degree decrease in the second largest angle and

Ground State Dynamics	Held at 10.0 Å Dissociation
170 ± 5	164 ± 8
162 ± 6	137 ± 7
102 ± 7	119 ± 7
98 ± 4	106 ± 5
94 ± 3	101 ± 5
91 ± 3	95 ± 3
88 ± 3	92 ± 3
85 ± 3	88 ± 3
82 ± 3	83 ± 3
79 ± 3	78 ± 5

Table 5.1: Average bond angles between datively-bound THF molecules of penta-coordinated Na^+ cores. During ground state dynamics, the orientation of the datively-bound THF molecules resembles the square pyramidal geometry from VSEPR theory, which is perhaps unsurprising because this Na^+ structure has five equivalent bonds to THF oxygen sites and sees approximately one whole electron at the center of the bond. The major differences between the average bond angles during ground state dynamics and when the molecule is held at a dissociative distance of 10.0 Å is a ∼25 degree decrease in the second largest angle and a ∼17 degree increase in the third largest angle. This indicates a shift toward a hybrid square pyramidal/trigonal bipyramidal structure since the Na^+ core now sees only approximately half an electron.

a ∼17 degree increase in the third largest angle, constituting a move away from the square pyramidal structure of the ground state.

Ground State Dynamics	Held at 10.0 ÅDissociation
156 ± 11	135 ± 12
115 ± 14	117 ± 7
98 ± 7	109 ± 5
89 ± 5	102 ± 5
83 ± 5	97 ± 5
77 ± 5	90 ± 6

Table 5.2: Average bond angles between datively-bound THF molecules of tetra-coordinated Na^+ cores. During ground state dynamics, the orientation of the datively bound THF molecules resembles the seesaw geometry from VSEPR theory. This makes sense because this Na^+ structure has four equivalent bonds to THF oxygen sites and sees approximately one whole electron at the center of the bond. The major differences between the average bond angles during ground state dynamics and when the molecule is held at a dissociative distance of 10.0 Å is a ∼21 degree decrease in the largest angle. This indicates a shift toward a hybrid seesaw/tetrahedral structure since the Na^+ core now sees only approximately half an electron.

Table 5.2 shows the average O–O bond angles between the datively-bound THF molecules

when there are four THFs coordinating a Na^+ core (tetra-coordinated), which only occurs for the $Na(THF)_4$−$Na(THF)_5^+$ molecular species, both during ground state dynamics and when the molecule is held at a dissociative distance of 10.0 Å. Four is also the expected coordination of Na^0 in THF, which our group has previously found must be understood as an (Na^+,e^-) tight contact pair due to the valence electron being significantly displaced from the sodium core by the four dative-bonded THF molecules.[86] During the ground state dynamics, the THFs around the tetra-coordinated Na^+ core arrange themselves with angles similar to those of a seesaw molecular geometry, with one ∼180 degree angle, one ∼120 degree angle, and the rest ∼90 degrees apart. Again, this is because the tetra-coordinated Na^+ core sees approximately the full valence electron similar to how a 'lone pair' would be seen by the central atom in VSEPR theory.[132] Once the molecule has dissociated, however, the coordinating THFs respond to the reduced electronic density by spreading out to take on a structure closer to a hybrid of seesaw and tetrahedral. Thus all of the O–O angles adjust toward ∼109.5 degrees, with the biggest change being a ∼21 degree decrease in the largest angle.

Now we know that the arrangement of the coordinating THF molecules around each Na^+ core cause the breakdown in LR observed for the rotation of the $Na_2(THF)_n^+$ excited state node shown in Fig 5.3 and that that node rotation is what gives rise to the 'kink' in the PECs of $Na_2(THF)_n^+$ predicted from the ground state, as observed in Fig. 5.1.

Now we can move on to comparing the more rigorous definition of LR, the comparison of equilibrium (umbrella-sampled) and nonequilibrium (dynamic) dissociation.

5.4.3 Linear Response Breakdown for the Nonequilibrium Dissociation Dynamics of Gas Phase $Na_2(THF)_n^+$ Species

Now that we understand the LR approximation for the photodissociation of the gas-phase $Na_2(THF)_n^+$ species and how the shift in molecular geometry around each sodium core allows the bonding electron to rotate from the π-like to σ^*-like orientation, we can delve into the

nonequilibrium dissociation dynamics of these molecules to explore how the datively-bound THF molecules cause a breakdown of LR. It is important to note that all of the surfaces shown in Fig. 5.1 are constructed by using umbrella sampling to hold the Na–Na bond at fixed distances at equilibrium. This means that the system has plenty of time to achieve the optimal arrangement of the coordinating solvent molecules at each bond distance. To observe actual dissociation dynamics, the molecule was placed in the first excited state from ground state configurations at the Na–Na equilibrium bond length. For gas-phase Na_2^+, the equilibrium bond length is 3.84 Å. For the gas-phase $Na_2(THF)_n^+$ species, the equilibrium bond length is 4.95 Å for $Na(THF)_4{-}Na(THF)_5^+$ and 5.70 Å for $Na(THF)_5{-}Na(THF)_5^+$. The system must then reorganize dynamically in order to reach the appropriate dissociative structure rather than following the smooth dissociative curve predicted from the LR excited state curves in Fig. 5.1, which will effect how the system behaves during dissociation.

Figure 5.4 plots the average Na–Na bond distances (solid lines) and node angles (dashed lines) during the dissociation of gas-phase Na_2^+ (panel (a), black lines) and the coordinated $Na_2(THF)_n^+$ species (panel (b), red lines for the $Na(THF)_4{-}Na(THF)_5^+$ state and purple for the $Na(THF)_5{-}Na(THF)_5^+$ state). As can be seen from Fig. 5.4a, the dissociation of gas-phase Na_2^+ occurs smoothly, as expected from its excited state PEC. Upon excitation, the two Na^+ cores immediately begin dissociating, building up momentum until the cores are far enough apart to no longer influence each other, after which the cores continue to move apart with a fixed velocity. At time zero, the node angle is already at the one position, indicating that the excited state electron's node is perfectly perpendicular to the Na–Na bond axis, a position which is retained throughout the entire dissociation trajectory.

However, in Figure 5.4b we can see that the $Na_2(THF)_n^+$ species take much longer to dissociate (about 2000 fs to reach the same 10 Å separation that gas phase Na_2^+ achieved in less than 200 fs). This is due to two primary factors. First, as discussed previously, although the Na–Na bond of $Na_2(THF)_n^+$ is immediately weakened upon excitation, the electronic density initially sits in a π bonding position, indicated by a node angle of about 0.25, which

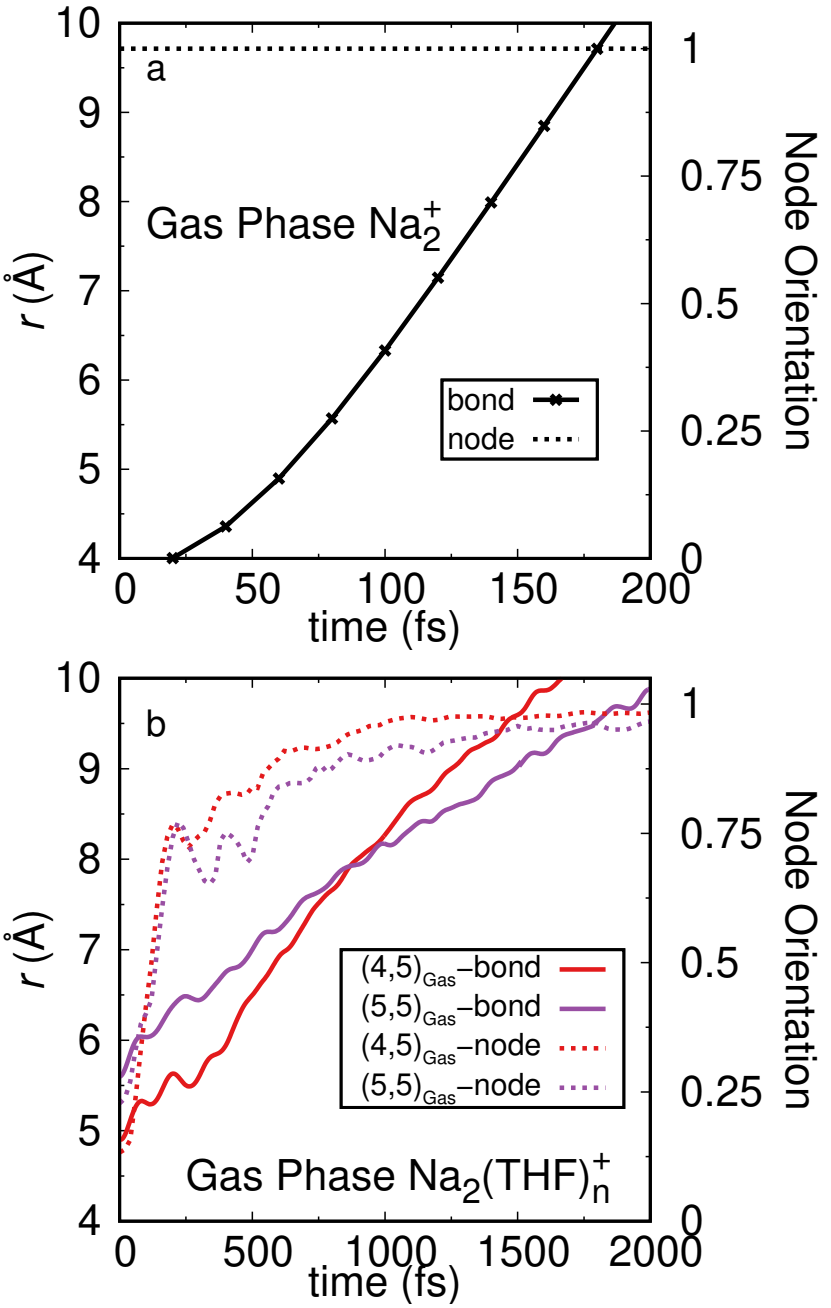

Figure 5.4: Nonequilibrium dissociation dynamics of gas-phase Na_2^+ and $Na_2(THF)_n^+$. Panel (a) shows the bond length (solid black line) and node angle (dashed black line) during the dissociation of gas phase Na_2^+. In panel (b), the solid red curve shows the Na–Na bond distance as a function of time for the $Na(THF)_4$−$Na(THF)_5^+$ species while the purple curve shows the same for $Na(THF)_5$−$Na(THF)_5^+$. Likewise, the dashed curves correspond to the node angle of the same species.

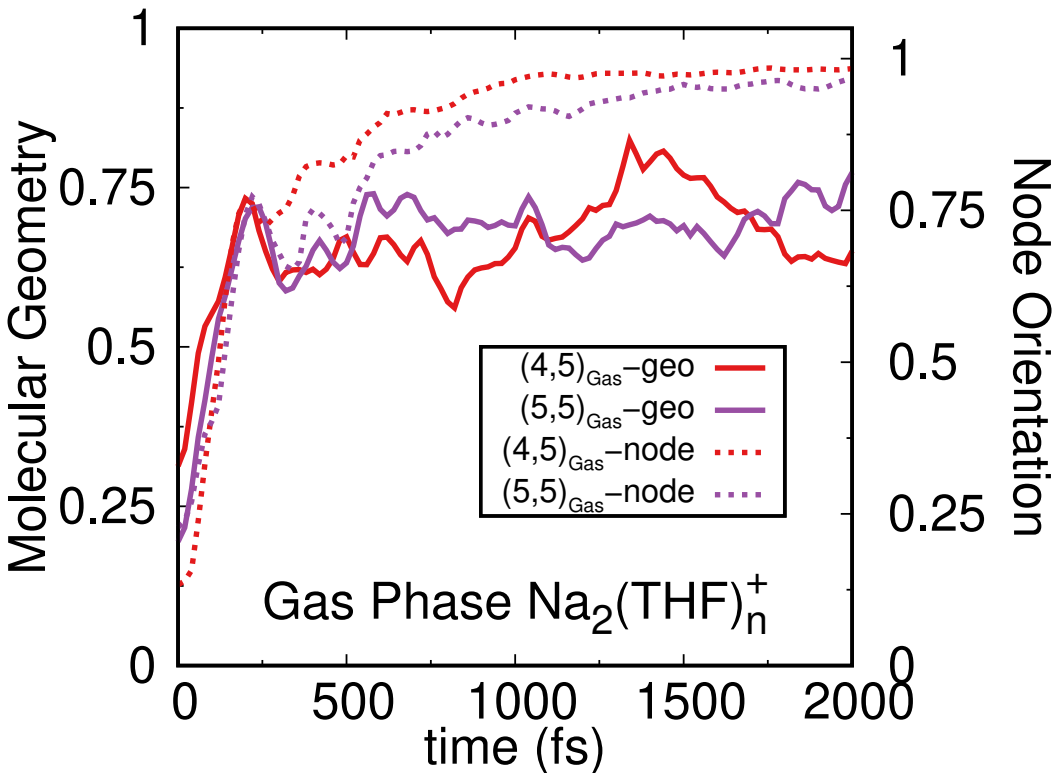

Figure 5.5: Node rotation correlates with the shift in the molecular geometry around each coordinated Na^+ core. The molecular geometry of each $Na_2(THF)_n^+$ molecule is defined by treating the average ground state O–O angles around each Na^+ core as the 'zero' state and the average O–O angles around each core at dissociation as the 'one' state, with each O–O angle weighted according to the magnitude of its shift from ground state to dissociation. The solid lines indicate the molecular geometry of each $Na_2(THF)_n^+$ species, with a red line for $Na(THF)_4$–$Na(THF)_5^+$ and a purple line for $Na(THF)_5$–$Na(THF)_5^+$, while the dashed lines indicate the node angles.

means that the excited state's node lies nearly parallel to the bond axis. This means that while the Na–Na bond is weakened, the molecule is not yet truly dissociative. While the umbrella sampled dynamics gave the system enough time to form the optimal configuration at each bond length, during dynamic dissociation, those rearrangements must take place on the fly. This leads to the initial 'hiccups' in the Na–Na bond length and node angle during the first few hundred femtoseconds of the dissociation trajectories, even though these properties have been averaged over twenty dissociation trajectories per $Na_2(THF)_n^+$ state, because the electronic density is trying to rotate into the dissociative position but must first wait for the coordinating THF molecules to move out of the way.

After about 250 fs, the node of the electronic density has rotated to an orientation of about 0.75, which indicates a position much closer to the σ^* orientation necessary for dissociation. This corresponds with a boost in the Na–Na dissociation. However, even after the $Na_2(THF)_n^+$ molecule has taken the optimal dissociation configuration, each Na^+ core must drag four to five THF molecules with it as it dissociates. Due to this increase in mass, the molecule falls apart more slowly. Furthermore, based on Fig. 5.4, during dynamic dissociation, the node of the valence bonding electron does not rotate to 0.75 until about 5.7 Å for the $Na(THF)_4{-}Na(THF)_5^+$ state and 6.5 Å for the $Na(THF)_5{-}Na(THF)_5^+$ state, later than the LR prediction of about 5.5 Å for both states shown in Fig. 5.3. This shows that LR fails for the photodissociation of the the $Na_2(THF)_n^+$ molecules: due to the need to account for on-the-fly changes to the solute's local solvent environment, it is only by propagating dynamically that we can fully understand this photodissociation process.

As predicted in Tables 5.1 and 5.2, the node rotation plotted in Fig. 5.4b is entirely controlled by the positions of the THF molecules coordinating each Na^+ core. Figure 5.5 compares the node angle during the $Na_2(THF)_n^+$ dissociation trajectories (dashed red and purple lines) with the shift in the molecular geometry around each Na^+ core (solid red and purple lines). The molecular geometry of the $Na_2(THF)_n^+$ molecule is defined by treating the average ground state O–O angles around each Na^+ core as the 'zero' state and the average O–O angles around each core at dissociation as the 'one' state, with each O–O angle weighted according to the magnitude of its shift from ground state to dissociation. Thus, those angles that change most dramatically have the largest influence on the molecular geometry coordinate whilst those with only a small shift have only a small effect.

As can be seen in Fig. 5.5, the rotation of the $Na_2(THF)_n^+$ electron density from the π bonding to the σ^* orientations correlates perfectly with the shift in molecular geometry around each Na^+ core. Due to the large variation in O–O angles, the molecular geometry never achieves a 'perfect one', but instead levels off around 0.75 at the precise point that the node angle achieves full rotation. This occurs at about 500 fs into the dissociation dynamics.

The 'wiggles' in the node angle/molecular geometry between ∼250 and ∼500 fs are due to minor reorientation of the electronic density after the σ^* orientation has been achieved.

5.4.4 Dissociation Dynamics of $Na_2(THF)_n^+$ Solvated in Liquid THF are Further Complicated by Changing Chemical Identity

Now that we understand the dissociation dynamics of the gas-phase $Na_2(THF)_n^+$ species, we turn our attention to Na_2^+ in full condensed phase THF. Exploring the dissociation dynamics of the $Na_2(THF)_n^+$ species in THF becomes even more complicated because in the full condensed phase, the coordination number on each Na^+ core can fluctuate. As we have seen previously, for $Na_2(THF)_n^+$ at equilibrium in full-condensed phase THF, the ground-state solute spends about 30% of its time in the $Na(THF)_4{-}Na(THF)_5^+$ state and about 70% of its time in the $Na(THF)_5{-}Na(THF)_5^+$. This means that when we photoexcite $Na_2(THF)_n^+$ in the full-condensed phase, we have a chance of starting on one of two primary dissociation pathways, which could be easily selected by the choice of excitation wavelength. This already indicates a new LR breakdown because equilibrium dynamics will wash out this important distinction because the interconversion from one coordination state to the other occurs on a time scale close enough to that of the dissociation dynamics that the two aren't fully separable.

To get a better sense of how the equilibrium LR and nonequilibrium dissociation dynamics differ, Figure 5.6 plots the umbrella-sampled potential of mean force (PMF) for the LR prediction of $Na_2(THF)_n^+$ dissociation in THF (blue diamonds) as compared to the PMFs for nonequilibrium, dynamic dissociation beginning from both the equilibrium Na–Na bond length of condensed phase $Na(THF)_4{-}Na(THF)_5^+$ (4.8 Å, red triangles) and the equilibrium Na–Na bond length of condensed phase $Na(THF)_5{-}Na(THF)_5^+$ (5.6 Å, purple circles). These dynamic PMFs were constructed in the same manner as we reported in previous work.[131]

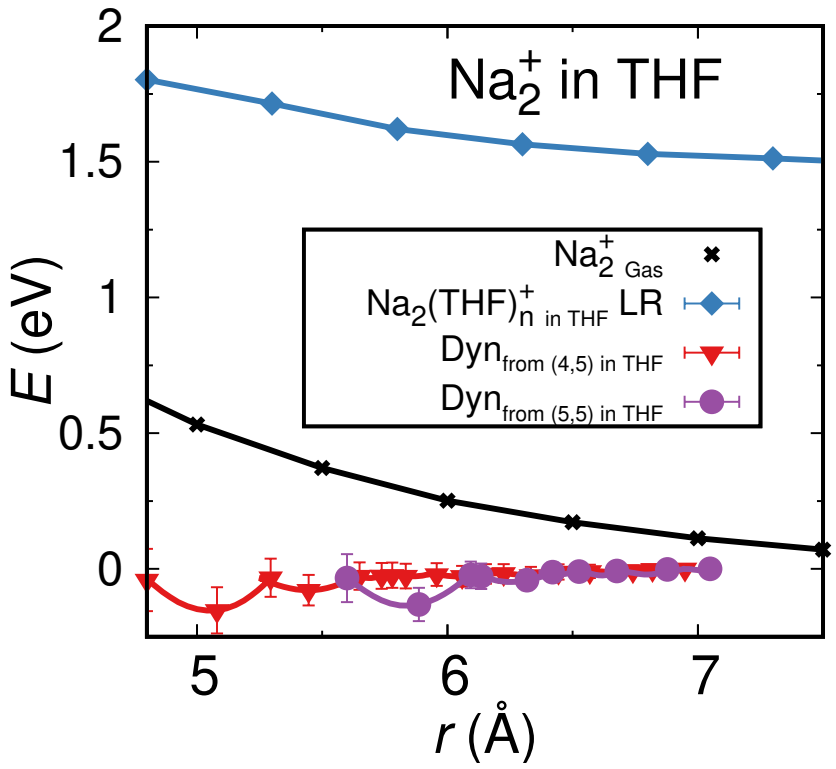

Figure 5.6: Comparison of the equilibrium, linear response prediction of $Na_2(THF)_n^+$ dissociation in full-condensed phase THF to the molecule's nonequilibrium dissociation dynamics reveals that, while both the LR prediction (blue diamonds) and dynamic dissociation from the $Na(THF)_4{-}Na(THF)_5^+$ (red triangles) and $Na(THF)_5{-}Na(THF)_5^+$ (purple circles) states are shallower than the potential energy curve of gas-phase Na_2^+, the dynamic curves show a distinctly different process. Thus, linear response breaks down for the dissociation of $Na_2(THF)_n^+$ in full-condensed phase THF just as it did for the $Na_2(THF)_n^+$ structures in the gas phase.

The gas-phase PEC of Na_2^+ is also included for comparison (black curve). Even the LR prediction for the $Na_2(THF)_n^+$ condensed phase dissociation is far shallower than that of gas-phase Na_2^+, but the dynamic PMFs are virtually flat except for a few dips at lower Na–Na bond lengths. This indicates that even though LR predicts $Na_2(THF)_n^+$ to be dissociative in the full-condensed phase, in reality the molecule struggles to come apart. We have described this process in general terms previously,[131] but will here go into more detail about the specific features of these dynamic curves.

To do so, we delve into the nonequilibrium dissociation trajectories to examine several key shifts in the $Na_2(THF)_n^+$ structure. We have already seen the dramatic rotation of the bonding electron's node that occurs during the dissociation of gas-phase $Na_2(THF)_n^+$. This same process occurs in the full condensed phase, but now it is complicated by the changing chemical identity of the solute as it forms new Na–THF oxygen-site dative bonds while dissociating. In particular, it is important to note that we would expect the photofragments of Na_2^+ in THF when fully dissociated to be one Na^+ cation solvated on average by six THF molecules and one Na^0 solvated on average by four THF molecules.[86] In the gas phase, no particles outside of the $Na_2(THF)_n^+$ species exist to make a measurement on the quantum mechanical valence electron. Thus, even at full dissociation, approximately half of the electron continues to reside on each Na^+ core. In the condensed phase, however, we would expect the uncoordinated solvent molecules to make measurements on the quantum mechanical electron, eventually forcing it to localize on one Na^+ core and thus reach the Na^+/Na^0 structure at full dissociation. The actual process, however, is complicated by the changing chemical identity of the molecule.

Figure 5.7 plots the node orientation of the $Na_2(THF)_n^+$ molecule at various umbrella-sampled bond lengths, both when residing on the ground state (a) and on the excited state (b). Notably, when propagating on the ground state, the node angle (black diamonds) never reaches one, instead leveling off around 0.5. This makes sense, however, when taking into account the number of solvent molecules coordinating each Na^+ core (n_{Na^+}), plotted

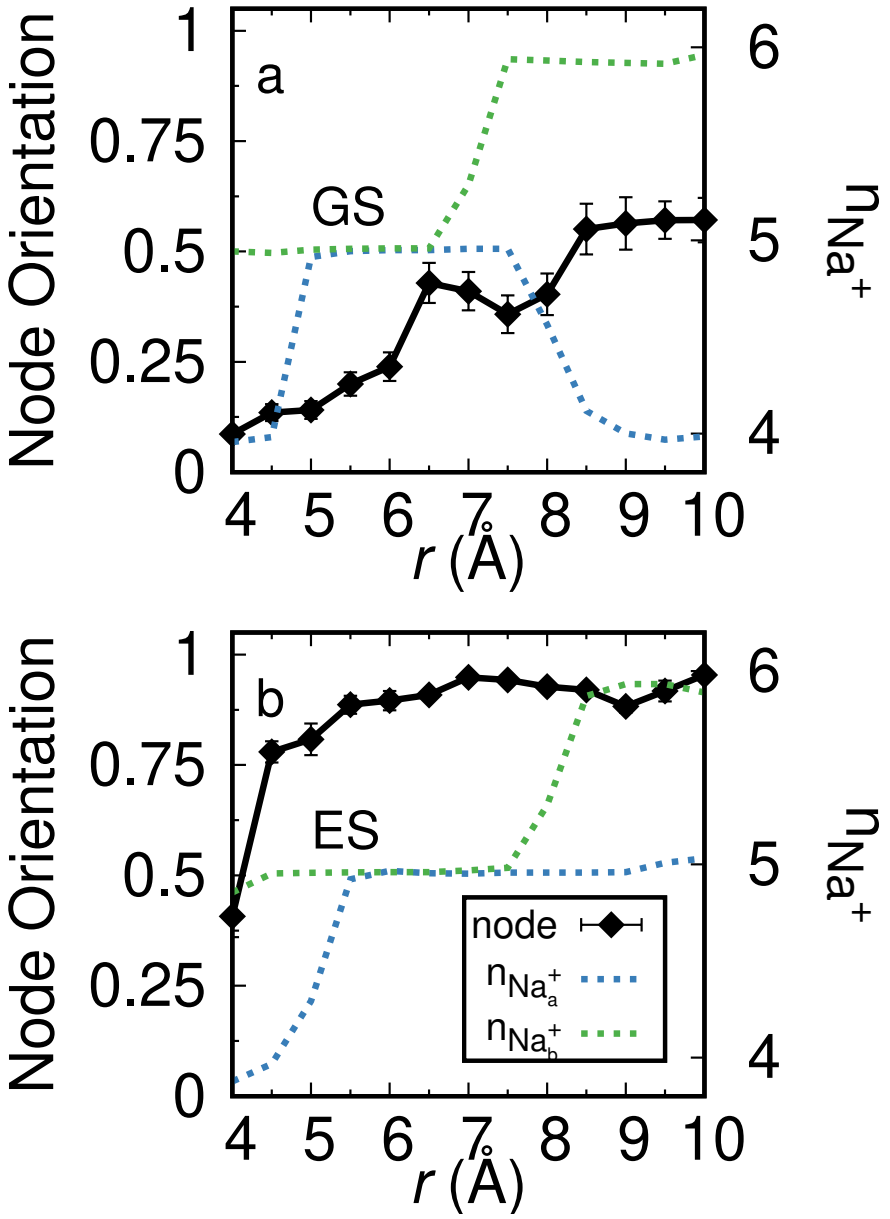

Figure 5.7: Node angle and n_{Na^+} coordinate differ when pulling the $Na_2(THF)_n^+$ molecule apart in the ground and excited state. Panel (a) shows the node angle and coordination number (n_{Na^+}) on each Na^+ core at the various umbrella sampled bond lengths while panel (b) shows the same for the $Na_2(THF)_n^+$ excited state. The node angle is plotted as black diamonds while n_{Na^+} is plotted in dashed blue and green to represent the coordination of the two Na^+ cores. For the ground state LR prediction, the electron eventually localizes as the solute comes apart, allowing the expected geometries of hexa-coordinated Na^+ and tetra-coordinated Na^0 at long distances. However, in the excited state prediction, the molecule instead retains some electronic density on each sodium core within the Na–Na distances studied, causing the molecule to remain in a $Na(THF)_5{-}Na(THF)_6^+$ state.

in Fig. 5.7a as dashed blue and green lines representing the coordination number of each sodium. At about 8 Å, the same bond length where the node angle levels off at 0.5, the electron localizes onto one of the Na^+ cores, resulting in one Na^0 with four coordinating THF solvent molecules and one bare Na^+ cation with six coordinating THF solvent molecules. When propagating in the excited state (Fig. 5.7b), however, entirely different dynamics are seen. First, the node rotates into a dissociative position even at low bond lengths, achieving 75% rotation at only a 4.5 Å Na–Na distance. Second, the coordination numbers of each Na^+ core indicate that even though the electron localizes primarily on one Na^+ core at long bond distances, the molecule never splits into the hexa-coordinated Na^+ and tetra-coordinated Na^0 components expected at full dissociation. Instead, the Na^+ that carries the electron prefers coordination by five THF molecules up to the distances we can accurately calculate inside our simulation box. Again, this shows the breakdown of linear response between propagation on the ground and excited state for the $Na_2(THF)_n^+$ species because the ground state equilibrium dynamics are clearly insufficient to understand even the LR of the excited state.

Finally, dissociation dynamics of Na_2^+ in THF reveal the difficulty the Na_2^+ molecule has fully dissociating in the full-condensed phase. Twenty dissociation runs were conducted from the equilibrium bond distance of each $Na_2(THF)_n^+$ state ($Na(THF)_4$−$Na(THF)_5^+$ and $Na(THF)_5$−$Na(THF)_5^+$) and the averaged results for the bond length and node angle are plotted in Fig. 5.8. The Na–Na bond distance over time (solid red curve for dissociation from the $Na(THF)_4$−$Na(THF)_5^+$ state and solid purple curve for dissociation from the $Na(THF)_5$−$Na(THF)_5^+$ state) reveals that the initial dissociation of $Na_2(THF)_n^+$ in the condensed phase occurs quite similarly to that of gas-phase $Na_2(THF)_n^+$: after an initial loosening of the bond due to the π bonding positioning of the electronic density, the molecule must then wait for the bonding electron to rotate into the dissociative σ^* position before normal dissociation dynamics can commence. The node angle for dissociation from each state (red and purple dashed lines) rotates at approximately the same point, after about 250 fs, which

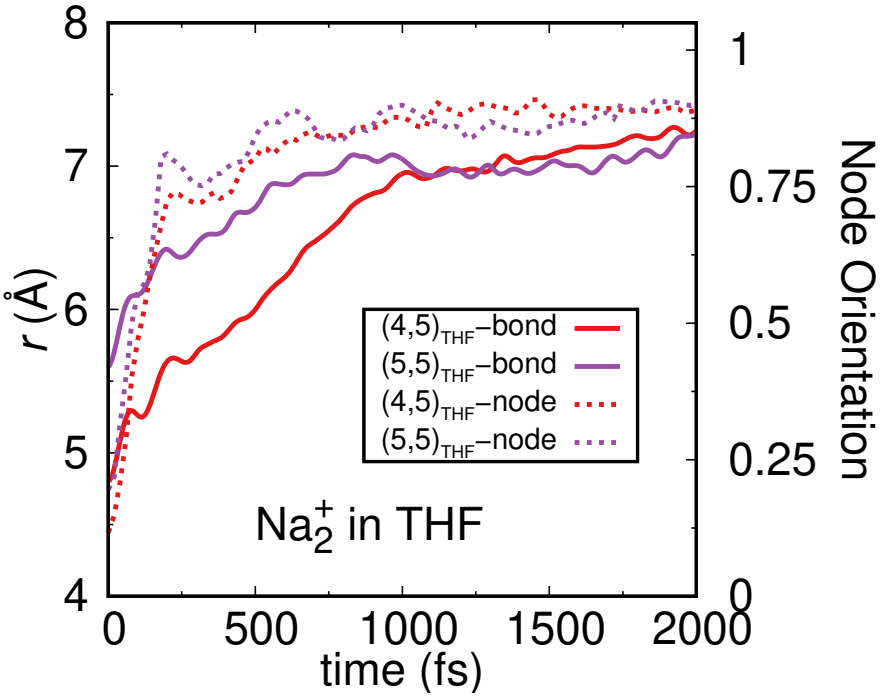

Figure 5.8: Nonequilibrium dissociation dynamics of $Na_2(THF)_n^+$ in THF begin similar to those of gas-phase $Na_2(THF)_n^+$. During the first few hundred picoseconds, the electronic density rotates from the π bonding to σ^* position, as evident by the jump in the node angle (dashed red for dissociation from the $Na(THF)_4{-}Na(THF)_5^+$ state and dashed purple for dissociation from the $Na(THF)_5{-}Na(THF)_5^+$ state) as well as the stall in the increase of the Na–Na bond length (solid red and purple curves) before normal dissociation dynamics can begin. However, around 7 Å, the molecule encounters the solvent cage of THF molecules which attempt to trap the Na_2^+ molecule. Lacking sufficient energy to escape the solvent cage, the molecule instead becomes trapped.

matches the point where the molecule becomes truly dissociative.

The molecule has difficulty, however, dissociating past a distance of about 7 Å. It is important to note when dissociating from the $Na(THF)_5{-}Na(THF)_5^+$ state, the molecule tends to remain in that state for the entire trajectory. However, when dissociating from the $Na(THF)_4{-}Na(THF)_5^+$ state, the molecule tended to convert to the $Na(THF)_5{-}Na(THF)_5^+$ within the first few hundred picoseconds, meaning that by ∼7 Å the $Na_2(THF)_n^+$ molecule behaves similarly regardless of the starting coordination as evidenced by the near overlap of their average dissociation trajectory beyond that point. In the LR prediction, it is just beyond that Na–Na bond distance of ∼7 Å that the $Na_2(THF)_n^+$ molecule transitions from the $Na(THF)_5{-}Na(THF)_5^+$ to the $Na(THF)_5{-}Na(THF)_6^+$ state, as shown in Fig. 5.7b. Because the process of rotating the electron density from the π-like to σ^* orientation consumes a large amount of energy, the solute now lacks sufficient energy to form the sixth dative bond on one sodium that would allow dissociation to continue. Thus, the $Na_2(THF)_n^+$ molecule becomes trapped during dissociation dynamics in full-condensed THF, a process that the LR approximation fails to capture due to the way the local solvent environment influences the electronic structure and chemical identity of the solute.

5.5 Conclusions

Through MQC MD simulations, we have explored the photodissociation of gas-phase Na_2^+, gas-phase $Na_2(THF)_n^+$, and $Na_2(THF)_n^+$ in liquid THF with particular investigation into how the modest solute–solvent interactions present between the Na^+ cores and their dative-bonded THF molecules intricately connects with the rotation of the excited state bonding electronic density from a π bonding to a σ^* position after photoexcitation of the $Na_2(THF)_n^+$ species. We have described how this rotation of the valence electronic density is facilitated by a shift in the molecular geometry of the THF molecules datively-bound to each sodium. Specifically, in the ground state, the tetra-coordinated sodium of

$Na(THF)_4{-}Na(THF)_5^+$ prefers a seesaw molecular geometry while the penta-coordinated sodiums of $Na(THF)_4{-}Na(THF)_5^+$ and $Na(THF)_5{-}Na(THF)_5^+$ prefer square pyramidal. However, the bonding electron density can only rotate when these geometries shift toward tetrahedral and trigonal bipyramidal, respectively. This process leads to a breakdown of LR. Because the LR approximation allows the local solvent structure to equilibrate, it fails to predict the nonequilibrium dynamic behavior of the dative-bonded THFs during actual dissociation dynamics.

Finally, dissociation of $Na_2(THF)_n^+$ in the full condensed phase becomes even more complex due to the potential for the solute to change identity dynamically during dissociation, thus further contributing to the breakdown of the LR approximation for this system. While the bonding electron resides on the electronic ground state, the $Na_2(THF)_n^+$ molecule comes apart in THF as a hexa-coordinated Na^+ and a tetra-coordinated Na^0, matching the expected equilibrium coordination of these fragments and indicating that the electron has fully localized. However, if the process is repeated with the electron residing the excited state, the molecule instead comes apart as a loosely bound $Na(THF)_5{-}Na(THF)_6^+$ species and the electron does not localize at the Na–Na bond lengths we can measure in our simulation. Furthermore, during nonequilbrium, dynamic dissociation, we find that the $Na_2(THF)_n^+$ lacks sufficient energy after the rotation of the electronic density to form the final dative bond to achieve the $Na(THF)_5{-}Na(THF)_6^+$ necessary to continue dissociation, instead becoming trapped in the $Na(THF)_5{-}Na(THF)_5^+$ after reaching a Na–Na bond length of ~ 7.0 Å. In sum, we have shown that when solute–solvent interactions of about the order of a hydrogen bond are present in a condensed phase system, the solute's electronic structure and thus dynamics and reactivity are actually controlled by the local solvent environment.

Appendices

Appendix A

Source Code for Running Molecular Dynamics Simulations

The source code used for this work can be found on the Schwartz Group Bitbucket, which is a code repository located at https://bitbucket.org/. The code used for simulations of Na_2 and Na_2^+ in THF is located in the folder "dimer_thf" while the code used for simulations of Na_2^+ in Argon is located in the folder "na2cat-liquidar-jaypseudo". All of the libraries needed to compile the source code are located on my Hoffman2 home directory (/u/home/w/widmer) in the folder "libraries". Likewise, the input files necessary to run the code are located on my Hoffman2 home directory in the folder "inputs".

The input file "param.input" contains various parameters that can be edited to influence either the type of simulation run or the type of data output. Here, I will outline some of the most important parameters and their functions:

- MAXSTEPS: how many time steps the simulation will run
- RESTART: if set to "T" the simulation will look for a restart.out file to restart a previously run simulation
- VRESCALE: if set to "T" the simulation will rescale velocities to equilibrate at a

specified temperature

- TEMP_TARGET: the target simulation temperature
- NSTEPDENS: determines how often to write out the electronic density as well as the file "density.cube" which can be used to create simulation snapshots in the program VMD
- NSTEPDIP: determines how often to write out the Frank-Condon overlap between the energy levels calculated which can be used to find the solute's absorption spectrum and node angle as discussed in chapter 5
- NCONFOUT: determines how often to write out the positions and velocities of all atoms in the simulation
- R_CELL: the length of one side of the simulation box
- NELEC: how many valence electrons are present in the simulation–1 for Na_2^+ and 2 for Na_2
- GRBXMX: how much of the simulation cell should the electronic grid span
- NGRID: how many grid points run along one side of the grid
- REFST: which electronic state will the system propagate on
- NSTATES: how many electronic states should the simulation calculate (note that this must be equal to or greater than REFST)
- DOBUMB: set to "T" to do umbrella sampling along the Na–Na bond axis
- BONDK: the force constant used for the Na–Na umbrella potential
- BONDZETA: the target Na–Na bond length

- DOUMB: set to "T" to do umbrella sampling of the coordination number around each sodium
- COORDK: the force constant used for the coordination number umbrella potential
- COORDKAPPA: a parameter that controls the steepness of the coordination cutoff
- COORDZETA1: the target coordination number around sodium 1
- COORDZETA2: the target coordination number around sodium 2
- COORDCUT: the Na–O cutoff distance
- NOSOLVENT: set to "T" to run a gas phase simulation
- NA_E_PP: determines which Na^+ pseudopotential to utilize during the simulation

When run, the code outputs a variety of output files. Here, I will outline some of the most important files:

- bondumb2.out: Na–Na bond length for use in calculating the umbrella sampled Na–Na potential of mean force
- out.conf: positions and velocites of all atoms in the simulation
- out.densityN: the electronic density of the Nth calculated electronic state
- out.dip: Frank Condon overlap between the calculated electronic states
- out.e_comN: the electron center of mass of the Nth calculated electronic state
- out.energies_mf: the various energies of the simulation components
- out.na1_pos: the position of sodium 1
- out.na2_pos: the position of sodium 2

- out.na1_vel: the velocity of sodium 1
- out.na2_vel: the velocity of sodium 2
- out.quanteN: the quantum energy of the Nth electronic state
- out.wavefunctionN: the wavefunction of the Nth electronic state
- restart.out: the information needed for the simulation to restart from the most recently calculated time step
- umb2.out: the number of THF molecules coordinating each sodium for use in calculating the umbrella sampled coordination potential of mean force

Appendix B

Analysis Scripts

The various codes used for analysis of the simulation trajectories are located on my Hoffman2 home directory in the folder "utilities". While not an exhaustive list, here, I will outline a few of the most useful analysis scripts:

- bond_coordinate_calc.f95: calculates the Na–Na bond coordinate from the file out.conf
- nodeangle.f95: calculates the orientation of the node of the lowest energy excited of Na_2^+ from the file out.dip
- absorbance_prep.f95: calculates the solute's absorption spectrum from the file out.dip
- closestArcube.f95: finds all argon atoms within a given radius of the solute and outputs a cube file used to generate a simulation snapshot in the program VMD
- closestTHFcube.f95: finds all THF molecules within a given radius of the solute and outputs a cube file used to generate a simulation snapshot in the program VMD
- na_coordinate_calc.f95: calculates the coordination coordinate around each sodium from the file out.conf

- bondvel.f95: calculates the bond velocity autocorrelation function from the files out.na1_pos, out.na2_pos, out.na1_vel, and out.na2_vel–the fourier transfer of the bond velocity autocorrelation then gives the power spectrum

- dipole_vector.f95: calculates the dipole moment and dipole moment autocorrelation function from the files out.na1_pos, out.na2_pos, and out.e_com1–the fourier transfer of the dipole autocorrelation then gives the infrared spectrum

- calculate_rdf.f95: calculates the Na–THF oxygen-site radial distribution function from the file out.conf

- calc_solvent_angles.f95: calculates the oxygen–oxygen angles of dative-bonded THF molcules

The mbar code used to calculate the potential of mean force from umbrella sampled data is stored on the Schwartz Group Bitbucket in the folder "util/umbrella-pmf.py".

References

[1] A. L. Harris, J. K. Brown, and C. B. Harris. The nature of simple photodissociation reactions in liquids on ultrafast time scales. *Ann. Rev. Phys. Chem.*, 39:341–356, 1988.

[2] M. J. Blandamer and M. F. Fox. Theory and applications of charge-transfer to solvent spectra. *Chem. Rev.*, 70:59–93, 1970.

[3] R. A. Marcus. On the theory of oxidation–reduction reactions involving electron transfer. *J. Chem. Phys.*, 24:966–978, 1956.

[4] R. A. Marcus and N. Sutin. Electron transfers in chemistry and biology. *Acta Biochim. Biophys.*, 811:265–322, 1985.

[5] E. R. Barthel, I. B. Martini, and B. J. Schwartz. How does the solvent control electron transfer? Experimental and theoretical studies of the simplest charge transfer reaction. *J. Phys. Chem. B.*, 105:12230–12241, 2001.

[6] M. S. Pshenichnikov, A. Baltuska, and D. A. Wiersma. Hydrated-electron population dynamics. *Chem. Phys. Lett.*, 389:171–175, 2004.

[7] D. Madsen, C. L. Thomsen, J. Thogersen, and S. R. Keiding. Temperature dependent relaxation and recombination dynamics of the hydrated electron. *J. Chem. Phys.*, 113:1126–1134, 2000.

[8] J. Lindner, A. N. Unterreiner, and P. Vohringer. Femtosecond relaxation dynamics of solvated electrons in liquid ammonia. *Chem. Phys. Chem.*, 7:363–369, 2006.

[9] P. J. Rossky and J. Scnitker. The hydrated electron: Quantum simulation of structure, spectroscopy, and dynamics. *J. Phys. Chem.*, 92:4277–4285, 1988.

[10] D. F. Coker, B. J. Berne, and D. Thirumalai. Path integral Monte-Carlo studies of the behavior of excess electrons in simple fluids. *J. Chem. Phys*, 86:5689–5702, 1987.

[11] E. Neria, A. Nitzan, R. N. Barnett, and U. Landman. Quantum dynamic simulations of nonadiabatic processes: Solvation dynamics of the hydrated electron. *Phys. Rev. Lett.*, 67:1011–1014, 1991.

[12] D. Chandler and K. Leung. Excess electrons in liquids: Geometrical perspectives. *Ann. Rev. Phys. Chem.*, 45:557–591, 1994.

[13] K. F. Wong and P. J. Rossky. Mean-field molecular dynamics with surface hopping: Application to the aqueous solvated electron. *J. Phys. Chem. A*, 105:2546–2556, 2001.

[14] M. Boero, M. Parrinello, K. Terakura, T. Ikeshoji, and C. C. Liew. First-principles molecular-dynamics simulations of a hydrated electron in normal and supercritical water. *Phys. Rev. Lett.*, 90:226403, 2003.

[15] A. Staib and D. Borgis. Reaction pathways in the photodetachment of an electron from aqueous chloride: A quantum molecular dynamics study. *J. Chem. Phys.*, 104:9027–9039, 1996.

[16] C. Nicolas, A. Boutin, B. Levy, and D. Borgis. Molecular simulation of a hydrated electron at different thermodynamic state points. *J. Chem. Phys.*, 118:9689–9696, 2003.

[17] B. J. Scwhartz and P. J. Rossky. Aqueos solvation dynamics with a quantum-mechanical solute: Computer-simulation studies of the photoexcited hydrated electron. *J. Chem. Phys.*, 101:6902–6916, 1994.

[18] B. J. Scwhartz and P. J. Rossky. Pump-probe spectroscopy of the hydrated electron: A quantum molecular-dynamics simulation. *J. Chem. Phys.*, 101:6917–6926, 1994.

[19] B. J. Scwhartz and P. J. Rossky. Hydrated electrons as a probe of local anisotropy: Simulations of ultrafast polarization-dependent spectral hold-burning. *Phys. Rev. Lett.*, 72:3282–3285, 1994.

[20] L. Turi, A. Mosyak, and P. J. Rossky. Equilibrium structure, fluctuations, and spectroscopy of a solvated electron in methanol. *J. Chem. Phys.*, 107:1970–1980, 1997.

[21] J. J. Zhu and R. I. Cukier. A quantum-molecular dynamics simulation of an excess electron in methanol. *J. Chem. Phys.*, 98:5679–5693, 1993.

[22] M. Mitsui, N. Ando, S. Kokubo, A. Nakajima, and K. Kaya. Coexistence of solvated electrons and solvent valence anions in negatively charged acetonitrile clusters, $(CH_3CN)_n^-$ (n=10-100). *Phys. Rev. Lett.*, 91:153002, 2003.

[23] E. Gallicchio and B. J. Berne. On the calculation of dynamical properties of solvated electrons by maximum entropy analytic continuation of path integral Monte Carlo data. *J. Chem. Phys.*, 105:7064–7078, 1996.

[24] C. Silva, P. K. Walhout, P. J. Reid, and P. F. Barbara. Detailed investigations of the pump-probe spectroscopy of the equilibrated solvated electron in alcohols. *J. Phys. Chem. A*, 102:5701–5707, 1998.

[25] X. L. Shi, F. H. Long, and K. B. Eisenthal. Electron solvation in neat alcohols. *J. Phys. Chem.*, 99:6917–6922, 1995.

[26] M. C. Cavanagh and B. J. Schwartz. Searching for solvent cavities via electron photodetachment: The ultrafast charge-transfer-to-solvent (CTTS) dynamics of sodide in a series of ether solvents. *J. Chem. Phys.*, 131:1–12, 2009.

[27] C. J. Smallwood, C. N. Mejia, W. G. Glover, R. E. Larsen, and B. J. Schwartz. A computationally efficient exact pseudopotential method. 2. Application to the molecular pseudopotential of an excess electron interacting with tetrahydrofuran (THF). *J. Chem. Phys.*, 125:1–9, 2006.

[28] M. J. Bedard-Hearn, R. E. Larsen, and B. J. Schwartz. Understanding nonequilibrium solvent motions through molecular projections: Computer simulations of solvation dynamics in liquid tetrahydrofuran (THF). *J. Phys. Chem. B.*, 107:14464–14475, 2003.

[29] M. J. Bedard-Hearn, R. E. Larsen, and B. J. Schwartz. Moving solvated electrons with light: Nonadiabatic mixed quantum/classical molecular dynamics simluations of the relocalization of photoexcited solvated electrons in tetrahydrofuran (THF). *J. Chem. Phys.*, 125:1–8, 2006.

[30] S. C. Doan and B. J. Schwartz. Ultrafast studies of excess electrons in qiquid acetonitrile: Revisiting the solvated electron, solvent dimer anion equilibrium,. *J. Phys. Chem. B*, 117:4216–4221, 2013.

[31] W. J. Glover and B. J. Schwartz. The fluxional nature of the hydrated electron: Energy and entropy contributions to aqueous electron free energies. *J. Chem. Theory and Comput.*, 16:1263–1270, 2020.

[32] J. M. Hermida-Ramon, A. Ohrn, and G. Karlstrom. Structure and spectrum of the hydrated electron: A combined quantum chemical statistical mechanical simulation. *J. Mol. Liq.*, 292:111300, 2019.

[33] R. E. Larsen, W. J. Glover, and B. J. Schwartz. Does the hydrated electron occupy a cavity? *Science*, 329:65–69, 2010.

[34] J. R. Casey, B. J. Schwartz, and W. J. Glover. Free energies of cavity and noncavity

hydrated electrons at the instantaneous air/water interface. *J. Phys. Chem. Lett.*, 7:3192–3198, 2016.

[35] J. R. Casey, R. E. Larsen, and B. J. Schwartz. Resonance raman and temperature-dependent electron absorption spectra of cavity and non-cavity models of the hydrated electron. *Proc. Nat. Acad. Sci.*, 110:2712–2717, 2013.

[36] J. R. Casey, A. Kahros, and B. J. Schwartz. To be or not to be in a cavity? The hydrated electron dilemma. *J. Phys. Chem. B*, 117:14173–14182, 2013.

[37] E. R. Barthel, I. B. Martini, and B. J. Schwartz. Direct observation of charge-transfer-to-solvent (CTTS) reactions: Ultrafast dynamics of the photoexcited alkali metal anion sodide (Na^-). *J. Chem. Phys.*, 112:9433–9444, 2000.

[38] R. M. Young and D. M. Neumark. Dynamics of solvated electrons in clusters. *Chem. Rev.*, 112:5553–5577, 2012.

[39] W. J. Glover, R. E. Larsen, and B. J. Schwartz. The roles of electronic exchange and correlation in charge-transfer-to-solvent dynamics: Many-electron non-adiabatic mixed quantum/classical simulations of photoexcited sodium anions in the condensed phase. *J. Chem. Phys.*, 129:1–20, 2008.

[40] D. Bhattacharyya, H. Mizuno, A. M. Rizzuto, Y. Y. Zhang, R. J. Saykally, J. Richard, and S. E. Bradroth. New insights into the charge-transfer-to-solvent spectrum of aqueous iodide: Surface versus bulk. *J. Phys. Chem. Lett.*, 11:1656–1661, 2020.

[41] W. J. Glover, R. E. Larsen, and B. J. Schwartz. First principles multi-electron mixed quantum/classical simulations in the condensed phase. ii. The charge-transfer-to-solvent states of sodium anions in liquid tetrahydrofuran. *J. Chem. Phys.*, 132:1–13, 2010.

[42] M. C. Cavanagh, R. E. Larsen, and B. J. Schwartz. Watching Na atoms solvate into Na^+-e^- contact pairs: Untangling the ultrafast charge-transfer-to-solvent dynamics of Na^- in tetrahydrofuran (THF). *J. Phys. Chem. A*, 111:5144–5157, 2007.

[43] J. Franck and E. Rabinowitch. Some remarks about free radicals and the photochemistry of solutions. *Trans. Far. Soc.*, 30:120–130, 1934.

[44] R. M. Noyes. Effects of diffusion rates on chemical kinetics. *Prog. React. Kinet.*, 1:129–160, 1961.

[45] B. J. Schwartz, J. C. King, and C. B. Harris. The molecular basis of solvent caging. In J. D. Simon, editor, *Ultrafast Dynamics of Chemical Systems. Understanding Chemical Reactivity*, chapter 8, pages 235–248. Springer, Dordrecht, 1994.

[46] W. J. Glover and B. J. Schwartz. How does a solvent affect chemical bonds? Mixed quantum/classical simulations with a full CI treatment of the bonding electrons. *J. Phys. Chem. Lett.*, 1:165–169, 2010.

[47] E. Rabinowitch and W. C. Wood. Dissociation of excited iodine molecules. *J. Chem. Phys.*, 4:358–362, 1936.

[48] E. Rabinowitch and W. C. Wood. Kinetics of recombination of iodine atoms. *J. Chem. Phys.*, 4:497–504, 1936.

[49] J. Douady, E. Jacquet, E. Giglio, D. Zanuttini, and B. Gervais. Non-adiabatic molecular dynamics of excited Na_2^+ solvated in Ar_{17} clusters. *Chem. Phys. Lett.*, 476:163–167, 2009.

[50] M. Y. Niv, M. Bargheer, and R. B. Gerber. Photodissociation and recombination of molecule in cluster: Nonadiabatic molecular dynamics simulations. *J. Chem. Phys.*, 113:6660–6672, 2000.

[51] N. Winter, I. Chorny, J. Vieceli, and I. Benjamina. Molecular dynamics study of the photodissociation and photoisomerization of ICN in water. *J. Chem. Phys.*, 119:2127–2143, 2003.

[52] D. Zanuttini, J. Douady, E. Jacquet, E. Giglio, and B. Gervaisa. Nonadiabatic molecular dynamics of photoexcited Li_2^+ Ne_n clusters. *J. Chem. Phys.*, 134:1–12, 2011.

[53] J. Zimmerman and R. M. Noyes. The primary quantum yield of dissociation of iodine in hexane solution. *J. Chem. Phys.*, 18:658–666, 1950.

[54] R. Marshall and N. Davidson. Photoelectric observation of the rate of recombination of iodine atoms. *J. Chem. Phys.*, 21:659–664, 1953.

[55] F. W. Lampe and R. M. Noyes. Absolute quantum yields for dissociation of iodine in inert solvents. *J. Am. Chem. Soci.*, 76:2140–2144, 1954.

[56] L. F. Meadows and R. M. Noyes. The dependence on wave length of quantum yields for iodine dissociation. *J. Am. Chem. Soci.*, 82:1872–1876, 1960.

[57] J. Troe. Atom and radical recombination reactions. *Ann. Rev. Phys. Chem.*, 29:223–250, 1978.

[58] L. Luther, J. Schroeder, J. Troe, and U. Unterberg. Pressure-dependence of atom recombination and photlytic cage effect of iodine in solution. *J. Phys. Chem.*, 84:3072–3075, 1980.

[59] B. Otto, J. Schroeder, and J. Troe. Photolytic cage effect and atom recombination of iodine in compressed gases and liquids: Experiments and simple models. *J. Chem. Phys.*, 81:202–213, 1984.

[60] M. G. Sceats, J. M Dawes, and D. P. Miller. Atom recombination in dense gases and fluids: A stochastic-model. *Chem. Phys. Lett.*, 114:63–70, 1985.

[61] R. Parson, J. Faeder, and N. Delaney. Charge flow and solvent dynamics in the photodissociation of solvated molecular ions. *J. Phys. Chem. A*, 104:9653–9665, 2000.

[62] J. Ka and S. Shin. One-electron model for photodissociation dynamics of diatomic anion. *J. Chem. Phys.*, 109:10087–10095, 1998.

[63] H. Schroder and H. Gabriel. Classical simulation of a cage effect in the dissociation of I_2Rg_n clusters (Rg=Ar,Kr,Xe; n<=5). *J. Chem. Phys.*, 104:587–598, 1996.

[64] W. N. Wang, K. A. Nelson, L. Xiao, and D. F. Coker. Molecular-dynamics simulation studies of solvent cage effects on photodissociation in condensed phases. *J. Chem. Phys.*, 101:9663–9671, 1994.

[65] R. M. Whitnell, K. R. Wilson, Y. J. Yan, and A. H. Zewail. Classical-theory of ultrafast pump-probe spectrscopy: Applications to I_2 photodissociation in Ar solution. *J. Mol. Liq.*, 61:153–165, 1994.

[66] R. Zadoyan, Z. Li, P. Ashjian, C. C. Martens, and V. A. Apkarian. Femtosecond dynamics of coherent photodissociation of I_2 isolated in matrix Ar. *Chem. Phys. Lett.*, 218:504–514, 1994.

[67] R. Zadoyan, Z. Li, C. C. Martens, and V. A. Apkarian. The breaking and remaking of a bond: Caging of I_2 in solid Kr. *J. Chem. Phys.*, 101:6648–6657, 1994.

[68] Z. Li, R. Zadoyan, and V. A. Apkarian. Femtosecond many-body dynamics of caging: experiment and simulation of I_2 photodissociation-recombination in solid Ar. *J. Phys. Chem.*, 99:7453–7465, 1995.

[69] V. A. Apkarian and N. Schwentner. Molecular photodynamics in rare gas solids. *Chem. Rev.*, 99:1481–1514, 1999.

[70] Z. Bihary, R. Zadoyan, M. Karavitis, and V. A. Apkarian. Dynamics and the breaking of a driven cage: I_2 in solid Ar. *J. Chem. Phys.*, 120:7576–7589, 2004.

[71] Q. L. Liu, J. K. Wang, and A. H. Zewail. Femtosecond dynamics of dissociation and recombination in solvent cages. *Nature*, 364:427–430, 1993.

[72] A. Kornath, A. Zoermer, and R. Ludwig. Formation of the magic cluster Na_8 in noble gas matrixes. *Inorg. Chem.*, 41:6206–6210, 2002.

[73] A. Kornath, R. Ludwig, and A. Zoermer. Small potassium clusters. *Angew. Chem. Int. Ed.*, 37:1575–1577, 1998.

[74] G. A. Ozin and H. Huber. The matrix optical spectra of sodium molecules containing from two to four atoms. *Inorg. Chem.*, 18:1402–1406, 1979.

[75] T. Welker and T. P. Martin. Optical-absorption of matrix isolated Li, Na, and Ag clusters and microcrystals. *J. Chem. Phys.*, 70:5683–5691, 1979.

[76] M. Hofmann, S. Leutwyler, and W. Schulze. Matrix isolation-aggregation of sodium atoms and molecules formed in a supersonic nozzle bean. *Chem. Phys.*, 40:145–152, 1979.

[77] F. W. Froben and W. Schulze. Raman measurements of matrix-isolated small metal-clusters. *Phys. Chem. Chem. Phys.*, 88:312–314, 1984.

[78] A. Kornath, A. Zoermer, and R. Ludwig. Raman spectroscopy investigation of matrix-isolated rubidium and cesium molecules: Rb_2, Rb_3, Cs_2, and Cs_3. *Inorg. Chem.*, 38:4696–4699, 1999.

[79] D. R. Scott and J. B. Allison. Solvent glasses for low temperature spectroscopic studies. *J. Phys. Chem.*, 66:561–562, 1962.

[80] V. S. Batista and D. F. Coker. Nonadiabatic molecular dynamics simulation of photodissociation and geminate recombination of I_2 liquid xenon. *J. Chem. Phys.*, 105:4033—4054, 1996.

[81] V. S. Batista and D. F. Coker. Nonadiabatic molecular dynamics simulation of ultrafast pump-probe experiments on I_2 in solid rare gases. *J. Chem. Phys.*, 106:6923—6941, 1997.

[82] J. Faeder, N. Delaney, P. E. Maslen, and R. Parson. Charge flow and solvent dynamics in the photodissociation of cluster ions: A nonadiabatic molecular dynamics study of I_2^- Ar_n. *Chem. Phys. Lett.*, 270:196—205, 1997.

[83] N. Delaney, J. Faeder, P. E. Maslen, and R. Parson. Photodissociation, recombination, and electron transfer in cluster ions: A nonadiabatic molecular dynamics study of $I_2^-(CO_2)_n$. *J. Phys. Chem. A*, 101:8147, 1997.

[84] P. E. Maslen, J. Faeder, and R. Parson. An effective Hamiltonian for an electronically excited solute in a polarizable molecular solvent. *Mol. Phys.*, 94:693—706, 1998.

[85] W. J. Glover, R. E. Larsen, and B. J. Schwartz. First principles multi-electron mixed quantum/classical simulations in the condensed phase. i. An efficient fourier-grid method for solving the many-electron problem. *J. Chem. Phys.*, 132:1–11, 2010.

[86] W. J. Glover, R. E. Larsen, and B. J. Schwartz. The nature of sodium atoms/(Na^+-e^-) contact pairs in liquid tetrahydrofuran. *J. Phys. Chem. B.*, 114:11535–115439, 2010.

[87] M. P. Allen and D. J. Tildesley. *Computer Simulation of Liquids.* Oxford University Press, London, 1992.

[88] J. C. Phillips and L. Kleinman. New method for calculating wave functions in crystals and molecules. *Phys. Rev.*, 116:287–294, 1959.

[89] C. J. Smallwood, R. E. Larsen, W. G. Glover, and B. J. Schwartz. A computationally efficient exact pseudopotential method. i. Analytic reformulation of the Philips-Kleinman theory. *J. Chem. Phys.*, 125:1–8, 2006.

[90] P. Suppan. Solvatochromic shifts: The influence of the medium on the energy of electronic states. *J. Photochem. Photobiol.*, 50:293–330, 1990.

[91] B. Bagchi. Isomerization dynamics in solution. *Int. Rev. Phys. Chem.*, 6:1–33, 1987.

[92] B. Gervais, E. Giglio, E. Jacquet, I. Ipatov, P. G. Reinhard, and E. Suraud. Simple DFT model of clusters embedded in rare gas matrix: Trapping sites and spectroscopic properties of Na embedded in Ar. *J. Chem. Phys.*, 121:8466–8480, 2004.

[93] L. Szaz. *Pseudopotential Theory of Atoms and Molecules*. Wiley, New York, 1985.

[94] Z. Liu, L. E. Carter, and E. A. Carter. Full configuration interaction molecular dynamics of Na_2 and Na_3. *J. Chem. Phys.*, 99:4355–4359, 1995.

[95] J. E. Lennard-Jones. The electronic structure of some diatomic molecules. *Trans. Faraday Soc.*, 25:668–686, 1929.

[96] C. A. Coulson. Representation of simple molecules by molecular orbitals. *Q. Rev. Chem. Soc.*, 1:144–178, 1947.

[97] H. Kato, T. Matsui, and C. Noda. $Na_2(a^1\Sigma^+{}_u \rightarrow x^1\Sigma^+{}_g)$ fluorescence accompanied by a continuous spectrum. *J. Chem. Phys.*, 76:5678–5683, 1982.

[98] K. K. Verma, J. T. Bahns, A. R. Rajeiriza, W. C. Stwalley, and W. T. Zemke. First observation of bound-continuum transitions in the laser-induced $a^1\Sigma^+{}_u \rightarrow x^1\Sigma^+{}_g$ fluorescence of Na_2. *J. Chem. Phys.*, 78:3599–3613, 1983.

[99] R. F. Barrow, J. Verges, C. Effantin, K. Hussein, and J. D'incan. Long-range potentials for the $x^1\Sigma^+{}_g$ and $(1)^1\ \sigma_g$ states and the dissociation energy of Na_2. *Chem. Phys. Lett.*, 104:179–183, 1984.

[100] O. Babaky and K. Hussein. The ground state $X^1\Sigma^+{}_g$ of Na_2. *Can. J. Phys*, 67:912–918, 1989.

[101] W. J. Glover, R. E. Larsen, and B. J. Schwartz. Simulating the formation of sodium:electron tight-contact pairs: Watching the solvation of atoms in liquids one molecule at a time. *J. Phys. Chem. A*, 115:5887–5894, 2011.

[102] A. E. Bragg, W. J. Glover, and B. J. Schwartz. Watching the solvation of atoms in liquids one molecule at a time. *Phys. Rev. Lett.*, 104:1–4, 2010.

[103] J. Chandrasekhar and W. L. Jorgensen. The nature of dilute-solutions of sodium-ion in water, methanol, and tetrahydrofuran. *J. Chem. Phys.*, 77:5080–5089, 1982.

[104] N. Mardirossian and M. Head-Gordon. ωB97M-V: A combinatorially optimized, range-separated hybrid, meta-GGA density functional with VV10 nonlocal correlation. *J. Chem. Phys.*, 144:214110–214200, 2016.

[105] O. Steinhauser. Reaction field simulation of water. *Mol. Phys.*, 45:335–348, 1982.

[106] B. Smit. Phase-diagrams of Lennard-Jones fluids. *J. Chem. Phys.*, 96:8639–8640, 1992.

[107] G. R. Ahmadi, J. Almlöf, and I. Røeggen. The interaction potential for the $X^1\sigma^+$ state of $ArNa^+$, $NeNa^+$ and $HeNa^+$. *Chem. Phys.*, 199:33–52, 1995.

[108] M. P. Allen and D. J. Tildesley. *ARPACK Users' Guide*. SIAM, Philadelphia, 1998.

[109] D. R. Widmer and B. J. Schwartz. Solvents can control solute molecular identity. *Nature Chem.*, 10:910–916, 2018.

[110] Q. Zhang, J. W. Hepburn, and M. Shapiro. Observation of above-threshold dissociation of Na_2^+ in intense laser fields. *Phys. Rev. A*, 78:1–3, 2008.

[111] J. A. Fayeton, M. Barat, J. C. Brenot, H. Dunet, Y. J. Picard, U. Saalmann, and R. Schmidt. Detailed experimental and theoretical study of collision-induced dissociation of Na_2^+ ions on He and H_2 target at keV energies. *Phys. Rev. A*, 57:1058–1068, 1998.

[112] J. C. Brenot, H. Dunet, J. A. Fayeton, M. Barat, and M. Winter. Analysis of collision induced dissociation of Na_2^+ molecular ions. *Phys. Rev. Lett.*, 77:1246–1249, 1996.

[113] A. Henriet and F. Masnou-Seuws. Model potential calculations for the ground, excited and Rydberg $^2\sigma$ states of Li_2^+, Na_2^+ and K_2^+: Core polarization effects. *Chem. Phys. Lett.*, 101:535–540, 1983.

[114] M. A. Morrison and L. A. Collins. Exchange in low-energy electron-gas model exchange potentials and applications to e-H_2 and e-N_2 collisions. *Phys. Rev. A*, 17:918–938, 1978.

[115] M. A. Morrison and L. A. Collins. The frozen-core approximation for diatomic molecules. *J. Phys. B*, 7:1782–1789, 1974.

[116] A. Kahros and B. J. Schwartz. Going beyond the frozen core approximation: development of coordinate-dependent pseudopotentials and application to Na_2^+. *J. Chem. Phys.*, 138:1–9, 2013.

[117] V. S. Batista and D. F. Coker. Nonadiabatic molecular dynamics simulations of the photofragmentation and geminate recombination dynamics in size-selected I_2^--Ar_n cluster ions. *J. Chem. Phys.*, 106:7102–7116, 1997.

[118] B. J. Schwartz, J. C. King, J. Z. Zhang, and C. B. Harris. Direct femtosecond measurements of single collision dominated geminate recombination times of small molecules in liquids. *Chem. Phys. Lett.*, 203:503–508, 1993.

[119] D. R. Widmer and B. J. Schwartz. The role of the solvent in the condensed-phase dynamics and identity of chemical bonds: The case of the sodium dimer cation in THF. *J. Phys. Chem. B*, Under Review 2020.

[120] D. Chandler. *Introduction to Modern Statistical Mechanics*. Oxford Univ. Press, New York, 1987.

[121] A. E. Bragg, M. C. Cavanagh, and B. J. Schwartz. Linear response breakdown in solvation dynamics induced by atomic electron-transfer reactions. *Science*, 321:1817–1822, 2008.

[122] M. J. Bedard-Hearn, R. E. Larsen, and B. J. Schwartz. Hidden breakdown of linear response: Projections of molecular motions in nonequilibrium simulations of solvation dynamics. *J. Phys. Chem. A.*, 107:4773–4777, 2003.

[123] A. C. Moskun, A. E. Jailaubekov, S. E. Bradforth, G. Tao, and R. M. Stratt. Rotational coherence and a sudden breakdown in linear response seen in room-temperature liquids. *Science*, 311:1907–1911, 2006.

[124] G. Tao and R. M. Stratt. The molecular origins of nonlinear response in solute energy relaxation: The example of high-energy rotational relaxation. *J. Chem. Phys.*, 125:1–17, 2006.

[125] B. M. Ladanyi and B. C. Perng. Solvation dynamics in dipolar-quadrupolar mixtures: A computer simulation study of dipole creation in mixtures of acetonitrile and benzene. *J. Phys. Chem. A*, 106:6922–6934, 2002.

[126] M. Maroncelli and G. R. Fleming. Computer simulations of the dynamics of aqueous solvation. *J. Chem. Phys.*, 89:5044–5069, 1988.

[127] D. Aherne, V. Tran, and B. J. Schwartz. Non-linear, non-polar solvation dynamics in water: The roles of electrostriction and solvent translation in the breakdown of linear response. *J. Phys. Chem. B*, 104(22):5382–5394, 2000.

[128] B. B. Laird and W. H. Thompson. On the connection between gaussian statistics and excited-state linear response for time-dependent fluorescence. *J. Chem. Phys.*, 126:1–4, 2007.

[129] A. J.Schile and W. H. Ward. Tests for, origins of, and corrections to non-gaussian statistics: The dipole-flip model. *J. Chem. Phys.*, 146:154109–154109, 2017.

[130] M. R. Shirts and J. D. Chodera. Statistically optimal analysis of samples from multiple equilibrium states. *J. Chem. Phys.*, 129:1–13, 2008.

[131] D. R. Widmer, A. Vong, and B. J. Schwartz. Linear response breakdown in liquid photodissociation: Caging and chemical identity. *Nature Chem.*, Submitted 2020.

[132] R. J. Gillespie. Fifty years of the VSEPR model. *Coord. Chem. Rev.*, 252:12–14, 2008.